A HISTOMORPHOMETRIC STUDY OF THE EFFECT OF AFRIPLEX GRT™ ON THE PANCREAS, LIVER AND KIDNEY OF RATS FED A HIGH-FAT DIET

by

Jodie Layman

Thesis presented in fulfilment of the requirements for the degree

Master of Science in Morphological sciences at

Stellenbosch University

Supervisor: Prof S.H. Kotzé

Co-supervisor: Dr N. Chellan

Faculty of Medicine and Health Sciences

December 2018

The financial assistance of the National Research Foundation (NRF) towards this research is hereby acknowledged. Opinions expressed, and conclusions arrived at, are those of the author and not necessarily to be attributed to the NRF.

DECLARATION

By submitting this thesis electronically, I declare that the entirety of the work contained therein is my own, original work, that I am the sole author thereof (save to the extent explicitly otherwise stated), that reproduction and publication thereof by Stellenbosch University will not infringe any third party rights and that I have not previously in its entirety or in part submitted it for obtaining any qualification.

December 2018

ABSTRACT

Obesity causes a wide range of disorders including insulin resistance, hepatic steatosis as well as renal glomerular and tubular pathology. These disorders are typically associated with oxidative stress and inflammation. Rooibos, *Aspalathus linearis*, is a South African plant which has antioxidative, anti-inflammatory, antilipidemic, and antihyperglycemic properties as shown *in vivo* and *in vitro*. Afriplex GRT™ is an unfermented green rooibos extract which is postulated to have enhanced effects compared to fermented rooibos, mostly due to its high aspalathin content. The present study aimed to determine the ameliorative effects of Afriplex GRT™ on the histomorphometry of the pancreas liver and kidney in a diet-induced obese rat model.

Male Wistar rats (N=28) were randomly sorted into four study groups (n=7) namely, control (C), GRT fed control (GRT), high-fat diet (HFD) and HFD supplemented with GRT (HFD-GRT). Animals were either fed a control feed or a HFD which contained fat, cholesterol and fructose. Animals in the GRT and HFD-GRT groups were supplemented with Afriplex GRT™ at a concentration of 60 mg per kg body mass per day. Body mass, and pancreatic, liver and kidney mass were determined after which samples were processed to wax. Tissues were sectioned at 4 – 5 µm in thickness and stained using haematoxylin and eosin for analysis by a histopathologist. Immunohistochemistry using anti-insulin and anti-glucagon double antibody labelling was performed on the pancreas. Other staining techniques included Masson's trichrome, Gordon and Sweet's reticulin impregnation and periodic acid Schiff. Additionally, frozen sections of the liver and pancreas were stained using Oil red O for lipid infiltration. Morphometric techniques included area, diameter, radii, point counting and ratios.

Body mass significantly decreased in the HFD-GRT group compared to the HFD group. Pancreas and kidney mass decreased significantly in the HFD-GRT group compared to the C-group, however liver mass significantly increased in both HFD groups. Islet area and β-cell area significantly decreased in the HFD-GRT group compared to all three control groups however, a greater number of islets was observed. Hepatic steatosis and liver pathology were reduced in the HFD-GRT group compared to the HFD group. Renal space and the proximal convoluted tubules were decreased in the HFD-GRT compared to C-group as indicated by trends. Additionally, a trend was observed in the arcuate artery media to lumen ratio which was increased in the GRT group compared to the HFD group.

Similar to the present study, a decrease in body mass has been observed with fermented rooibos and its polyphenols in HFD-fed animals. In the HFD-GRT group, increased islets per section area and smaller islet areas are associated with increased insulin secretion, which suggests improved glucose tolerance. This study suggests that Afriplex GRT™ may effectively reduce hepatic steatosis, an effect previously seen in studies on fermented rooibos and rooibos polyphenols. More in-depth studies on the effects of Afriplex GRT™ in the kidney are needed, potentially for a longer study period. Therefore, Afriplex GRT™ has observable ameliorative effects on the histomorphology of the liver and the pancreas; the effects on the kidney requires further investigation.

OPSOMMING

Vetsug veroorsaak 'n groot verskeidenheid van afwykings, wat insluit insulienweerstandigheid, hepatiese steatosis, asook renale glomerulêre en tubulêre patologie. Hierdie afwykings word tipies geassosieer met oksidatiewe stres en inflammasie. Rooibos, *Aspalathus Linearis*, is 'n Suid-Afrikaanse plant wat anti-oksidatiewe, anti-inflammatoriese, anti-lipidemiese en anti-hiperglukemiese eienskappe toon, volgens *in vivo* en *in vitro* studies. Daar word gepostuleer dat Afriplex GRT™, wat 'n ongefermenteerde groen rooibos uittreksel is, ‘n versterkte effekt toon in vergelyking met gefermenteerde rooibos, hoofsaaklik as gevolg van die hoë aspalatien inhoud. Die doel van die huidige studie was om die verbeterende effekte van Afriplex GRT™ op die histomorfometrie van die pankreas, lewer en nier in ‘n dieet-geïnduseerde obesitiet rotmodel vas te stel.

Manlike Wistar rotte (N = 28) was verdeel in vier studiegroepe (n = 7) naamlik, kontrole groep (K), kontrole GRT groep (GRT), hoëvet diet groep (HVD) en HVD met GRT groep (HVD-GRT). 'n Beheer voer of 'n HVD (wat vet, cholesterol en fruktose bevat) was vir rotter gevoer. Die voer van rotte in die GRT en HVD-GRT groepe was aangevul met Afriplex GRT™, met 'n konsentrasie van 60 milligram per kg liggaamsmassa per dag. Liggaamsmassa as ook pankreas, lewer en nier massa was bepaal, waarna weefsel in was verwerk was. Weefsels was gesny teen ‘n 4 - 5 µm dikte en gekleur met hematoksilien en eosien vir analise deur 'n histopatoloog. Immunohistochemiese kleuring vir anti-insulien en anti-glukagon was op die pankreas uitgevoer. Masson’s trichrome, Gordon en Sweet’s retikulien saturasie, en periodic acid Schiff was ook gedoen. Verder was bevrore snitte van die lewer en pankreas met Oil red O gekleur vir lipied infiltrasie. Morfometriese tegnieke het ingelsuit in area, deursnee, radius, punt telling en verhoudings.

Liggaamsmassa het aansienlik afgeneem in die HVD-GRT-groep in vergelyking met die HVD-groep. Pankreas- en niermassa het aansienlik afgeneem in die HVD-GRT-groep in vergelyking met die K-groep, maar die lewermassa het aansienlik toegeneem in beide HVD-groepe. In die HVD-GRT-groep het die eiland- en beta-selgebied aansienlik afgeneem in vergelyking met al drie beheergroepe, maar 'n groter aantal eilandjies is waargeneem. Hepatiese steatosis en lewerpatologie was in die HVD-GRT-groep verlaag in vergelyking met die HVD-groep. Renale spasie en die proksimale kronkelbuisies is in die HVD-GRT verlaag in vergelyking met K-groep soos aangedui deur tendense. Daarbenewens was 'n tendens

waargeneem in die arcuate arterie media tot lumen verhouding wat in die GRT groep vergroot is in vergelyking met die HVD groep. 'n Vermindering in liggaam gewig, vergelykbaar met die huidige studie, was geassosieer met gefermenteerde rooibos en sy polyfenole in die HVD-gevoerde diere. In die HVD-GRT-groep het die toenemende eilandjies per area en aantal kleiner eilandjies per area gelei tot ‘n verhoogde insulienafskeiding, wat verbeterde glukosetoleransie aandui. Hierdie studie dui daarop dat Afriplex GRT™ hepatiese steatosis effektief kan verminder, 'n effek wat voorheen gesien is in studies oor gefermenteerde rooibos en rooibos polifenole. Meer in-diepte studies oor die gevolge van Afriplex GRT™ in die nier is nodig, ideal vir 'n langer tydperk. Dus, Afriplex GRT™ het waarneembare verbeterende effekte op die histomorfologie van die lewer en die pankreas. Hierdie effekte op die nier vereis verdere ondersoek.

ACKNOWLEDGEMENTS

All honour, glory and praise to my Lord and Savior Jesus Christ for the completion of this masters thesis.

- My sincere gratitude to my supervisor, Prof. S Kotzé, for sharing your knowledge, guiding and being patient with me. Baie Dankie Prof.
- Thank you to my co-supervisor, Dr. N Chellan, for your support, patience and guidance.
- The following people are thanked for their technical assistance: Mr R Williams and Mr J Pieterse from the Division of Clinical Anatomy and Ms. Charna Chapman, Ms Ruzayda Van Aarde and Mr Desmond Linden from the South African Medical Research Council. Lastly, Prof. Martin Kidd for assistance with statistical analysis.
- Thank you to Prof B Huisamen, Marlouw Kroukamp and Mignon van Vuuren from the Division of Medical Physiology.
- Thank you to the South African Medical Research Council for the use of their facilities and equipment.
- Thank you to my friends, colleagues and staff members from the Division of Clinical Anatomy. You are an amazing team.
- The National Research Foundation and Stellenbosch University are hereby acknowledged for their financial support.
- To my colleagues and friends, Daniella Pereira, Lauren Sahd, Karen Cilliers, Mikal Aylward and Leandrie Beselaar thank you for support and friendship. I really appreciate you.
- Thank you to Karen Cilliers for thorough editing.
- To Nomatolo Nqula and Joseph Risinamhodzi, for your friendship and prayers.
- A special thank you to my parents, Jerome and Lillian Layman, as well as my brother, Luther Layman, without your love and support none of this would have been possible.
- Lastly, to my best friend, Victor Lemphane, thank you for your love and support, for always believing in me and motivating me.

May God richly bless all of you.

DEDICATION

This thesis is dedicated to my grandmother, Irene Layman, a hardworking woman who loved her family, especially her grandchildren.

To Kyle Bevan Thompson and his family who live to honour his memory.

Lastly, this thesis is dedicated to my friends and family

CONTENTS

TABLES

Addenda

FIGURES

Addenda:

EQUATIONS

ADDENDA

ABBREVIATIONS

ACU	Animal Care and Use
AMP	Adenosine monophosphate
AMPK	AMP-activated protein kinase
ANOVA	Analysis of variance
BCL_2	B-cell lymphoma 2
BM	Body mass
C	Control group
CAT	Catalase
CI	Confidence interval
Control	Control feed
DAB	3'3-diaminobenzidine
DCT	Distal convoluted tubule
DIO	Diet-induced obesity
DPX	Dystyrene Plasticiser and xylene
ER	Endoplasmic reticulum
eNOS	endothelial nitric oxide synthase
FFA	Free fatty acids
G	Gastric portion
GFR	Glomerular filtration rate
GLUT-4	Glucose transporter -4
GPx	Glutathione peroxidase
GRT	Green rooibos group
H_2O_2	Hydrogen peroxide
HDL	High density lipoproteins
HFD	High-Fat Diet
HPLC	High performance liquid chromatography
IR	Insulin resistance
LD	Lower duodenal portion
LDL	Low density lipoprotein
LSD	Least Significant Difference
LPS	Lipopolysaccharide

MDA	Malondialdehyde
MFPOG	Masson Fuchsin Ponceau-Orange G
MRC	Medical Research Council
N	Study population size
n	Study sample size
NBF	Neutral buffered formalin
NaCl	Sodium chloride
NADPH	Nicotinamide adenine dinucleotide phosphate
NAFLD	Non-alcoholic fatty liver disease
NAFPD	Non-alcoholic fatty pancreas disease
NAS	Non-alcoholic fatty liver disease activity score
NASH	Non-alcoholic steatohepatitis
NBF	Neutral Buffered Formalin
NF-κβ	Nuclear factor kappa beta
OECD	Organization for Economic Co-operation and Development
OH	Hydroxyl group
ORO	Oil red O
PAS	Periodic acid Schiff
PCT	Proximal convoluted tubule
PKB	Protein kinase B
PPAG	Phenylpyruvic acid-2-O-glucoside
PPAR	Peroxisome Proliferator- activated receptor
PBS	Phosphate buffered saline
RAAS	Renin angiotensin aldosterone system
REC	Research Ethics Committee
RGB	Red/green/blue colour segmentation
RNS	Reactive nitrogen species
ROS	Reactive oxygen species
S	Splenic portion
SA	South Africa
SEM	Standard error of the mean
STZ	Streptozotocin
SOCS	Suppressor of cytokine signalling
SOD	Superoxide dismutase

SOP	Standard operating procedure
T2DM	Type 2 diabetes mellitus
TBS	Tris buffered saline
TG	Triglycerides
UD	Upper duodenal portion
VAT	Visceral adipose tissue
VLDL	Very low-density lipoproteins
WAT	White adipose tissue
WHO	World Health Organisation

Units of measurement

°	degrees
C	Celsius
g	Gram
l	litre
M	molar
m	milli
%	percent
±	plus or minus
α	alpha
β	beta
γ	gamma
δ	delta
κ	Cohens kappa score
µ	Micro

CHAPTER ONE:

INTRODUCTION

Aspalathus linearis, commonly known as rooibos, is a South African plant with proven effects on metabolic related disorders. Rooibos may be prepared in its fermented, traditional form or unfermented green form. The effects of fermented rooibos, its extracts and individual polyphenols *in vitro* and *in vivo* are established. These effects include: decreasing hyperglycaemia (Kawano *et al.*, 2009; Son *et al.*, 2013; Kamakura *et al.*, 2015), improving hyperlipidaemia and liver steatosis (Beltran-Debon *et al.*, 2010), reducing oxidative stress (Joubert *et al.*, 2004), cardiovascular disease (Pantsi *et al.*, 2011), inflammation (Ajuwon *et al.*, 2013), and nephroprotective effects (Alhoshani *et al.*, 2017). More recently, the use of unfermented rooibos in research is gaining popularity, mostly due to its high aspalathin content.

Afriplex GRT™ is a laboratory standardized unfermented rooibos extract developed by African Plant Extracts Pty, Ltd. (Afriplex). Improvement of vascular function, myocardial insulin resistance and mitochondrial function, liver antioxidant profile, liver and body mass reducing properties of Afriplex GRT™ have been determined in two unpublished masters theses on the same experimental animals (Kroukamp, 2018; Maqeda, 2018). Organs from the same studies were studied on a histological level to determine whether the effects of Afriplex GRT™ reflected on histology and morphology of the pancreas, liver and kidney.

Obesity is a chronic, lifestyle-related metabolic disorder which results from the imbalance of caloric intake and energy expenditure. An unhealthy sedentary lifestyle (Wang *et al.*, 2016) and unhealthy diet are associated with obesity, which promotes excessive deposition of visceral and ectopic white adipose tissue (Noeman *et al.*, 2011). Obesity is associated with insulin resistance, type two diabetes mellitus, fatty pancreas and liver disease, hypertension and chronic kidney disease. Many of these effects can be replicated in animal models to study the mechanisms behind these disorders. Disorders commonly observed in animal models include: increased body and organ mass (Buettner *et al.*, 2007; Beltran *et al.*, 2011), alterations in islet morphology, number and size (Slavin *et al.*, 2010; Oliveira *et al.*, 2014), hepatic steatosis (Catta-Preta *et al.*, 2011; Schultz *et al.*, 2013), glomerulomegaly and tubular dysfunction in the kidney (Altunkaynak *et al.*, 2008; Stemmer *et al.*, 2012). As obesity and its associated disorders increase, the need to comprehend the consequences of these conditions and provide solutions is vital. Animal models of metabolic disorders have been studied extensively with several herbal extracts, including fermented rooibos (Beltran *et al.*, 2011; Mathijs et a., 2014; Sanderson *et al.*, 2014; Sasaki *et al.*, 2018); however, the potential effects of an unfermented green rooibos extract in a diet-induced obese rat model requires further investigation.

Therefore, the present study, aimed to determine the effects of Afriplex GRT™, on the histomorphology of pancreas, liver and kidney of rats fed a HFD. Morphometric and histological study of pancreatic islets, liver hepatocytes, the renal corpuscle, proximal convoluted tubules and arcuate arteries of the kidney were performed. In addition, study of Afriplex GRT™ as a protective supplement will determine whether the protective effects of Afriplex GRT™ are visible on a histomorphometric level.

CHAPTER TWO:

LITERATURE STUDY

2.1 OBESITY: THE GLOBAL EPIDEMIC

Obesity is defined as constant caloric intake which exceeds energy expenditure and results in the excessive formation of white adipose tissue (WAT) (Akoum *et al.,* 2011; Sanderson *et al.,* 2014). The World Health Organization (WHO) reported that obesity has more than doubled since 1980 (Obesity & Overweight., 2016). According to the Organization for Economic Co-operation and Development (OECD), globally one in two adults and almost one in six children are overweight and or obese. Further they stated that more than one in four adults in countries including South Africa, are obese (Obesity update, 2017). South Africa has the highest obesity rate in sub-Saharan Africa (The Heart and Stroke foundation of South Africa, 2016). Statistics from the South African demographics survey (2016) revealed that 31% of males and 68% of females were reported to be obese, and that the Western Cape is the obesity capital of South Africa.

Obesity results in ectopic and visceral WAT infiltration and accumulation which may result in fatty deposition in the liver, skeletal muscle, heart (Noeman *et al.,* 2011) and pancreas (Ou *et al.,* 2013). Insulin resistance, chronic kidney disease, hepatic steatosis (Stemmer *et al.,* 2012), diabetes mellitus, and hypertension (Sanderson *et al.,* 2014) are all obesity associated disorders of major public health concern (Park *et al.,* 2012). Many of these disorders fall under the term 'metabolic syndrome' which is characterised by insulin resistance, glucose intolerance, hypertension, systemic inflammation, atherogenic dyslipidaemia and abdominal obesity (Roberts & Sindhu, 2009). These disorders are usually associated with inflammation (Park *et al.,* 2012) and oxidative stress (Roberts & Sindhu, 2009; Beltran-Debon *et al.,* 2011; Noeman *et al.,* 2011; Favero *et al.,* 2013).

2.1.1 Diet-induced obesity (DIO)

Obesity may be induced in rodents and other animal models by dietary, neuroendocrine or genetic means (Noeman *et al.,* 2011). Consumption of a HFD is the major risk factor in metabolic disorders and is central to disorders linked to obesity (Beltran *et al.,* 2011; Akoum *et al.,* 2011). The adverse effects associated with an HFD occur due to the imbalance between energy use and calorie intake. The purpose of diet-induced obesity in rodents is to replicate the Western-diet (Lozano *et al.,* 2016) and lifestyle associated with obesity (Wang *et al.,* 2016). In animal studies, a HFD usually consists of corn-starch, sucrose, fructose or maltodextrose, a source of fat e.g. lard or soybean oil, casein, minerals and vitamins as well as a source of fibre (Warden & Fisler, 2008). In contrast, chow diets can be defined as high-carbohydrate or -fibre

diets as they usually consist of corn, oats or ground wheat, alfalfa and soybean meals, vitamins and minerals, vegetable oil and a protein source such as fish (Warden & Fisler, 2008; Pellizon & Ricci, 2018). Several organs are negatively affected by HFD consumption the pancreas, liver and kidney are organs frequently injured by metabolic disorders associated with unhealthy lifestyles and eating habits. The anatomy, histology and the effects obesity on the pancreas, liver and kidney will be discussed briefly.

2.2 PANCREAS

2.2.1 Anatomy and histology

The pancreas is a lobulated organ located in the abdominal cavity consisting of two main functional units, exocrine and endocrine glands (Young *et al.*, 2006). The exocrine portion consists of the pancreatic acini which secrete enzymatic juices to assist digestion while the endocrine portion, consisting of pancreatic islets (Islet of Langerhans), and is responsible for glucose homeostasis (Young *et al.*, 2006). Figure 2.2 illustrates the morphology and histological arrangement of the rodent pancreas; the micrograph shows an anti-insulin (pink) and anti-glucagon (brown) labelled β- and α-cells, respectively. This organ consists of more exocrine tissue than endocrine tissue, with the latter only making up 2 to 4 % of the total organ volume (Williams *et al.*, 2016).

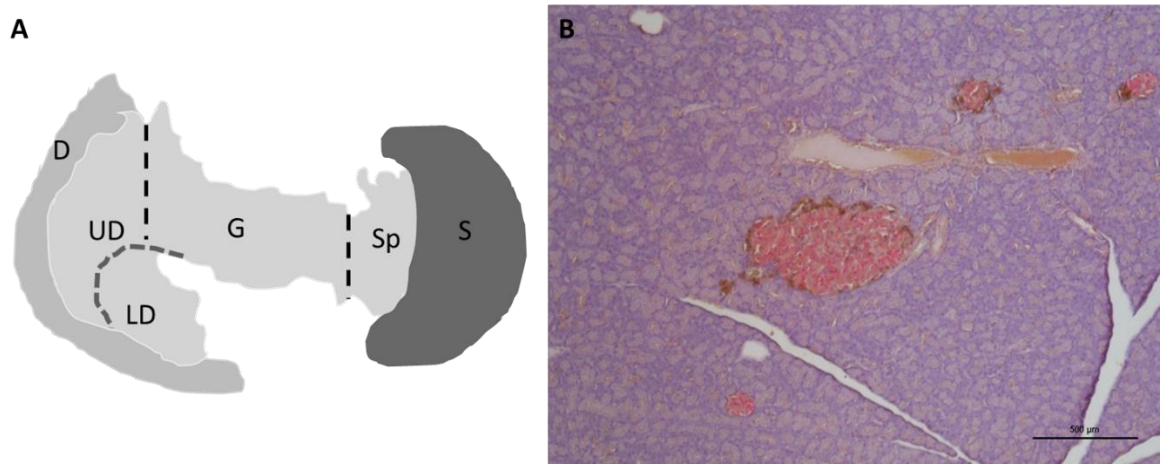

Figure 2.1: Morphology of the rodent pancreas. (A) macroscopic anatomy of the pancreas and (B) micrography of pancreatic histology double antibody labelled with anti-insulin and anti-glucagon (B). The rodent pancreas is generally divided into four regions the upper duodenal (UD), lower duodenal (LD), gastric (G) and splenic regions (S) (Elayat *et al.*, 1995). Histologically, the pancreas consists of endocrine pancreatic islets and exocrine acinus. The pancreatic islets area labelled with anti-glucagon (brown) and anti-insulin (pink) for α- and β-cells. Figure A adapted from Elayat et al. (1995). Micrography by Jodie Layman.

The rat pancreas extends from the end of the duodenal fold towards the gastro-splenic omentum (Greene, 1955; Baker *et al.,* 1979). The rat pancreas may be characterized into four regions namely the duodenal upper (UD) and lower (LD), splenic(S) and gastric (G)regions (Elayat *et al.,* 1995).The human pancreas consists of five regions, the head, neck, body, tail and uncinate process. Similair to the rodent pancreas, the head of the human pancreas is encircled by the duodenum and the tail extends towards the spleen. Both pancreatic islets of rodents and humans consist of four cell types: alpha (α-) secreting glucagon cells, beta (β-) secreting insulin, delta (δ-) secreting somatostatin and pancreatic polypeptide (pp-) cells. Different species each have their own distinct arrangement of the cell types however the functions of cells are consistent (Quesada, Todorova & Soria, 2006). In rodents pancreatic islets are made up of 60-80% β-cells and 10-15% α-cells mantle (Quesada, Todorova & Soria, 2006; Steiner *et al.,* 2010). Structurally, rodent islets cells arrange themselves with a β-cells core and a mantle of α-cells with interspersed δ- and pp-cells. In human pancreatic islets, α-cells make up the majority forming a central core (Steiner *et al.,* 2010) while the remainder of cells are scattered throughout the islets. Collectively these cell types control glucose homeostasis. After a meal insulin is secreted to assist glucose absorption into cells all over the body. Thereafter, glucagon assists secretion of glucose from storage sites to maintain cell function. However, in metabolic disorders this balance is compromised especially in obese individuals who consume copious amounts of unhealthy foods. In these individuals, hyper secretion of insulin occurs, and glucagon is under secreted. Hyperglycaemia persists due to peripheral insensitivity to insulin leading to further injury. This has particular effects on the β-cells which have very few endogenous antioxidants (Sakuraba *et al.,* 2002; Kim *et al.,* 2009). The exocrine portion also experiences injury as the increase in nutrients leads to intra-pancreatic adipocyte deposition. Therefore, both damage to the endocrine and exocrine portions can be problematic.

2.2.2 The effects of obesity on the pancreas

As of 2017, four hundred and twenty-five million people are estimated to be living with diabetes mellitus (Sasaki *et al.,* 2018). Type two diabetes mellitus (T2D) is associated with obesity and is characterised by high blood glucose (Slavin *et al.,* 2010; Nolan *et al.,* 2011), peripheral insulin resistance, and deficient insulin secretion from the pancreas (Sasaki *et al.,* 2018). Alterations in pancreatic islets including: increased islet number, size and morphology as well as insulin secretion are associated with obesity (Slavin *et al.,* 2010). Generally, obese individuals consume copious amounts of carbohydrates which places significant strain on

glucose balance which is maintained by glucagon secreted by pancreatic islet α- cells and insulin secreted by β- cells. As a result of these eating patterns, pancreatic β-cells experience excessive stimulus to secrete insulin. Insulin resistance results in impaired insulin signalling to the liver for the inhibition of glucose release, and stimulation of glucose uptake by the peripheral organs (Reaven *et al.,* 2005). As peripheral insulin resistance in the liver, muscle, adipose tissue, kidney and other organs (Reaven *et al.,* 2005) is present, excessive glucose levels persist in the blood (hyperglycaemia). To attenuate this, β-cells secrete more insulin (hyperinsulinemia) however, after prolonged hyperglycaemia and insulin resistance, β-cells apoptosis (Donath *et al.,* 1999), and resultant decrease in β-cells mass and function occurs and results in T2D.

Diabetes mellitus and insulin resistance are associated with changes in islet size and number (Slavin *et al.,* 2010) β-cells mass, and function (Nolan *et al.,* 2011). Animals fed an HFD usually present with larger islets (Fraulob *et al.,* 2010) which suggests increased hormone secretion. However, smaller islets are associated with increased insulin secretion in both rodent and human islets (Kim *et al.,* 2009; Kotze, 2015). Similar to islets, β-cells also increase with the presence of a HFD (Falcoa *et al.,* 2016) however, HFDs are associated with β-cell related lipotoxicity which may result in β-cell apoptosis (Mathijs *et al.,* 2014). In pancreatic islets, β-cells secrete insulin whereas α-cells oppose insulin by secreting glucagon (Young *et al.,* 2006) when blood glucose is low. Glucagon targets the liver to increases glucose production (Hanhineva et al., 2010). The balance between glucagon and insulin secretion is altered in obesity associated disorders like insulin resistance and diabetes mellitus. Previously in a diabetic rat model, increased body and organ mass as well as degenerated pancreatic islets, vacuolized and degranulation of β-cells was observed in control and HFD fed animals (Anyakudo & Omotayo, 2015).

Obesity results in fat infiltration in many organs including the pancreas where it is known as non-alcoholic fatty pancreas disease (NAFPD). The latter is characterized by increased pancreas mass which compromises pancreatic function (Fraulob *et al.,* 2010). Pancreatic mass is usually increased in obese human individuals (Yagahashi, 2016), or in animals exposed to a HFD (Fraulob *et al.,* 2010; Carter *et al.,* 2014; Anyakudo & Omotayo, 2015). However, pancreas mass is rarely reported in human autopsy due to the difficulty with which it can be accurately dissected as it has obscure borders (Yagahashi *et al.,* 2016; Yu & Wang, 2017). The presence of pancreatic steatosis is associated with insulin resistance and pancreatic islet related

lipotoxicity (Mathijs *et al.*, 2014; Yagihashi, 2016). Intra- and interlobular fat accumulation associated with chronic HFD exposure in rodentsts and results in damage to pancreatic architecture and islets morphology (Fraulob *et al.*, 2010; He *et al.*, 2010; Carter *et al.*, 2014), fibrosis as well as inflammatory cell infiltration (Ou *et al.*, 2013). Histology and biochemical measurements are used frequently to assess pancreatic steatosis. However, as the pancreas is prone to rapid autolysis and difficult to clearly dissect no precise pattern of pancreatic steatosis has been clearly defined (Yu & Wang, 2017).

The excessive lipid infiltration and deposition associated with NAFPD leads to the death and replacement of the pancreatic acinar cells with adipose tissue known as pancreatic steatosis (intralobular) and has a suggested role in T2DM (Yagahashi, 2016; Ou *et al.*, 2013). Furthermore, NAFPD compromises pancreas function due to the release of local fat-derived cytokines which may result in inflammation (Fraulob *et al.*, 2010). Consensus as to whether the alterations in the pancreas are due to fat infiltration associated with insulin resistance or β-cell function in humans is still unknown (Yu & Wang, 2017). The presence of fatty pancreas diseases promotes chronic pancreatitis, exacerbates acute pancreatitis and may lead to pancreatic cancer (Ou *et al.*, 2013). Figure 2.2 describes the link between the liver, pancreas and visceral adipose tissue in insulin resistance and hyperglycaemia and how they contribute to NAFLD and NAFPD.

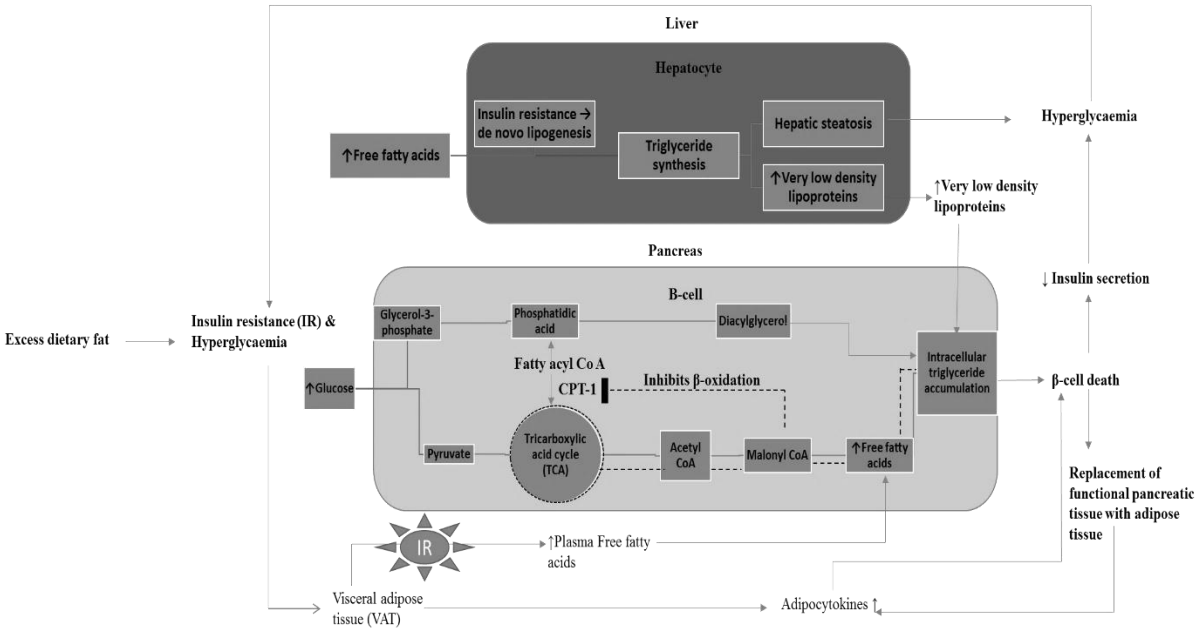

Figure 2.2: Summary of the effects of a diet high in fat on pancreas, liver and visceral adipose tissue (VAT). In the pancreas β-cell death occurs as a result of intracellular triglyceride (TG) accumulation due to the inhibition of β-oxidation (fatty acid catabolism). β-cell death results in decreased insulin secretion and the replacement of pancreatic tissue with adipose tissue (pancreatic steatosis). In the liver, hepatocytes are overwhelmed by the increase in free fatty acids (FFA), TG synthesis is favoured and increased intracellular accumulation of lipids and the release of very low-density lipoproteins (VLDL) occurs. Furthermore, within hepatocytes *de novo* lipogenesis is triggered further increasing TG production. Increased VLDL secretion from the liver increases intracellular TG accumulation in the pancreas. The presence of hepatic steatosis increases hyperglycaemia as hepatic insulin resistance is present and hepatic glucose balance is lost (hepatocyte failure). Visceral adipose tissue (VAT) stores increase due to increased FFA, insulin resistance (IR) and hyperglycaemia. The VAT stores secrete FFA triggered by IR, and adipocytokines. (Adapted fromYagihashi, 2016).

Non-alcoholic fatty pancreas disease is associated with non-alcoholic fatty liver disease (NAFLD); ectopic fat infiltration in the liver parenchyma (Ou *et al.*, 2013). Non-alcoholic fatty liver disease (NAFLD) is the clinical manifestation of insulin resistance associated with chronic intake of a HFD (Schultz *et al.*, 2013). Study of NAFPD is relatively new and was only recently established in both animal and human studies (Della Corte *et al.*, 2015). Insulin and glucagon, hormones secreted by the pancreas, maintains the balance between lipid metabolism in the liver (Campbell *et al.*, 2006) further emphasizing the link between the liver and pancreas (Yu & Wang, 2017) especially in metabolic disorders. Synergistic effects of NAFLD and

NAFPD have shown effects on β-cell function and glucose metabolism (Della Corte *et al.,* 2015) however, further investigation is required to confirm this.

2.3 LIVER

2.3.1 Anatomy and histology

The liver is a largest organ found in the abdominal cavity of humans and rats (Young *et al.,* 2006). The rodent liver is divided into four main lobes namely: the median lobe, a right lateral lobe, a small caudate lobe and a large left lateral lobe (Baker *et al.,* 1979; Malarkey *et al.,* 2005; Shi *et al.,* 2015) (Figure 2.3 B). The liver is involved in glucose, lipid and protein storage and synthesis (Young *et al.,* 2006) and acts as the main organ responsible for eliminating and detoxifying toxins (Ajuwon *et al.,* 2013). Glycogenesis, glycogenolysis and gluconeogenesis are glucose processing pathways in the liver which help maintain glucose balance. These pathways are also responsible for metabolizing carbohydrates to fatty acids and triglycerides (Young *et al.,* 2006; Hanhineva *et al*., 2010) which is important for plasma lipoprotein production. Lipids are usually used to synthesize plasma lipoproteins (very-low, low- and high-density lipoproteins) and oxidised to triglycerides for energy (Hanhineva *et al*., 2010). In comparison to humans, rats do not have a gallbladder the organ responsible for storing bile which assists fat digestion. In rats, their bile ducts anastomose and secrete bile directly into the duodenum (Suckhow *et al.,* 2005). Some proteins such as those involved with haemostasis and fibrinolysis as well as albumin and other hormone and pro-hormones are produced and secreted by the liver (Young *et al.,* 2006; Kierszenbaum & Tres, 2015). In addition to nutrient homeostasis, protein storage and synthesis, the liver filters the blood and plays significant role in neutralizing toxic of substances (Ajuwon *et al.,* 2013).

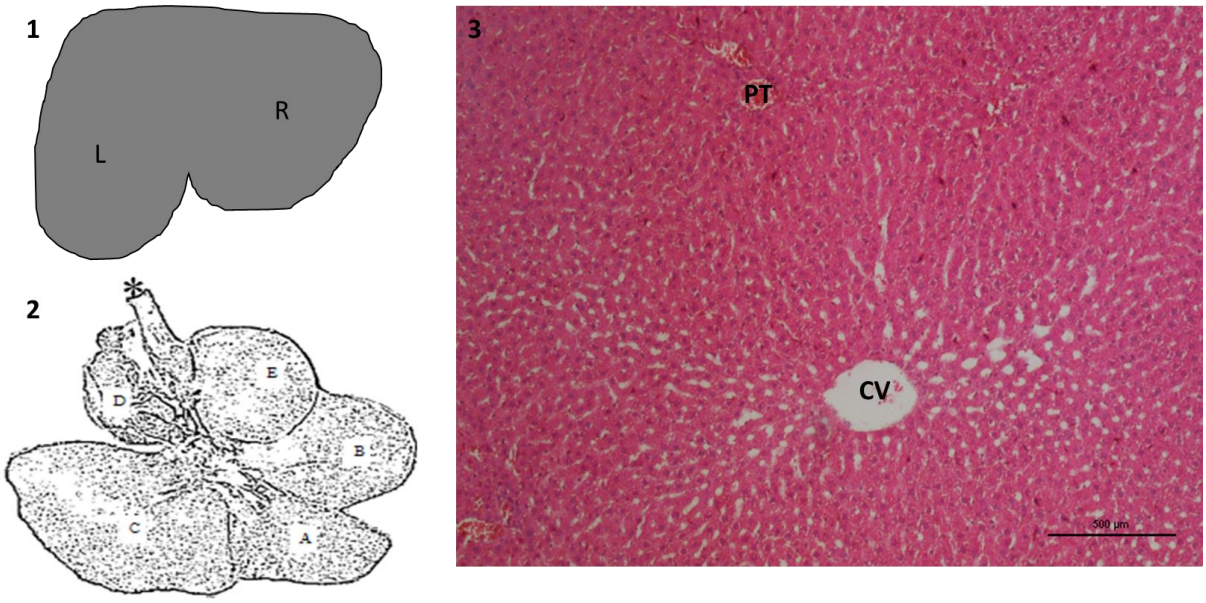

Figure 2.3: Illustration of the liver of humans (1) and rodents (2) and a representative micrograph of the rodent liver (3). The human liver is divided into two anatomical lobes, right (R) and left (L), and two accessory lobes, caudate and quadrate (not shown).The rodent liver lobes may be divided into the (A) median lobe (right and left), (B & E) right lateral lobe, (C) left lateral lobe(largest) and the caudate lobe (D). (* indicates the oesophagus). C) The histology of the liver, with hepatocytes radiating from the central veins with interspersed sinusoids. (CV) central vein, (PT) portal triad. Bar indicates 500µm. (1) Schematic illustration of liver (Netter *et al.*, 2005). (2) Adapted from Baker *et al.*, 1979. (3) Micrography by Jodie Layman.

The liver histologically has various cell types namely, hepatocytes, Kupffer cells, stellate cells and endothelial cells (sinusoidal and biliary) (Malarkey *et al*., 2005; Young *et al.*, 2013; Pellicoro *et al.*, 2014). Hepatocytes make up the parenchymal portion of the liver which accounts for 80% of the liver volume. Furthermore, these cells make up 66% of the total cells within the tissue and are responsibly for metabolism and secretion of various substances (Sherwood, 2013). Hepatocytes are polyhedral shaped cells, with a large central nucleus which may be mono- or bi-nucleated (Gupta, 2000). Kupffer cells are the residing macrophages of the liver located frequently in the periportal regions and the sinusoids (Young *et al.*, 2006). The Space of Disse is located between the sinusoids and the hepatocytes. Specialized cells namely the stellate cells are found in the space of Disse and are the main determinants of fibrogenesis, cirrhosis and regeneration of the liver (Malarkey *et al.*, 2005).

Hepatic lobules are the structural and functional units of the liver. Three arrangements of hepatic lobules exist: classic, portal and acinus (Malarkey *et al.*, 2005). The classical lobule

consists for five to six portal triads surrounding a central terminal hepatic vein. A portal vein, hepatic artery and bile duct form the portal triads, a specialized trio forming the "border" of liver lobules. Portal lobules involve three central veins where the bile canaliculi join into a single bile duct (Malarkey *et al.*, 2005; Kierszenbaum & Tres, 2015). Hepatic physiology and pathology are best described by the third type of hepatic lobule, the hepatic acinus. The hepatic acinus consists of a portal triad and two central veins on either side. The acinus splits this area into three zones: zone one (periportal), two (midzonal) and three (centrilobular) (Malarkey *et al.*, 2005; Young *et al.*, 2006; Kierszenbaum & Tres, 2015).

2.3.2 The effects of obesity on the liver

The current obesity epidemic is associated with increased lipid infiltration in the liver, known as a chronic liver disease namely, Non-alcoholic fatty liver disease (NAFLD). Non-alcoholic fatty liver disease (NAFLD) is the most common liver disease globally with a prevalence of 10-45% (Brunt et al., 2011; Wang *et al.*, 2016). A full spectrum of disease falls under the umbrella term of NAFLD, which includes hepatic steatosis, steatohepatitis, cirrhosis and hepatocellular carcinoma. Atherosclerosis, metabolic syndrome, insulin resistance and T2DM are all associated with NAFLD. As a result of the synergistic effects of metabolic disorders, NAFLD can assist early detection of metabolic disorders in normal mass individuals (Ou *et al.*, 2013). NASH is the more aggressive form of NAFLD associated with metabolic syndrome and obesity which may lead to cirrhosis and hepatocellular carcinoma. NASH is characterized by inflammation, steatosis and progressive fibrosis as well as a decrease in fatty acid oxidation and an increase in lipid oxidation (Choi *et al.*, 2013; Wang *et al.*, 2016).

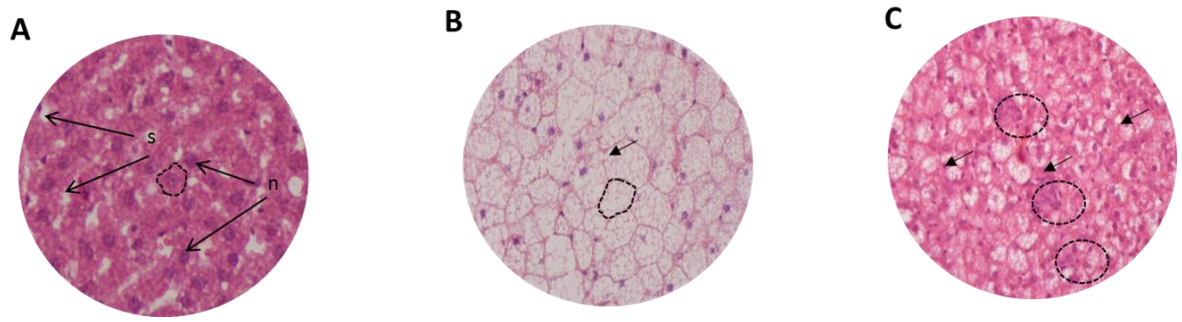

Figure 2.4: Representative micrographs of normal liver (A) and two livers with fatty disease (B & C). In comparison to (A), (B) shows severely ballooned hepatocytes with microvesicular steatosis. (C) shows the presence of inflammatory foci and some microvesicular steatosis. Sinusoids are obscured due to hepatocyte ballooning in both (B) and (C). Black arrows indicate microvesicular steatosis. Dash lines encircle hepatocyte in (A) & (B) and inflammatory foci in (C). Micrography by Jodie Layman.

Hepatic steatosis is closely associated with metabolic syndrome and obesity. High-fat diet induced hepatic steatosis is characterized by a decrease in fatty acid oxidation as well as an increase in lipid oxidation (Choi *et al.*, 2013). Normally, the liver recruits' fatty acids for β-oxidation in the mitochondria of hepatocytes. Additionally, it esterifies fatty acids to glycerol for storage as triglycerides or packages them as very low-, low-or high-density lipoproteins (Brown & Goldstein, 1986). Steatosis occurs upon the imbalance of hepatic lipid intake and synthesis to triglycerides within hepatocytes which is greater than beta-oxidation and export of plasma lipoproteins and results in increased liver mass (Fraulob *et al.*, 2010; He *et al.*, 2010). Lipid infiltration becomes evident as micro- and or macrovesicular steatosis within the tissue. Due to the excess lipid intake, lipid containing vacuoles become present in the hepatocyte cytoplasm (microvesicular) which with the continuation of excessive lipid intake vacuoles increase, enlarge and displace the nucleus (macrovesicular); (Wang *et al.*, 2016). The presence of microvesicular steatosis is not a key pathological marker in NAFLD, although focal regions of microvesicular steatosis associated with macrovesicular steatosis is (Wang *et al.*, 2016). In fatty liver disease, the micro- and macrovesicular vacuoles may narrow and even occlude the hepatic sinusoids (Farrel *et al.*, 2006). The degree of hepatic steatosis is directly correlated with fibrosis and inflammation (Wang *et al.*, 2016). Fibrosis indicates disease progression and is observed in more than 80% of people diagnosed with NASH (Farrel *et al.*, 2006).

Liver pathology associated with obesity usually includes hyperlipidaemia, increased lipid peroxidation and oxidative stress with the reduction of antioxidants and glutathione levels in the liver (Beltran-Debon *et al.*, 2010; Noeman *et al.*, 2011; Park *et al.*, 2012). Park *et al.* (2012)

showed increased triglyceride and total cholesterol infiltration in the liver associated with HFD feeding. The presence of hepatic steatosis in HFD fed rat and mice models is common (Cattapretta *et al.,* 2011; Levene *et al.,* 2011;Schults *et al.,* 2013). In addition, tumour promotion in the liver has been linked to liver inflammation caused by an HFD (Park *et al.,* 2010).

2.4 KIDNEY

2.4.1 Anatomy and histology

The kidneys are two bean shaped organs attached to the posterior body wall responsible for filtering the blood and producing urine. In the rat, the right kidney and its suprarenal gland are located more cranially than the left (Greene, 1955). The rat kidney has one calyx, specialized fornixes of the renal pelvis helps to concentrate urine in the papilla and well-developed renal pyramids. The functional unit of the kidney is the nephron; made up of the renal corpuscle (glomerulus and Bowman's capsule), proximal and distal convoluted tubules, loop of Henle ending in collecting ducts (Young *et al.,* 2006). The kidneys form part of the urinary system which functions to filter fluids from blood and excrete wastes. Specifically, the kidney is responsible for water homeostasis by filtering glucose, sodium and other small molecules (Kierszenbaum & Tres, 2015).

The glomerulus is a lobulated capillary mass within a specialized thin walled capsule lined with squamous epithelium, the Bowman's capsule (Kierszenbaum & Tres, 2015). The capsule has 2 layers a visceral layer in contact with the glomerulus which has podocytes and a parietal layer which covers Bowman's capsule. The space between these layers is known as the renal or urinary space. The proximal convoluted tubule is a characteristic structure in most rodents. It has cuboidal shaped cells lining the lumen of the tubule with large round nuclei (Kierszenbaum & Tres, 2015). The PCT is stained with periodic acid Schiff stain due to is glycogen rich brush border. In contrast to PCTs, distal convoluted tubules (DCT), have larger lumens and more nuclei. As DCTs lack a brush border they are not stained with periodic acid Schiff (PAS).

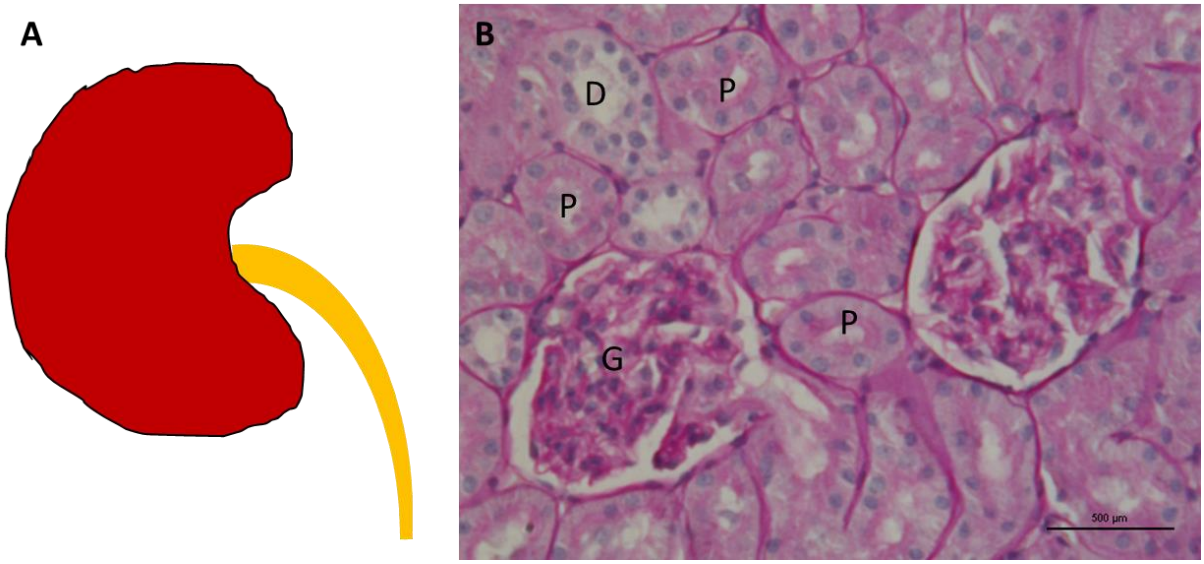

Figure 2.5: Morphology of the kidney (A) and a photomicrograph of the rat kidney cortex (B). (G) Glomerulus, (P) Proximal convoluted tubule, (D) Distal convoluted tubule (40x). Bar represents 500 µm. Micrograph by Jodie Layman.

The kidney is supplied with blood via a single renal artery. Renal arteries split into interlobar arteries which in turn branch into arcuate arteries. The arcuate arteries are found at the corticomedullary junction (the border between the cortex and medulla) (Reddi *et al.*, 2001). Arcuate arteries give rise to interlobular arteries which branch and give rise to afferent arterioles which form the glomerular capillary network (Kierszenbaum & Tres, 2015).

2.4.2 The effects of obesity on the kidney

Chronic obesity has numerous consequences on the structural and functional components of the kidney. Functionally, tubular reabsorption is increased by activation of the sympathetic nervous system and the renin-angiotensin systems leading to a higher blood pressure (obesity related hypertension) (Hall *et al.*, 1998). Hypertension is defined as systolic and diastolic blood pressure greater than 140/90 mmHg. Primary and secondary causes of hypertension are well defined. Primary causes are related to behavioural and lifestyle related choices while secondary hypertension is related to abdominal obesity (Ritchie & Connel, 2007). Activation of the renin-angiotensin (RAAS) system plays an important role in blood pressure regulation and fluid regulation in the kidney (Young *et al.*, 2006). These changes physiologically lead to structural alterations in the arterial system and parts of the kidney.

Structurally, obesity results in increased renal vasodilation, glomerulosclerosis, a greater glomerular surface area, mesangial thickening and podocyte injury (Altunkaynak *et al.,* 2008; Stemmer *et al.,* 2012). Collectively this may be termed obesity-related glomerulopathy and is usually associated with proteinuria (Ekonoyan, 2011; Stemmer *et al.,* 2012). Furthermore, other obesity associated pathologies include increased glomerular filtration rate, renal hypertrophy, glomerulomegaly and increased albuminuria which may lead to renal cell carcinoma (Ekonoyan, 2011). In obese individuals, increased visceral adipose tissue especially around the kidneys causes increased renal pressure. This pressure affects renal tubular absorption especially sodium reabsorption and affects the excretion of sodium in the urine.

Obesity exacerbates the onset and progression of nephropathy and preneoplasia in the kidneys (Stemmer *et al.,* 2012). In diabetic individuals, decreased renal mass is common and is associated with renal disease progression (Tobar *et al.,* 2013). In contrast, Crinigan *et al.* (2015) reported increased renal mass following a short term HFD of six weeks. Similarly, increased renal mass was observed in C57BL/6J mice fed a HFD over a period of 52-weeks (Van Der Heijden *et al.,* 2015). Chronic exposure to a HFD produced pronounced nephropathy in the corticomedullary region of the kidney in male wistar rats which were sensitive or resistant to diet induced obesity for eleven-months (Stemmer *et al.,* 2012). They reported nephropathy which include dilated glomerular blood vessels, proteinaceous casts, thickened basement membranes, interstitial inflammation, shedding and exfoliation of proximal tubular cells in the tubular lumen, hyperplasia, increased cell number and multi-layered tubules as well as glomerulosclerosis and tubule-interstitial fibrosis (Stemmer *et al.,* 2012). Altunkaynak *et al.* (2008) studied the morphometric parameters and structure of kidneys exposed to a HFD. They reported glomerular capillary and blood vessel dilation, glomerular sclerosis, tubule defects, thickened basement membranes and fibrosis (increased connective tissue). They concluded that a significant relationship existed between structural changes in the kidney and fatty diet intake (Altunkaynak *et al.,* 2008). Thus, the effects of a HFD may negatively effect on the structure and function of the kidney.

Although obesity negatively effects the pancreas, liver and kidney, the main cause is increased oxidative stress, inflammation and the inability to maintain homeostasis.

2.5 OXIDATIVE STRESS AND OBESITY

Obesity is associated with oxidative stress and inflammation (Roberts & Sindhu, 2009; Beltran-Debon *et al.,* 2011; Noeman *et al.,* 2011; Favero *et al.,* 2013). Oxidative stress occurs when the production of free radicals overwhelms the endogenous antioxidant systems (Roberts & Sindhu, 2009) resulting in pathology. Oxygen, nitrogen, chlorine and sulphur are sources of free radicals. Reactive oxygen and nitrogen species (ROS and RNS) specifically include superoxide, hydroxyl radical and hydrogen peroxide while RNS include nitric oxide and peroxynitrite radicals (Pizzino *et al.,* 2017).

Physiologically, ROS forms part of many normal processes in the human body (Rahal *et al.,* 2013). Mitochondria are the main cell organelles responsible for the production of ROS as a by-product of normal cellular aerobic metabolism. In the mitochondria, reduction reactions occur which remove electrons from oxygen producing free radicals, oxygen containing molecules with unequal electrons. Production of ROS can be from both exogenous and endogenous sources however ROS is primarily produced by the mitochondrial electron transport chain (Pizzino *et al.,* 2017). Exogenous sources of ROS include ultraviolet radiation, pharmaceutical drugs, pollutants, toxins and foods. Other sources of ROS include xanthine oxidase, NADPH oxidase and eNOS coupling. The production of ROS can be deleterious or beneficial as it forms part of cellular metabolism, cell signalling (Burton & Jauniax, 2011), apoptosis, defence from pathogens as mediators of inflammation (Roberts & Sindhu, 2009) and inducing cell division (Ajuwon *et al.,* 2013). However, excess production of ROS in pathophysiological conditions can result in oxidative stress in the form of degradation of lipids, proteins, cell membranes and nucleic acids (Roberts & Sindhu, 2009; Pizzino *et al.,* 2017).

Pro-oxidants are highly reactive ions or atoms (free radicals) which have an unpaired electron in their outer orbital. These free radicals are unstable and usually react with macromolecules to attempt to complete their outer orbital (Burton & Jauniax, 2011). When binding to macromolecules, they induce oxidation and the production of oxidative species. Antioxidants are endogenous or exogenous molecules which counteract the production and elimination of ROS to reduce oxidative stress (Pizzino *et al.,* 2017). Endogenous antioxidants include the enzymatic molecules superoxide dismutase (SOD), catalase (CAT), and glutathione peroxidase (GPx) (Roberts & Sindhu, 2009; Pizzino *et al.,* 2017). In the event of excessive ROS production, the addition of exogenous antioxidants like vitamin C, E and A, β-carotene, metals

and plant polyphenols can be beneficial (Pizzino *et al.,* 2017). Although, excess antioxidants can also result in oxidative stress, thus the pro-oxidant-antioxidant balance is important.

The complete absence of ROS or the addition of too many antioxidants can result in tissue damage. Pancreatic β-cells are particularly sensitive to oxidative stress as they lack sufficient antioxidant enzymes, specifically GPx and SOD (Abdollahi *et al.,* 2004). Thus, in the event of type two diabetes mellitus or hyperglycaemia β-cells experience significant strain which may lead to reduced β-cells mass. The liver is responsible for detoxification of various substances, thus oxidative imbalance is likely to occur. An oxidant, *tert*-butyl hydroperoxide (*t*-BHP), once metabolized by hepatocytes can result in lipid peroxidation which decreases membrane fluidity and results in damage to nucleic acids (Ajuwon *et al.,* 2013). The kidney is highly susceptible to ROS induced injury, as a result of the high content of polyunsaturated fatty acids which when exposed to ROS, undergo lipid peroxidation (Pizzino *et al.,* 2017).

Plant polyphenols from fruit, vegetables and teas due to their antioxidant rich polyphenol content can be beneficial in conditions associated with oxidative stress (Ajuwon *et al.,* 2013; Rahal *et al.,* 2013; Pizzoni *et al.,* 2017). Globally a surge in metabolic disorders is occurring linked to unhealthy diets. Diets high in fruits and vegetables have shown promising effects against oxidative stress as a result of their antioxidant content (Rahal *et al.,* 2013; Pizzoni *et al.,* 2017). In addition, the use of teas has shown promising effects due to the antioxidant rich polyphenol content they contain (Ajuwon *et al.,* 2013). Aspalathin found in rooibos, contributes 43% of the total antioxidant capacity (Joubert *et al.,* 2005).

2.6 *ASPALATHUS LINEARIS* (ROOIBOS) DISTRIBUTION AND BOTANY

Rooibos, *Aspalathus linearis* (Brum.f.) Dahlgren (family *Fabaceae*; tribe *Crotalariae*) is an indigenous South African plant with more than 270 endemic species. This polymorphic shrub has various wild forms each with their own characteristic morphology and geographical distribution. *A. linearis* is found in the Cederberg wilderness extending into the Citrusdal, Niewoudtville (Beelders *et al.,* 2012) and Clanwilliam regions of the Western Cape (Joubert *et al.,* 2008). Generally, *A. linearis* has bright green coloured needle-like leaves which turn red-brown once they are bruised (Morton, 1983). The leaves have short internodes (Joubert & de Beer, 2011) with “pea-shaped” yellow flowers usually found in clusters (the flowers affect the taste of the tea and are thus removed) on long slender stems (Morton, 1983). As many

morphological adaptations of rooibos exist, rooibos plants may occur in straggling forms less than 30 cm to erect bushes up to 1.35-2 m in height. Figure 2.5 describes two types of rooibos and the forms used in research of its health benefits.

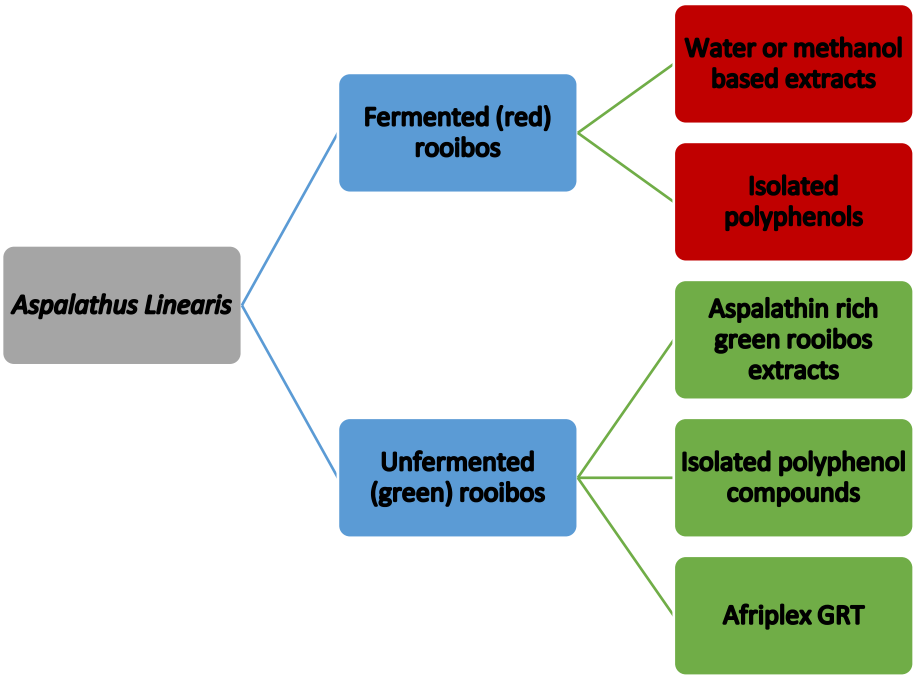

Figure 2.6: The types of Rooibos, *Aspalathus linearis*, fermented and unfermented used in various studies.

2.6.1 Rooibos history and commercialization

Rooibos was first listed as a medicinal African plant by Watt and Breyer-Brandwijk in 1932 however, no applications of the plant were specified. Carl Thunberg, a European Botanist visited the Western cape in 1722 where he observed the Khoi san people using rooibos as a beverage (Joubert *et al.*, 2008). Later, Benjamin Ginsberg, a Russian merchant, also observed the Khoi san harvesting, processing and brewing the plant which he later commercialized in 1904 (Joubert & de Beer, 2011).

During World War II, the early Dutch settlers drank rooibos as an alternative to Oriental (black) tea which was very expensive and unavailable. After World war II, the rooibos market collapsed as more convenient forms of Oriental tea's (tea bags) and inexpensive coffees became available (Joubert *et al.*, 2008). The rooibos industry has since recovered and become a household brand based on its caffeine-free and low-tannin content (Joubert *et al.*, 2008). The popularity of rooibos has increased globally (Marnewick *et al.*, 2011) with increasing consumer

interest in natural antioxidant containing products (Beelders *et al.*, 2012) as well as its pleasant flavour (Joubert & de Beer, 2011).

Initially, the quality of rooibos `was not standardized, thus the composition of polyphenols, and antioxidants reaching consumers was not guaranteed. This prompted the establishing of the Rooibos Tea Control Board to ensure the quality and marketing of the tea (Joubert & de Beer, 2011). The health benefits associated with rooibos have been linked to its phenolic composition (Joubert & de Beer, 2011; Muller *et al*., 2017). Rooibos is believed to have several medicinal and health promoting properties however many of them are yet to be scientifically substantiated (Joubert & de Beer, 2011; Marnewick *et al.*, 2011)

Due to the proposed medicinal effects of rooibos its development into extracts and products has become increasingly popular. The first use of rooibos as a supplement was in the treatment of a one-year old child who suffered from colic. The mother Annique Theron used rooibos to heat the milk and found the condition of the child dramatically improved. (Morton, 1983). This finding resulted in the development of a cosmetic care range (Joubert & de Beer, 2011). Since then, the use of fermented rooibos for extracts and supplements in foods and beverages is well established. In various forms, rooibos is added to beverages, foods, cosmetic products, tablets, and supplements (Joubert & de Beer, 2011). Unfermented rooibos products have now become more common and are available commercially. Freshpak™ has launched its green rooibos variant available in most stores in the Western cape.

2.6.2 Processing *Rooibos*

Rooibos processing originated from the Khoi san people who harvested rooibos by chopping the shoots with an axe, mashing them with a mallet, fermented and sun-dried the bruised fragments in hollows of stones (Joubert *et al.*, 2008). Processing of rooibos has been modernized in terms of the machinery and methods used but the principle remains the same (Joubert & de Beer, 2011). The current processing procedure follows the same sequence beginning with comminution or shredding of the leaves. Thereafter, the leaves are bruised to initiate browning and left to ferment (sweat) and dry out in the open. Tea makers believed sunlight was essential for the development of the characteristic red colour (Joubert, 1996; Joubert & de Beer, 2011). The addition of tea pasteurization was introduced in the 1980's to ensure low microbial activity after a *Salmonella* contamination scare, however, this process may jeopardize the content of essential rooibos flavonoids (Joubert & de Beer, 2011).

General rooibos processing results in the production of the traditional red (fermented) rooibos product. During fermentation, enzymatic and structural changes occur which result in the characteristic red-brown colour and taste as well as a substantial decrease in the phenolic composition (Canda *et al.*, 2014) especially the antioxidant potential (Vilano *et al.*, 2010). Throughout the fermentation process a significant amount of the dihydrochalcone, aspalathin, is lost resulting in only 7% of the original aspalathin content remaining in the fermented rooibos product (Joubert, 1996; Canda *et al.*, 2014). Fermentation, processing techniques and genetic variation all affect the antioxidant (flavonoid) content and phenolic composition of rooibos (Marnewick, 2014).In the 1990's the Agricultural research council (ARC) proposed a new method of processing to produce an unfermented rooibos product, rich in antioxidants (Vilano *et al.*, 2010) especially aspalathin (De Beer *et al.*, 2016) namely unfermented (green) rooibos.

Unfermented (green) rooibos is processed in conditions to maintain the green colour and polyphenol content lost during bruising or traditional processing techniques (Joubert & de Beer, 2011). Unfermented rooibos contains several polyphenols of which aspalathin, nothofagin, Z-2-(β-D-Glucopyranoloxy)-3-phenylpropenoic acid (PPAG), quercetin as well as orientin and iso-orientin all have promising medicinal properties (Muller *et al.*, 2017). A comparison of fermented and unfermented rooibos polyphenol values per 100 g of leaf solids is shown in Table 2.1.

Table 2.1: The mean content of rooibos polyphenols and resultant antioxidant capacity per 100 g of leaf solids of fermented and unfermented rooibos leaves &stems. Adapted from Beelders *et al*. (2012) & Marnewich *et al*. (2014)

Chemical group	Polyphenols	Fermented rooibos* (g/100 g leaf solids)	Unfermented rooibos (g/100 g leaf solids)
Dihydrochalcones	Aspalathin	0.64±0.17	12.4±0.1
	Nothofagin	0.10±0.03	1.7±0.16
Flavones	Orientin,	0.92±0.05	0.81±0.08
	Iso-orientin,	1.3±0.08	1.3±0.16
	Vitexin	0.19±0.02	0.18±0.02
	Iso-vitexin	0.20±0.01	0.23±0.03
Flavanols	Quercetin	0.94±0.16	0.91±0.12
	Iso-quercetin	0.18±0.11	0.24±0.04
	Hyperoside, Rutin	0.26±0.08	0.18±0.04
Phenylpropanoid	Phenylpyruvic acid-2-o-glucoside	0.53±0.10	0.44±0.06
Hydroxycinnamic acid	Ferulic acid	0.09±0.04	Not detected
Total polyphenol capacity# (mg gallic acid equivalents)		**73.43±1.79**	**106.46±2.14**
Total antioxidant capacity$		**1537.60±27.40**	**2093.57±50.20**

* Fermented rooibos based on one cup = 200 mL prepared by steeping one rooibos tea bag in 200 mL fresh boiled water. # Folin-Ciocalteu methods measured against gaelic acid equivalents(GAE).
$ Based on the oxygen radical absorbance capacity (± Standard deviation) of ten samples.

Aspalathin is a cyclic dihydrochalcone C-C glycoside which has only been found in rooibos, more in the unfermented form than the fermented form. During traditional rooibos processing aspalathin is converted to vitexin (Vilano *et al.*, 2010), orientin and iso-orientin via its flavanone analogues (Krafczyk & Glomb, 2008; Krafczyk *et al.*, 2009). A patented method of vacuum-drying has been found to produce green rooibos with a high aspalathin content however at this point it is too expensive to commercialize (Joubert & de Beer, 2011). Other methods proposed to ensure high aspalathin content include a rapid extraction process, low temperatures and pH, as well as the exclusion of oxygen during fermentation to hinder loss of the compound. Several countries, with Japan at the forefront, have produced patents for green rooibos extracts using these methods. Aspalathin is extremely sensitive to heat, oxidation, light and varying pH and thus orientin and iso-orientin are more stable and easier to quantify.

Aspalathin has negligible bioavailability (Joubert & de Beer, 2011); thus, its combination with other rooibos polyphenols may be essential for its efficacy

2.6.3 Bioavailability of *Rooibos* and its extracts

The use of green rooibos extracts and purified isolated polyphenol compounds as commercial products and as treatments in research is dependent on its bioavailability. Absorption, metabolism, excretion and distribution of polyphenols in the gastrointestinal system are influenced by several factors (Manach *et al.,* 2005). These factors specifically affect the ability of rooibos *in vivo*. namely the medium by which the compound is administered *ad libitum* in e.g. in drinking water, mixed in feed, jelly blocks or orally gavage (Muller *et al.,* 2017). The method by which rooibos is administered (*in vitro* or *in vivo*) is essential to its ability to have the required affects. Many *in vitro* studies have published remarkable results which cannot always be reciprocated in *in vivo* studies. Furthermore, the form in which the compound is given for example in water-based extracts, laboratory prepared extract powders or as purified isolated compounds affect its ability to have the required effects (Snijman *et al.,* 2007; Kawano *et al.,* 2009; Perold, 2009; Beltran *et al.,* 2011; Canda *et al.,* 2014).

Many authors agree that the purified polyphenol compounds are effective in various disorders (Snijman *et al.,* 2007; Kawano *et al.,* 2009; Perold, 2009) however the rooibos extract, works synergistically to produce the beneficial effects (Canda *et al.,* 2014). The use of a pure compound may allow easier transport across the intestinal epithelium. Even thou polyphenols may reach the intestinal epithelium intact its interaction with the intestinal microflora may result in its transformation to its metabolites. Thus, the isolation of a single polyphenolic compound may not be as effective as the whole extract (Beltran-Debon *et al.,* 2011; Joubert & de Beer, 2011; Canda *et al.,* 2014; Kamakura *et al.,* 2015).

When rooibos is ingested, its polyphenols are predominantly metabolized in the liver and colon (Vilano *et al.,* 2010).Most rooibos flavonoids may be passed from the small intestine to the large intestine where they interact with the colonic microflora (Kreuz *et al.,* 2008). The interaction with the microflora results in the release of the aglycones of aspalathin and isomers of iso-orientin which may be detected in urine and/or plasma (Muller *et al.,* 2017). The absorption and metabolism of aspalathin has been elaborated on due to the increasing interest in its use in research and health products. As aspalathin does not undergo extensive processing and employs a concentration gradient to traverse the intestinal epithelium by paracellular

means (Courts & Williamson, 2009; Bowles *et al.,* 2017) thereafter it enters the portal venous system (Stalmach *et al.,* 2009).

The absorption of aspalathin has been evaluated in animal and human studies and will be outlined briefly below (Kreuz *et al.,* 2008; Courts & Williamson, 2009; Stalmach *et al.,* 2009; Courts & Williamson, 2015). A study using caco-2 cells model noted that C-glucosyl flavonoids such as aspalathin cross the intestinal epithelium by passive diffusion without metabolism (de-glycosylation) (Kreuz *et al.,* 2008; Courts & Williamson, 2015). The absorption of aspalathin *in vitro* using caco-2 cells in a monolayer showed an improved aspalathin bioavailability when ingested as a green rooibos extract versus an isolated compound (Huang, du Plessis, du Preez, Hamman, & Viljoen, 2008). This places further emphasis on the theory that the synergistic effects of rooibos as an extract and not as individual polyphenols are what make it viable (Muller *et al.,* 2017).

The absorption of aspalathin *in vivo* was first evaluated in pig studies by Kreuz *et al.* (2008). They fed the animals an aspalathin-enriched green rooibos extract and measured the amount of aspalathin in blood and urine after seven and 11 days. They concluded that aspalathin did not require de-glycosylation to be absorbed and detected aspalathin conjugated to methyl, glucuronic acid or both in urine samples but no aspalathin or its metabolites could be detected in plasma (Kreuz *et al.,* 2008). The explanation for the low concentration of aspalathin in plasma samples is as a result of affinity for plasma proteins (Muller *et al.,* 2017) however, aspalathin can be detected in plasma if a large dose of green rooibos is ingested as was the case in a human study (Breiter *et al.,* 2011).

Human studies have also evaluated the bioavailability of green rooibos metabolites found in urine (Stalmach *et al.,* 2009), as well as plasma (Breiter *et al.,* 2011). Stalmach *et al*. (2009) reported that aspalathin metabolites were the major excretory products 0-24 hours after consumption of fermented and unfermented rooibos. The main metabolite excreted after green rooibos ingestion was O-methyl-aspalathin-O-glucuronide, whereas, eriodyctiol-O-glucosides was the main metabolite excreted after fermented rooibos consumption. Aspalathin metabolites can be detected in urine within 5h of consumption whereas fermented rooibos metabolites between 5-12 h. This indicates different sites of absorption; for green rooibos, the small intestine, and fermented rooibos, the large intestine (Muller *et al.,* 2017). Breiter *et al.* (2011), found no significant rise in plasma antioxidant activity after the consumption of unfermented

rooibos (tea or extract form) but trace amounts of unchanged rooibos polyphenols such as aspalathin were detected. The urine analysis identified methylated aspalathin as the major excretory product, with many other forms of aspalathin and nothofagin being detected (Breiter *et al.*, 2011).

2.6.4 The effects of fermented and unfermented *Aspalathus linearis*

The benefits of rooibos can be attributed to the major flavonoids it contains, which have been shown to have several promising effects including: antioxidant (Sanderson *et al.*, 2014; Monsees & Opuwari, 2016), cancer modulating (Marnewick *et al.*, 2009; Joubert & de Beer, 2011; Canda *et al.*, 2014), antimutagenic (Canda *et al.*, 2014; Snijman *et al.*, 2007), anti-histaminic (Morton, 1983), hepatoprotective (Beltran-Debon *et al.*, 2011), immune system modulating (Vilano *et al.*, 2010), anti-inflammatory (Ajuwon *et al.*, 2013; Scholms *et al.*, 2013; Canda *et al.*, 2014), antidiabetic (Muller *et al.*, 2012; Ajuwon *et al.*, 2013), dermatological (Shindo & Kato, 1991), anti-hypouricemic (Najafian *et al.*, 2016), hypoglycaemic effects (Kawano *et al.*, 2009; Beltran-Debon *et al.*, 2011; Mathjis *et al.*, 2014; Kamakura *et al.*, 2015), anti-lipogenic effects (Beltran-Debon *et al.*, 2011; Sanderson *et al.*, 2014), anti-viral and anti-atherosclerotic effects (Canda *et al.*, 2014), and antimicrobial effects (Hübsch *et al.*, 2014). Rooibos has also been said to improve appetite, reduce anxiety, promotes sleep and soothe digestive disorders (Morton, 1983). Anti-obesity effects have previously been shown in vivo (Beltran-Debon *et al.*, 2011) and in vitro (Sanderson *et al.*, 2014). The effects of a high aspalathin green rooibos extract in an obese model has not yet been evaluated. Table 2.2. illustrates a summary of metabolic effects associated with unfermented rooibos and rooibos polyphenols

Table 2.2: The use of unfermented rooibos extracts in various models adapted from (Muller *et al.*, 2017).

Rooibos type/ extract/ infusion	Effect	Model	Finding	Reference
Unfermented and fermented	Anti-carcinogenic	Skin carcinogenic mouse model	Reduced incidence and volume of tumours reduced oxidative stress	Petrova *et al.*, 2009
Unfermented methanol extract	Anti-inflammatory	*In vitro*, COS-1 cells transfected with baboon DNA	Reduced output of steroids compounds (4-fold) and reduced the precursors of aldosterone and cortisol	Scholms *et al*, 2012
Green, aspalathin enriched extract	Anti-diabetic	*In vitro* and *in vivo*, C_2Cl_2 and Chang cells and Wistar rats respectively	Reduction in high blood sugar, increased ability for glucose uptake, inhibited α-glucosidase	Muller *et al*, 2012
Green, aspalathin enriched extract and a fermented extract	Anti-diabetic	*In vitro*, insulin resistant C_2Cl_2 muscle cells	Reverse palmitate induced insulin resistance	Mazibuko *et al*, 2013
Fermented and unfermented rooibos extracts		Male wistar rats standard control diet	Liver mass was significantly increased in 5% unfermented rooibos. No effect on absolute liver and kidney mass or kidney mass expressed as a percentage of body mass. Liver catalase activity significantly improved.	Monsees & Opuwari, 2013
Green rooibos extract	Anti-diabetic	L6 myotubes and RIN-5F pancreatic β-cells and obese diabetic KK-Ay rat model	L6 myotubes: promoted glucose uptake via AMPK and AKT phosphorylation RIN-5F: protected against AGE induced ROS. *In vivo* protected against fasting high blood sugar	Kamakura *et al*, 2015
Fermented and unfermented rooibos extracts		Female wistar rats	Increased serum creatinine, no changes in histology of the liver or kidney.	Monsees & Opuwari, 2017

2.6.4.1 Anti-diabetic effects of rooibos

Standard type 2 diabetes treatment includes metformin and diet control, an alternative strategy is that of green rooibos. Two strategies have been proposed as control strategies for postprandial glucose elevation, one being agents which are able to inhibit α-glucosidase and hydrolases enzymes found in the brush border of the small intestine (Muller et al., 2012). An alternate strategy is the inhibition of glucose reabsorption by glucose transporters in the kidney (Jesus *et al.*, 2017; Sasaki *et al.*, 2018). Muller *et al.* (2012) demonstrated the use of green rooibos as an effective agent to inhibit yeast α-glucosidase. Using HPLC, they determined the extract with the highest inhibitory aspalathin activity and used it in STZ-induced diabetic rats. Their extract showed a sustained and effective lessening effect on blood glucose comparable to that of metformin (Muller *et al.*, 2012). Aspalathin and nothofagin, major polyphenols in green rooibos, have shown the ability to alter glucose reabsorption in the kidney further suggesting a role for green rooibos extracts as antidiabetic compounds (Jesus *et al.*, 2017; Lui *et al.*, 2015).

A rooibos polyphenol of interest in anti-diabetic research is Z-2-(β-D-Glucopyranoloxy)-3-phenylpropenoic acid (PPAG) which has shown anti-diabetic properties. In a HFD- rat model PPAG effectively protected against pancreatic β-cell mass loss as well as β-cell endoplasmic reticulum (ER) stress by increasing anti-apoptotic molecule expression (BCL_2). Furthermore, PPAG prevented hyperglycaemia in obese rats (Mathijs *et al.*, 2014). Another study made use of PPAG in an *in vitro* Chang cell model and in rats fed a high-fat and sucrose/fructose diet. There they showed an improvement in glucose uptake by the cells and increased expression of glucose regulating proteins: glucokinase, glucose transporters (GLUT) 1 & 2, insulin receptors, peroxisome proliferator- activated receptor alpha (PPARα) and suppressor of cytokine signalling (SOCS) in the liver of the rats. In the same study, improved glucose tolerance and fasting glucose concentration were observed (Muller *et al.*, 2013). Lastly, in Balb/c mice exposed to STZ, PPAG effectively protected β-cells from apoptosis and maintained expression of anti-apoptotic molecule BCL-2 (Himpe *et al.*, 2016).

Aspalathin, as an isolated polyphenol compound has been associated with antidiabetic effects in several *in vitro* and *in vivo* models. Its analogues, orientin and iso-orientin have been linked to antidiabetic effects as well as cardioprotective and anti-inflammatory effects. A few authors have reported antidiabetic properties with aspalathin (Kawano *et al.*, 2009; Muller *et al.*, 2012; Son *et al.*, 2013; Mazibuko *et al.*, 2015). One such study was on type-two diabetic mice where

aspalathin was shown to potentially suppresses fasting blood glucose and improve glucose tolerance (Son *et al.*, 2013). A study by Kawano and colleagues (2009) showed increase glucose break-down and insulin secretion in cultured RIN-5F pancreatic β-cells *in vitro* with aspalathin. Similarly, Kamakura *et al.* (2015) made use of an *in vitro* β-cell model and showed that both the use of an aspalathin-enriched green rooibos extract and aspalathin as an isolated compound was effective against cell death and ROS-induced cell dysfunction and suppressed fasting blood glucose in vivo (Kamakura *et al.*, 2015). Iso-orietin has also been associated with anti-diabetic effects such as decreasing high blood sugar (Sezik *et al.*, 2015) and enhancing insulin signalling and genetic expression. Furthermore, orientin was able to improve the blood lipid profile (Sezik *et al.*, 2015) and inflammatory conditions by regulating inflammatory cytokines (Wedler *et al.*, 2014).

Mazibuko *et al.* (2013) showed anti-diabetic effects of fermented and unfermented rooibos in palmitate-induced insulin resistant C_2C1_2 muscle cells *in vitro*. Rooibos effectively resolved the palmitate induced injury and nullified its effects on mitochondrial activity, glucose consumption and cell ATP levels (Mazibuko *et al.*, 2013). In a study of adipocytes (3T3-L1 cells) in combination aspalathin and a green rooibos extract relieved the palmitate induced insulin resistance, suppressed protein expression of nuclear factor kappa beta (NF-κB), adenosine monophosphate (AMP)- activated protein kinase (AMPK), and insulin receptor and increased protein kinase B (AKT). The green rooibos extracts increased protein expression of GLUT4, a glucose channel, and the expression of peroxisome proliferation receptor while the isolated aspalathin increased carnitine palmitoyl transferase 1 (Mazibuko *et al.*, 2015). These effects collectively propose that green rooibos extracts which contain aspalathin may possess hypoglycaemic properties which may reduce the effects of a HFD.

2.6.4.2 Hepatoprotective and Hepatotoxic effects of rooibos

The hepatoprotective effects of rooibos may be related to its effects on liver steatosis. Beltran-Debon *et al*. (2011) showed rooibos effectively protected the liver from lipid retention in the presence of excessive calorie intake induced by a HFD. In the same study, fermented rooibos showed hypolipidemic effects and notable changes in lipid metabolism in rats fed a high-fat diet supplemented with an aqueous rooibos extract (Beltran-Debon *et al.*, 2011). Additionally, they observed decreased hyperlipidaemia with rooibos supplementation in HFD animals however, no significant effects in the control animals. This suggests that rooibos only works in

severely metabolically disturbed conditions (Rodriguez-Sanabria *et al.,* 2010; Beltran-Debon *et al.,* 2011) especially in mice fed a diet mimicking the western diet (Joubert & de Beer, 2011).

Rooibos ameliorated the effects of the HFD on the liver by decreasing the lipid storage and helping to break down the stored fat (Beltran-Debon *et al.,* 2011). Another study similarly reported anti-lipogenic properties using a fermented rooibos extract. They concluded that the addition of fermented rooibos effectively inhibited adipocyte differentiation and metabolism, suggesting its potential as an anti-obesity therapy (Sanderson *et al.,* 2014).

Rooibos may possess additional hepatoprotective effects such as anti-cirrhotic effects reported in a carbon tetrachloride (CCl_4)-rat model of fibrosis (Ulicna *et al.,* 2003). Lee & Bae (2015) showed anti-mutagenic effects of isolated rooibos compounds (aspalathin and nothofagin) in response to lipopolysaccharide (LPS) induced liver injury. Alternatively, Monsees and Opuwari (2016) reported that a 5% unfermented rooibos extract significantly increased liver mass (related to an increase in hypertrophy) but maintained liver architecture (no fibrosis).

In contrast to the above mentioned hepatoprotective affects, three case reports have reported hepatotoxic effects associated with rooibos consumption. All three are associated with excessive or recent introduction of rooibos into the diet thereafter liver related symptoms e.g. raised ALT and AST which lead to the diagnosis (Sinsalo *et al.,* 2010; Engels *et al.,* 2013; Zacharia & Whitlatch, 2013).Therefore, collectively the effects of rooibos on the liver can be protective however, the effects of chronic rooibos consumption should be monitored.

2.6.4.3 Nephroprotective effects of rooibos

To date, limited studies have studied the effect of both fermented and unfermented rooibos on the kidney and even fewer the histomorphometric effects. Nephrotoxicity, hepatotoxicity and oxidative stress caused by tert-butyl hydroperoxide were alleviated by rooibos supplementation in rats (Ajuwon *et al.,* 2013). A 2% and 5% unfermented rooibos extract showed no effect on kidney mass in female rats on a control diet (Monsees & Opuwari, 2016) whereas in male rats a 5% unfermented and fermented rooibos extract respectively, significantly decreased kidney mass relative to body mass (Opuwari & Monsees, 2013). Monsees and Opuwari (2016) reported no histological changes in morphology or structure of the kidney after rooibos exposure however, an increase in creatinine, a marker of kidney function, was present in the fermented treatment group only. In contrast to Monsees and Opuwari, fermented rooibos

protected kidney function in male wistar rats (Ajuwon *et al.*, 2016). A study by Pereira (2017) reported no significant changes in the renal corpuscle or proximal convoluted tubules in male wistar rats supplemented with a 2% fermented rooibos solution. Therefore, the effects of rooibos on the kidney are under reported and as kidney function is paramount to many metabolic disorders establishing the effects of rooibos on the kidney need to be clearly defined.

2.7 RATIONALE AND MOTIVATION OF THE STUDY

Afriplex GRT™ is a unfermented green rooibos laboratory standardized extract that may attenuate obesity related histomorphometric changes due to the polyphenols it contains. This extract contains 12% aspalathin, a polyphenol which has promising effects antidiabetic effects (Kawano *et al.*, 2009; Muller *et al.*, 2012; Son *et al.*, 2013). Orientin and iso-orientin, metabolites of aspalathin, have shown possible antidiabetic effects as well (Sezik *et al.*, 2015). Quercetin, another component of Afriplex GRT™ may have possible anti-obesity effects (Jung *et al.*, 2013; Liu *et al.*, 2015). As the synergistic effects of extracts are believed to make them superior to individual polyphenol compounds (Muller *et al.*, 2017) this green rooibos extract may effectively reduce the effects of a HFD.

A major concern in current research is the use of the term “HFD” which is not clearly defined, reported or delineated. In the literature anything from 30-60% calories from fat (Jang, 2017) can be defined as a HFD which has led to substantial variability in results reported (Buttener *et al.*, 2006). As diet pairings used in animal studies (control and HFD) are essential for producing results which are meaningful, comparable, and can be replicated (Jang, 2017; Pellizon & Ricci, 2018) a few key factors should be considered. The type and source of fat (unsaturated versus polyunsaturated versus saturated), animal strain, phytoestrogen content, and the sugar source (Warden & Fisler, 2008). The sugar source used in animal models is extremely relevant to closely replicate the effcts produced from excesss sugar intake associated with an unhealthy western diet.

Fructose is used commercially as an alternative sugar source to sucrose (Elliot *et al.*, 2002). Sufficient evidence has determined that fructose aggravates body mass gain and may contribute to dyslipidaemia and insulin resistance (Warden & Fisler, 2008; Mathijs *et al.*, 2014). Dietary consumption of fructose has also been associated with a decrease in plasma leptin and post-meal insulin secretion as fructose does not activate pancreatic β-cells. Fructose is preferentially

metabolized to lipids in the liver (Elliot *et al.,* 2002) where it directly and indirectly inhibits free fatty acid oxidation (Schultz *et al.,* 2013). Daily fructose consumption is associated with increased hepatic fibrosis and inflammation (Schultz *et al.,* 2013) and is associated with increased hepatic macrovesicular steatosis and triglycerides (Lee *et al.,* 2015). In the liver, fructose suppresses glucose uptake, which results in increased blood glucose and increased insulin secretion which may be related to insulin resistance (Schultz *et al.,* 2013). As fructose consumption has increased due to the use of fructose corn syrup commercially, a link to obesity and insulin resistance is suggested (Elliot *et al.,* 2002). Therefore, the present study aimed to determine whether a green rooibos extract could effectively ameliorate the histomorphometric effects of a HFD in a rodent model.

CHAPTER THREE:

RESEARCH QUESTIONS,

AIM AND OBJECTIVES

3.1 RESEARCH QUESTION

- Does Afriplex GRT™ have ameliorative histomorphometric effects in diet-induced obese rats and their age matched controls?
- Can Afriplex GRT™ prevent morphological changes and or pathology in the pancreas, liver and kidney of obese rats?

3.2 AIM

To determine the histomorphometric effects of a HFD and a HFD in combination with Afriplex GRT™ on the pancreas, liver and kidney in male Wistar rats.

3.3 OBJECTIVES

I. Routine histomorphological examination of the pancreas, liver and kidney in four study groups namely three control groups control (C), green rooibos control (GRT), high-fat diet control (HFD) and a high-fat diet fed green rooibos supplemented (HFD-GRT) experimental group.

II. Pancreas, to determine;
   a. Pancreatic islet size, number and volume per tissue reference area;
   b. α- and β-cell areas;
   c. Lipid infiltration with Oil red O; and
   d. Evaluate pathology on H&E stained tissue.

III. Liver, to determine:
   a. Volume of steatosis;
   b. Area of steatosis;
   c. Evaluate pathology using the Non-Alcoholic Fatty Liver Disease (NAFLD) Activity Score (NAS); and
   d. Liver structural integrity by studying reticular fibres using Gordon and Sweet's Reticulin impregnation technique.

IV. Kidney, to determine
   a. Morphometric changes on the renal corpuscle, proximal convoluted tubules and arcuate arteries using periodic acid Schiff stain; and
   b. Evaluate pathology using H&E.

3.4 HYPOTHESIS

H_0 Afriplex GRT™ has no ameliorative effects on the histomorphometry of the pancreas, liver and kidney in diet-induced obese rats.

H_1 Afriplex GRT™ has ameliorative effects on the histomorphometry of the pancreas, liver and kidney in diet-induced obese rats.

CHAPTER FOUR:

MATERIALS AND METHODS

4.1 ETHICAL CLEARANCE

Ethical approval was granted for the use of tissue in the present histomorphometric study (SU-ACUD16-00139). The present study used tissue harvested from related studies that were ethically cleared. One study focused on vascular function and liver antioxidant capacity in this HFD-GRT model (SU-ACUD15-00102); (Maqeda, 2018) while another focused on myocardial insulin resistance and mitochondrial function (Kroukamp, 2018); (SU-ACUD 16-00179). Both studies are unpublished masters theses from which the liver, pancreas and kidney samples used in the present study were harvested. The present study conformed to the key principles for humane animal research outlined by Stellenbosch University Research Ethics Committee: Animal Care and Use (REC: ACU). Animal care was guided by the "South African National Standards: The care and use of animals for scientific purposes" (SANS, 10386, 2008) as set out by the South African Bureau of Standards. Animals were monitored for stress, illness or injury daily to ensure their wellbeing.

4.2 ANIMAL HOUSING AND STUDY GROUPS

Male Wistar rats (N=28) of body mass 150 g to 210 g (eight weeks old) were randomly allocated into the following four groups: control (C), green rooibos (GRT) control, high-fat diet (HFD) control and HFD-GRT experimental group (Figure 4.1). Rats were housed in plastic cages, four animals per cage in the Central Animal unit, Faculty of Medicine and Health Science, Stellenbosch University. Animals were kept under a 12-hour light and 12-hour dark cycle, 40% humidity at room temperature (± 23 ˚C).

4.3 ANIMAL FEEDING PROGRAMME

Two feeding programs were used for a period of 16 weeks. The control (C) and GRT groups were fed rodent breeder feed (*Labchef, Nutritionhub,* South Africa), while the HFD and HFD-GRT animals received a diet additionally containing fat, fructose and cholesterol. The composition of the main dietary components is shown in Table 4.1.

Table 4.1: A comparison of the control and high-fat diets treatments, contribution of each food group in the diets fed to the animals for the duration of the study.

Food group	Control diet	High-fat diet
Carbohydrate (%)	51.9	28.8
Protein (%)	25	14.3
Fat g/100 g	4.8	27.9
Fructose g/100 g	-	11
Sucrose g/100 g	6.6	13.3
Cholesterol	-	6.4
Kilojoules/100 g	**1272**	**1829**
Kilocalories	**304.02**	**437.14**

4.4 PREPARATION OF FEEDS AND SUPPLEMENTATION

4.4.1 High-fat diet preparation according to Huisamen *et al.*, 2013

The HFD was prepared by soaking rodent breeder feed pellets (390 g) (*Labchef, Nutritionhub*, South Africa) in a large bowl with boiling water (200 ml) until soft. The additional ingredients were added, which included cholesterol (10 g), fructose (100 g), Holsum™ cooking fat (750 g), Nestle™ sweetened condensed milk (790 g) and casein (100 g). This combination was mixed forming a homogenous product. The mixture was rolled into balls approximately 50 g in weight and refrigerated at -4 º C. One ball was placed into each cage daily.

4.4.2 Afriplex GRT™ supplementation

Animals from the GRT and HFD-GRT groups were supplemented with the Afriplex GRT™ extract, an unfermented *Aspalathus linearis* extract high in aspalathin. The extract and its polyphenolic composition were supplied by the South African Medical Research Council (SA-MRC) (Addendum D). The extract was fed to the animals in the form of jelly blocks since rats have been shown to like sweet tasting foods (Chellan *et al.*, 2008). The animals received a dosage of 60 milligrams per kilogram body mass of the animal per day. This ensured that each animal received a dosage according to their body mass (Addendum D). From week 11 to 16 the GRT and HFD-GRT animals were given one GRT supplemented jelly block, while the control and HFD animals received placebo jelly blocks. To ensure absolute compliance and dose control, a single block of jelly was given daily by hand. This helped to control that all animals received jelly to normalize the dietary sugar content (refer to Figure 4.1).

Jelly blocks were prepared by dissolving 4 g of Moir's™ strawberry jelly and gelatine respectively, in 25 ml of boiling water. The mixture was cooled, followed by the addition of

the Afriplex GRT™ extract powder, at the calculated dosage according to the body mass was added. The mixture was placed on a magnetic stirrer to ensure the jelly and gelatine granules dissolved. A repetitive pipette (Gilson™ Distriman™ Positive displacement repetitive pipette) was used to transfer 1 ml of the mixture into an ice-block container. The jelly was made weekly and kept in sealed containers protected from light and precipitation in a freezer (-4 ºC).

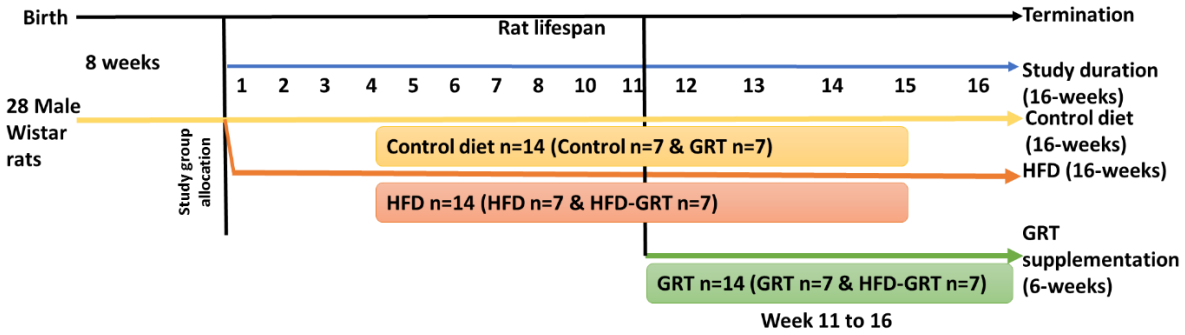

Figure 4.1: Summary of animal lifespan, dietary and Afriplex GRT™ supplementation. Twenty-eight male Wistar rats were allocated to the four study groups; control (C), high-fat diet (HFD), control diet and Afriplex GRT™ supplemented (GRT) and high-fat diet fed and Afriplex GRT™ supplemented (HFD-GRT).

The dosage of Afriplex GRT™ was deduced by reviewing the literature, as no previous study used this exact extract (Muller *et al.*, 2012; Kamakura *et al.*, 2015). Muller and colleagues used an aspalathin-rich green rooibos extract where a 25mg/kg dosage showed a glucose lowering effect while a 30mg/kg extract was more effective at reducing oral glucose tolerance compared to vildagliptin (a dipeptidyl peptidase 4-inhibitor) an antidiabetic drug. Previously, Kamakura *et al*. 2015 similarly showed a decrease in fasting blood glucose with a green rooibos extract (same as Muller *et al.*, 2012) in KK-A^{y} mice, a dosage calculated to be about 250mg/kg/day. Further consultation revealed that primates receive a dosage of 90mg/kg/day which relates to 180mg/kg/day in rats. Therefore, the dosage of 60mg/kg/day was determined as a mid-point between Muller *et al.*, 2012 and the dosage received by primates (Kroukamp, 2018).

4.5 ANIMAL ANAESTHESIA AND TISSUE HARVESTING

At the end of the study period (16-weeks), animals were weighed using an electronic scale. An overdose of sodium pentobarbital (Euthanze©, *Bayer*, South Africa) was administered to each animal (160 milligrams per kilogram body mass, intra-peritoneally) by a researcher authorised by the South African Veterinary Council. Once corneal, pedal and withdrawal reflex were

absent, the thoracic cavity was opened, and the heart removed (death by exsanguination). The pancreas, liver and right kidney were removed, weighed and fixed as detailed in Addendum C.

4.6 HISTOLOGY

4.6.1 Tissue preparation

Tissues allocated for standard histological processing were stored in 10% neutral buffered formalin (NBF) for a period of 36 to 48 hours. Thereafter, organs were placed into labelled plastic embedding cassettes. The tissues were processed in the Shannon Eliot Duplex™ tissue processer (*OptoLaboratory*, South Africa) on a 17-hour cycle according to the protocol in Addendum F. Processed tissue was embedded in paraffin wax using the Leica™ EG 116 embedder (*SMM instruments*, Germany). Blocks were cooled on a cold plate for an hour and kept in the refrigerator for 15 minutes prior to sectioning. Tissues were sectioned using the Lecia™ RM 2125 rotary microtome (*SMM instruments*, Germany). Sections were transferred to a water bath heated to 34 to 37 ºC and placed on standard microscope slides for standard stains or positively charged microscope slides for immunohistochemistry and Oil red O. Slides were placed in the oven to remove wax. After the sections were stained, a cover slip was mounted using distyrene, a plasticizer, and xylene (DPX) mounting media.

The frozen pancreas and liver tissue were removed from storage and kept in liquid nitrogen (-196 ºC). A portion of the pancreas and liver (approximately 10 mm^2) was placed on the tissue mount, covered with tissue freezing media (SHH0026, *Merck*, North America) and set by submersion in liquid nitrogen. The Leica™ CM1850 UV cryostat microtome (*SMM instruments*, Germany) was used to section the tissue. Sections were placed on positively charged microscope slides and kept in the freezer prior to staining. After staining, slides were left to air dry and aqueous mounting media (G 0918, *Merck*, Pty, Ltd) was used to mount the coverslip and stabilized with clear nail varnish.

4.6.2 Tissue staining

Haematoxylin and Eosin stain

To study morphology and diagnose pathology in the pancreas, liver and kidney, the haematoxylin and eosin (H&E) stain was used. Haematoxylin stains the nuclei blue (affinity for acidic structures) and eosin stains the remainder of the tissue pink to red (affinity for basic structures); (Bancroft & Gamble., 2008). The Leica™ Auto-Stainer XL (*SMM instruments*, Germany) was used to stain 5 µm sections of the pancreas, liver and kidney (Addendum G).

The H&E stain was used for histopathological analysis, to determine if special stains were necessary and for histomorphometry.

4.6.3 Pancreas

Double antibody labelling of pancreatic islets

Formalin fixed pancreata were sectioned at 4 µm at three levels, with the three levels 20 and 30 µm apart (serial sections). A manual double antibody staining approach, using anti-glucagon and subsequently anti-insulin antibodies, was used. The tissue was labelled according to the standard operating procedure of the SA-MRC, ICC\B7-V01(Addendum H).

The sections were dewaxed in an oven at 60 ºC for 30 minutes and dehydrated to water. To block for endogenous peroxidases, a 3% hydrogen peroxide (H_2O_2) was prepared in a staining jar, and the slides were placed in the solution for five minutes. To ensure contrast and heightened antibody signal, thorough washing of slides with 0.05 M Tris Buffered Saline (TBS) pH 7.2 was performed between steps. After washing, the area around the sections were dried and traced with a Dako™ pen to ensure even coverage of the small quantities of antibody solution(s).

Thereafter, the pancreata were incubated in a moisture chamber for 20 minutes with a 1:20 dilution of normal goat serum to block for non-specific background staining. The primary antibody, 100 µl polyclonal anti-glucagon (1:50) (A0564, *Dako*, North America, Inc) was applied to the slides in a moisture chamber at room temperature (±25 ºC) for 30 minutes. The washing step was repeated, the area around the sections were dried, and the tissue was incubated with biotinylated rabbit anti-IgG in a moisture chamber for a further 30 minutes. The slides were washed once more, after which they were incubated with Vectastain® Avidin biotin (PK6100, *Vector laboratories*,) complex in a moisture chamber for one-hour to detect biotin molecules. After washing, the area around the section was dried with tissue paper and liquid 3’3-diaminobenzidine (DAB) (K5355. *Dako*, North America, Inc) as well as substrate chromogen solution were added to slides for five minutes. During the DAB staining, the progress was viewed under a standard light microscope to prevent overstaining. The slides were washed with distilled water followed by a 0.05 M TBS washing step to conclude anti-glucagon labelling.

The second labelling procedure using anti insulin was applied to the slides whereby the area around the section was dried and slides placed in a moisture chamber. To block non-specific binding, a 1:20 dilution of normal horse serum was added, and the slides were incubated for 20 minutes at room temperature. Subsequently, a 1:5000 dilution using monoclonal anti-insulin antibody (K5355. *Dako*, North America, Inc) was added, and the slides were incubated overnight (20-24 hours) in a refrigerator at 4 ºC. Following incubation, the slides were brought to room temperature and the Envision™ G/2 double stain system rabbit/mouse kit (K5361. *Dako*, North America, Inc) was used according to manufacturer's instructions to complete the anti-insulin antibody labelling.

This staining procedure labelled insulin secreting β-cells red-pink and glucagon secreting α-cells brown. Internal positive, external and method controls were included to validate the stains and the staining procedure. Control pancreas tissue from the C-group of the present study was used as an internal positive control, kidney tissue from an unrelated study was used as a method control and pancreas tissue from an unrelated study as an external control.

4.6.4 Pancreas and Liver

The following stains were done on both the pancreas and liver tissue to determine the presence of lipid infiltration.

Oil red O stain

Oil red O stains triglycerides, fatty acids and lipoproteins (Mehelm *et al.*, 2013). Frozen pancreas and liver tissue were prepared as detailed in section 4.6.1. The cryostat was used to produce serial sections of the pancreas (n=3) and liver (n=5) at 8 µm and 10-12 µm respectively on positively charged microscope slides. The internal microtome environment was maintained at -15 ºC and -12 ºC, respectively. Tissue was stained within 24-hours of sectioning, and imaged immediately after staining

Slides were incubated in an Oil red O-dextrin solution (01391, *Merck,* North America) and counterstained with a 50% Crystal violet solution (V5265,*Merck*, North America) to create contrast and visualize cellular anatomy (Bancroft & Gamble, 2008); (detailed in Addendum I). Intraperitoneal fat attached to muscle was used as an external positive control and the pancreas and liver tissue of the C-group as the internal control.

4.6.5 Liver

4.6.5.1 Masson's trichrome

Masson's trichrome staining technique is a specialized stain which stains collagen type-1 fibres blue-green (light green solution), nuclei black-purple (haematoxylin) and the tissue parenchyma red-orange (Fuchsin Ponceau Orange G working solution) (Bancroft & Gamble, 2008; Saxena, 2010). This stain was used to detect fibrotic changes in the liver. Tissues were sectioned at 5 µm and placed on standard microscope slides for a manual protocol (Addendum J). Human skin was used as an external control and liver tissue from the C-group as an internal control.

4.6.5.2 Gordon and Sweet's silver impregnation technique (Reticulin stain)

The reticulin technique is based on the nature of reticulin fibres to be argyrophilic and was used to demonstrate the supportive reticulin network in the liver by impregnating fibres black (Saxena, 2010). Disruption of this network may result in reticulin fibres collapsing or forming thickened plates (Singhi *et al.,* 2012). Formalin fixed liver tissue was sectioned at 5 µm and stained according to Addendum K (Bancroft & Gamble, 2008). The C-group acted as an internal control, and human skin was used as an external positive control.

4.6.6 Kidney

4.6.5.3 Periodic acid Schiff stain

Periodic acid Schiff (PAS) is used routinely to determine alterations in the basement membrane of the renal corpuscle and tubules of the kidney. Periodic acid oxidizes the hydroxyl (-OH) group of glycogen, glycoproteins, glycolipids and mucins. The exposed aldehyde groups react with the chromophores in Schiff's reagent to produce a bright purple-magenta colour (Saxena, 2010). Tissue was sectioned at 5 µm, placed on standard microscope slides and stained using a manual protocol detailed in Addendum L. External positive and internal controls were run simultaneously with the staining of the study tissue, namely, rat colon and control tissue from the control study group.

4.7 MORPHOMETRIC TECHNIQUES

Morphometry is the measure of form and is frequently used in histopathology to describe measurements made from two-dimensional tissue sections (Zaitoun *et al.,* 2001). A summary of the morphometric techniques used per organ is illustrated in figure 4.2. Composite images of the entire tissue sections on each slide of the pancreas and kidney were taken using the Nikon

software and camera (Table 4.2). Images of the liver were taken using the Zeiss software and camera (Table 4.2) detailed in the liver morphometry section. Histomorphometric analysis was completed using ImageJ (https://imagej.net/ImageJ), STEPanizer © Stereology Tool, and Zen Lite™ 2012 software packages. Each software package was calibrated using the scale bar indicated on the images.

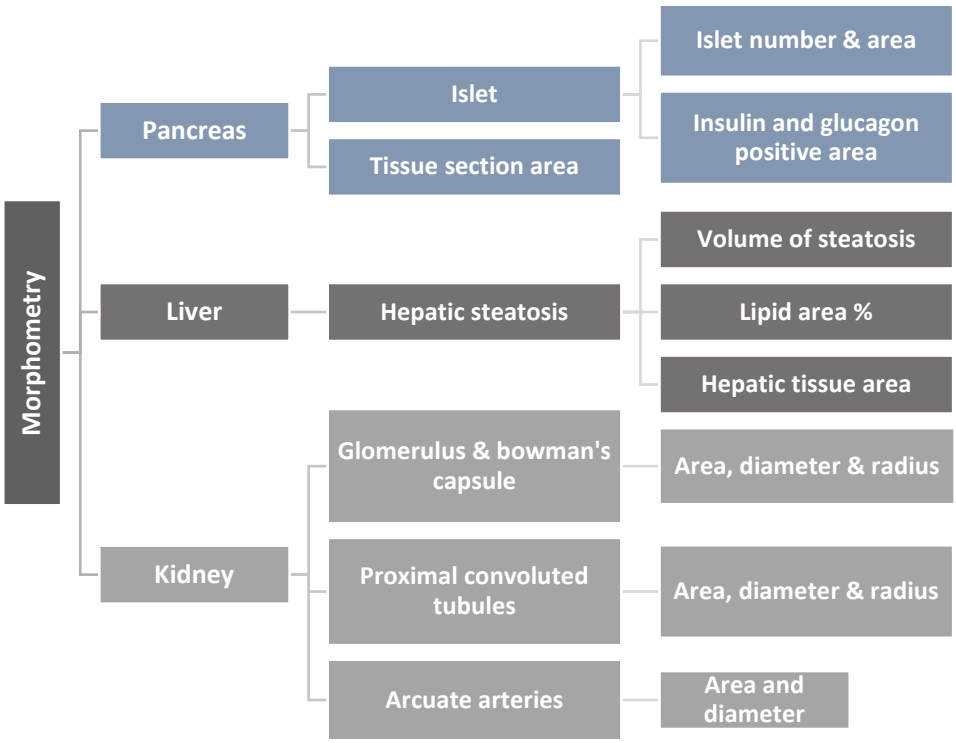

Figure 4.2: A summary of the morphometric measurements performed on the various components of the pancreas, liver and kidney.

Table 4.2: The microscope systems used for scanning, production of micrographs and analysis of the pancreas, liver and kidney.

	Nikon system	**Carl Zeiss system**
Equipment	Nikon Eclipse Ti-S microscope (*Nikon instruments Inc.*, Copyright 1991-2015) - PRIOR ProScan III, Nikon automated tissue scanning software - Nikon NIS Imaging Software version 4.40 - Nikon Digital Sight DS-Fic, *Nikon corporation*, Japan attached camera	Zeiss Axioskop 2 light microscope (801452) (*Carl Zeiss*, AG, Oberkochen, Germany) - Axiovision version 4.7.2.0 software - Zen (2012) blue edition Version 1.1.2.0 - Axiocam 105 (Camera)
Tissue	Pancreas and kidney	Liver

4.7.1 Morphometry of the pancreas

Morphometric analysis of the pancreatic islets, α- and β-cells surface areas was performed on the double antibody labelled sections using methods adapted from Ricculio *et al*. (2004). Each section was scanned at 100x magnification with a 15% overlap per image. The individual images were stitched to form a composite image of the full tissue section to determine section area as a reference point. Furthermore, individual images of the pancreatic islets were used for morphometric analysis.

A basic macro was designed which converted the composite image to a red/green/blue (RGB) stack greyscale image (Addendum M). The tissue section was manually traced, and the tissue selected using the threshold function. ImageJ then automatically determined the section area in μm^2. The section area in μm^2 was converted to mm^2 (Figure 4.3).

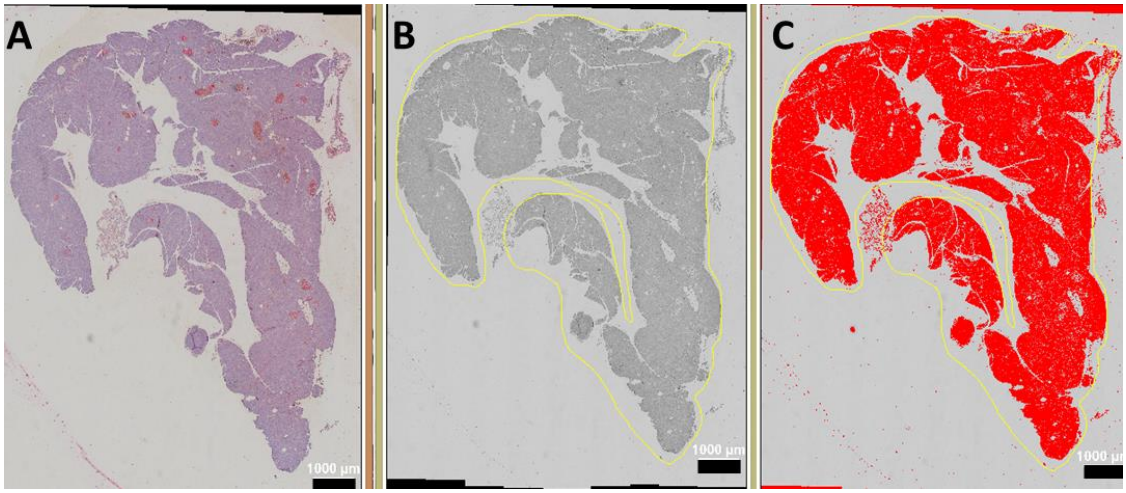

Figure 4.3: Determination of tissue section area in µm^2 as a reference point. (A) Each pancreas was double antibody labelled with anti-glucagon and anti-insulin antibodies and scanned using the Nikon microscope and automated scanning software. (B) Composite images of the entire section area were converted to a red/green/blue stack (greyscale images). (C) The tissue section was manually traced (yellow) excluding blood vessels, peripancreatic fat and lymphoid tissue. The tissue section was selected using the threshold bar (red) and the section area (µm^2) determined by ImageJ. Bar represents 1000 µm.

Immunohistochemistry was used to differentiate the glucagon and insulin secreting hormone cells in the pancreatic islets. The area of the islets, α- and β-cells as well as the percentage of α- and β-cells positive areas were determined in µm^2. The individual images of the pancreatic islets were evaluated and any images in which the full islet was absent, were excluded. The islet circumference was traced to determine total islet surface area (Figure 4.4). The image was converted to an RGB stack, the red filter was selected and the α- and β-cell positive areas were measured individually. The threshold was adjusted for each image to account for changes in staining intensity.

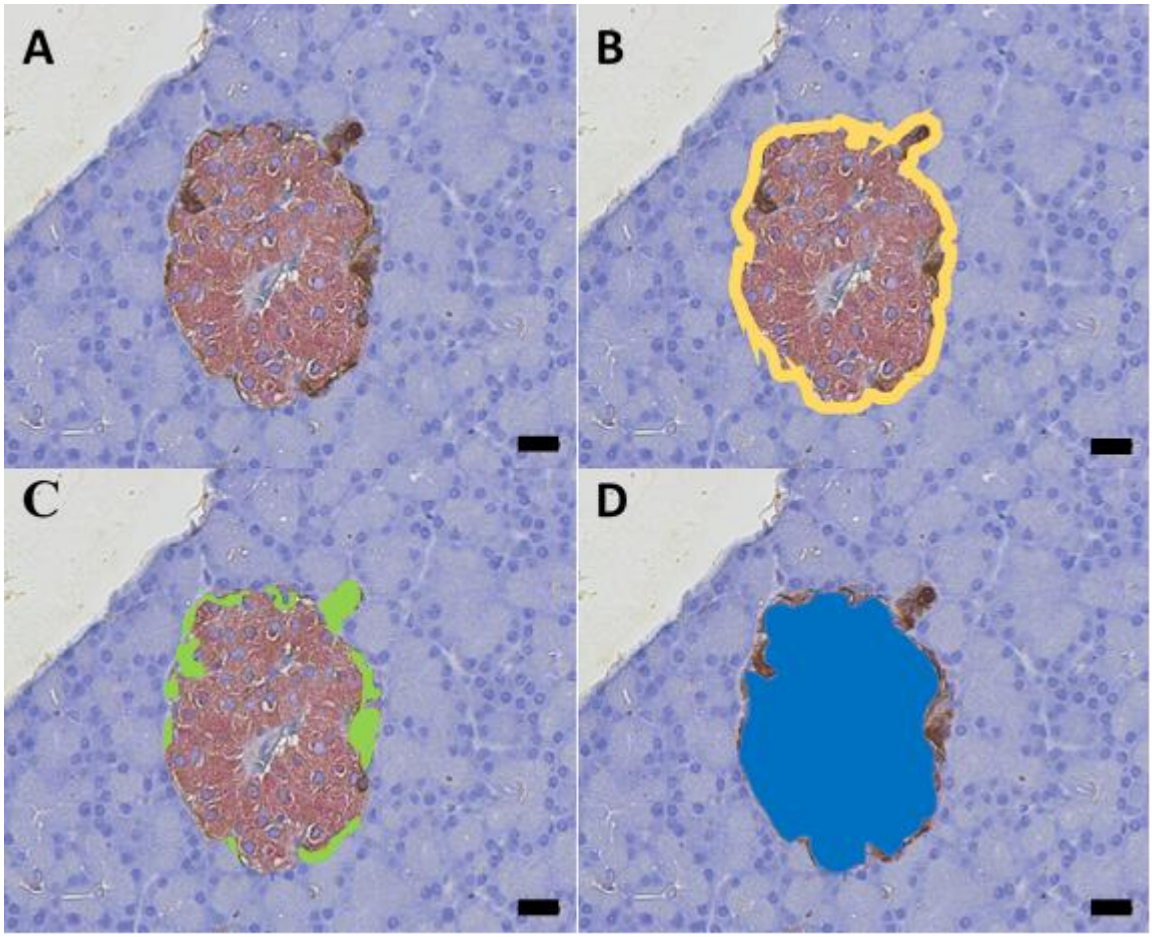

Figure 4.4: Morphometric measurements on the pancreatic islets, α- and β-cells (µm^2). (A) A representative pancreatic islet double antibody labelled with anti-glucagon (brown) and anti-insulin (pink/red). (B) The perimeter of the pancreatic islets was manually traced (yellow). (C) the α- cell area was selected (green) using the threshold bar and area determined (µm^2). (D) The β-cell area was determined by selecting the pink (blue) stained region within the perimeter of each islet (µm^2). Bar represents 20 µm.

A total of 400 islets in each experimental group were compared. For each animal all the islets analysed were organized into a data sheet in Microsoft Excel. Any islets which did not show both α- and β-cells were excluded. The remaining islets were then numbered and using a random number generator, islets were selected based on the number allocated to them. The selected islets were organized into a separate data sheet and means calculated so that statistical analysis could take place.

Islet volume was determined by applying a 1000 µm^2 grid to the composite image (Figure 4.5) and determining the number of points touching islets ($P_{(Islets)}$) versus the points touching the reference area (pancreatic exocrine tissue, $P_{(Reference\ area)}$) (Equation 4.1). The three levels of

tissue (20 and 30 µm apart, section 4.6.3.1) were scanned using the Nikon system and a 1000 µm^2 grid was superimposed over the composite images using ImageJ. The average islet volume per group was determined. This grid size was used to determine the number of islets per 1000 µm^2 to standardize islet number per (1000 µm^2) section area.

$$Vv = P_{(Islet)} - P_{(Reference\ area)}$$

Equation 4.1: The volume of pancreatic islets per total pancreatic section area.

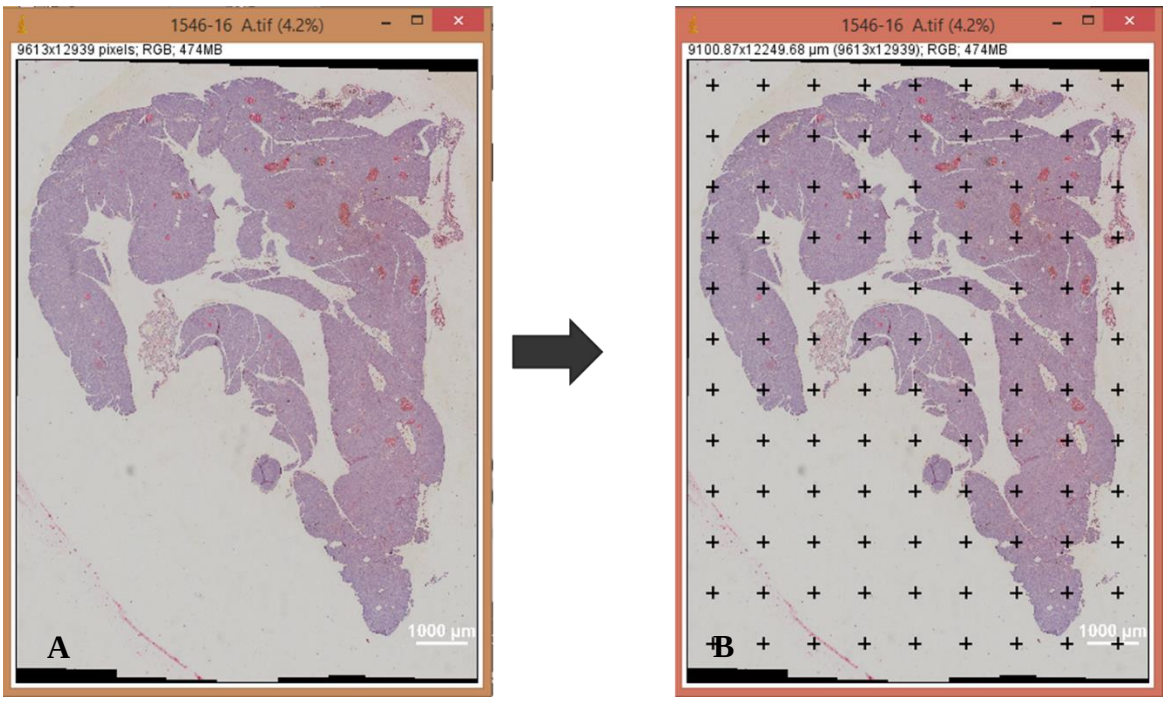

Figure 4.5: Determination of pancreatic islet volume using ImageJ. A 1000 µm^2 grid was superimposed over the composite image (A) and the points touching islets divided by the total number points on the tissue was used to determine islet volume (B).

4.7.2 Morphometry of the Liver

For morphometry, 12 images of both the H&E (200X) and Oil red O stained liver tissue (100X) per animal were captured using the Zeiss system by a blinded observer (Figure 4.6). The images were used to quantify the volume of steatosis using a 36-point grid and area of steatosis by image processing according to methods described by Catta-Pretta *et al*. (2011).

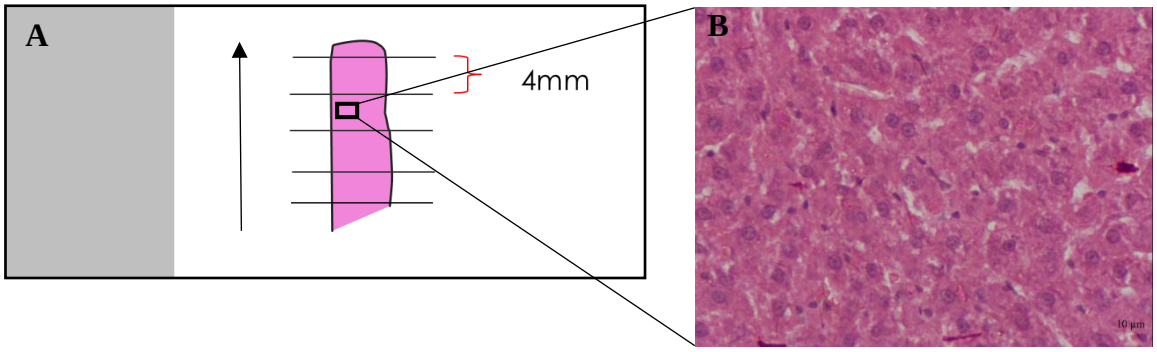

Figure 4.6: Method of image capture. On the left schematic representation of a standard microscope slide with a section of liver tissue (A) (pink). The tissue was divided, into four equal parts on the slide, approximately 4 mm apart using a permanent maker. Three images per part were captured on the H&E (200X) and the Oil red O stained liver tissue (100X). Images were captured systematically in the direction of the arrow (black). An example of a micrograph of control liver tissue stained with H&E is seen on the right (B).

To assess the volume of steatosis, a ratio of points touching lipid vacuoles (P_p) compared to the total number of test points (P_T) was determined (Equation 4.2). A 36-point grid was applied to ten randomly selected H&E and Oil red O micrographs using the STEPanizer © software. A guard area (10 µm^2), to ensure that only hepatocytes shown completely was applied per image. The image was studied from left to right and points touching the white unstained area where lipid deposits were located prior to alcohol processing were counted. The count was collected for all images per animal and transferred to an Excel spreadsheet where Equation 4.2 was applied to determine the volume of steatosis (Figure 4.7).

$$V_v\,(steatosis) = \frac{P_p\,(steatosis)}{P_T}$$

Equation 4.2: Volume of steatosis was determined by dividing the number of points touching lipid vacuoles by the total number of points in the grid (36).

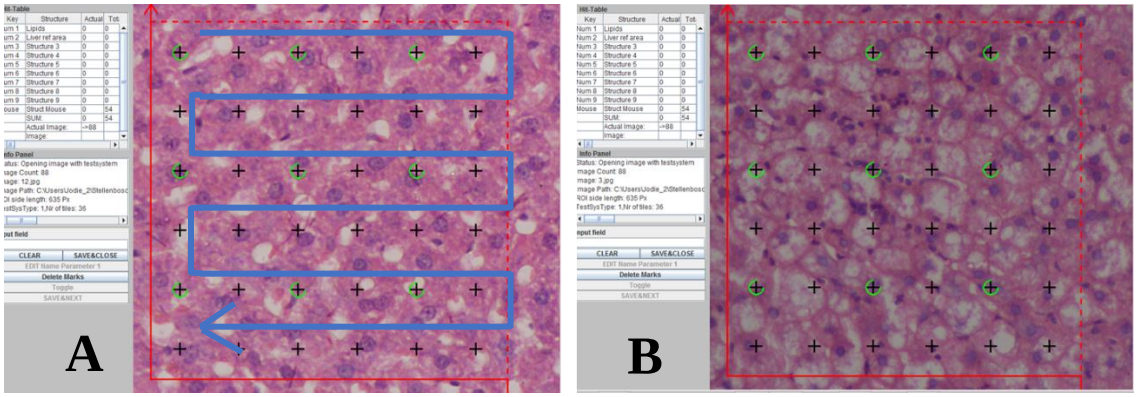

Figure 4.7: Determination of the volume of steatosis. The 36-point grid and guard area (red box) produced using the STEPanizer © software to determine the volume of steatosis in control livers (A) and fatty livers (B). Images were analysed from left to right following the blue arrow illustrated on figure A. Green circles referred to the subsampling area.

To determine the area (μm^2)of lipid deposits, ten images of H&E and Oil red O stained liver tissue from each study group were randomly selected (Figure 4.8 A-H). Each individual image (Figure 4.8 A & E) was converted to a greyscale RGB image (Figure 4.8 B & F) where a threshold was applied to assist selection of the unstained white areas in the micrograph. Subsequently, that image was converted to a black and white binary image (Figure 4.8 C & G) and the hepatic tissue area was determined. The binary image was inverted (Figure 4.8 D & H) to determine area of steatosis. In the control and GRT groups, the white area in the binary image (C) represented the sinusoids and the black area the hepatic tissue. Whereas, in the HFD fed groups the white area represented lipid infiltration and the black area the hepatic tissue.

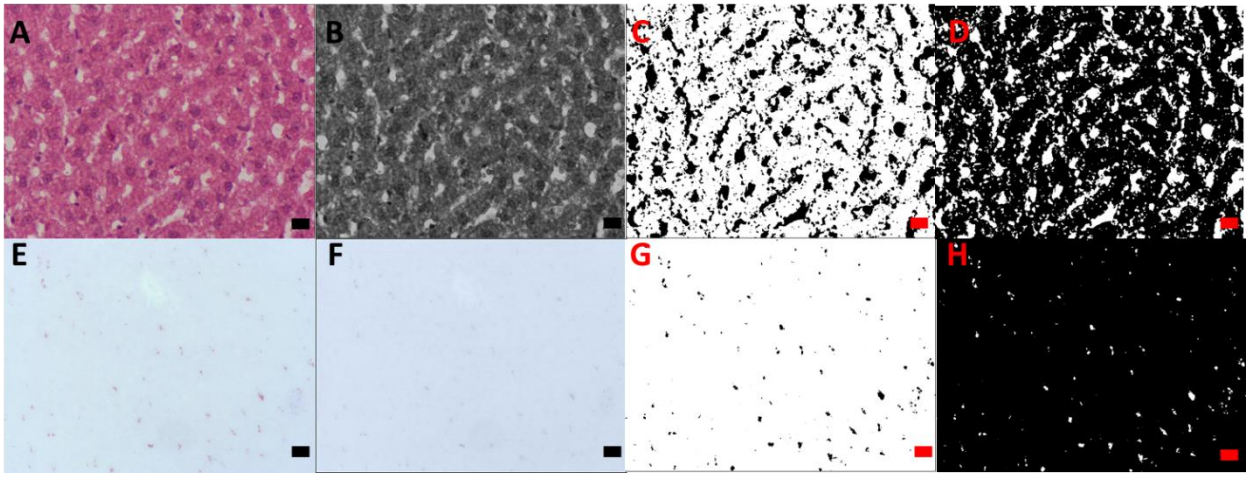

Figure 4.8: Illustration of image transformation to determine the area of hepatic tissue and steatosis in haematoxylin and eosin (A-D) and Oil red O stained tissue (E-H). Individual images (A & E) were first transformed to RGB stacks (B & F) and then converted to binary images (C & G) to measure the tissue area. The binary images were inverted (D & H) to allow the sinusoid area to be measured in control fed animals. In contrast in the HFD fed animals, sinusoids were obscured due to extensive hepatocyte swelling. Thus, the inverted binary images measured steatosis. Bar represents 10 µm.

4.7.3 Morphometry of the Kidney

Morphometric analysis of the kidney was performed on the glomeruli, Bowman's capsule, proximal convoluted tubules (PCT), and arcuate arteries. The full tissue sections of the PAS stained kidney were scanned at 200X using the Nikon software and camera (Table 4.2). Individual images were captured with a 15% overlap and stitched to form a composite image.

The circumference of the glomerulus, Bowman's capsule, inner and outer perimeter of the PCT's were traced (Figure 4.9 A & B). Area, diameter, and radius of the various structures were derived by the Zen lite™ 2012 software. The renal space was determined by subtracting the glomerular area from the Bowman's capsule area. To determine the PCT wall area, the difference between the outer surface area and inner surface area was determined. Similarly, the PCT wall diameter was determined by subtracting the outer surface diameter from the inner surface diameter.

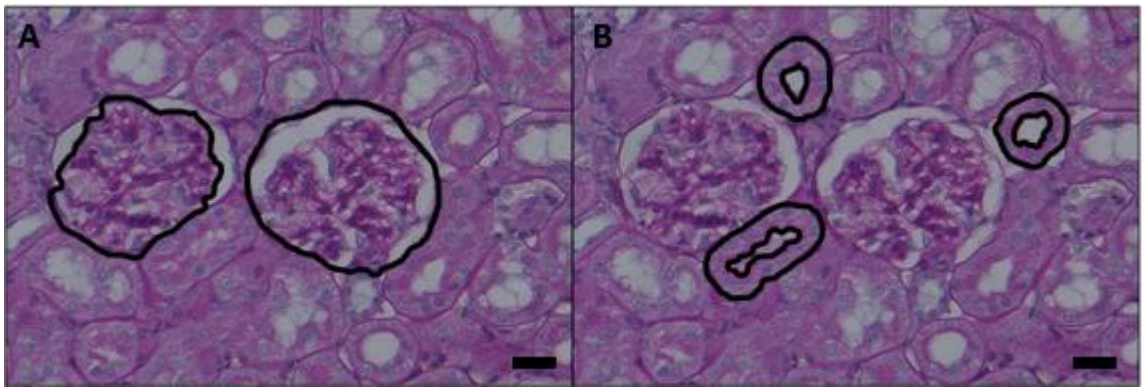

Figure 4.9: Morphometric measurements of the renal corpuscle (Bowman's capsule and glomerulus) and proximal convoluted tubules. (A) The glomerulus and Bowman's capsule perimeters were traced, and the area, diameter and radii determined in μm^2. (B) Three closely related proximal convoluted tubules per glomerulus, inner and outer perimeter were traced to determine the area, diameter and radii determined in μm^2. Bar represents 20 µm.

Additionally, the renal arcuate arteries were analysed using methods adapted from Reddi *et al.* (2001). The circumference of the artery and arterial lumen were traced to determine the outer and luminal areas of the arterial wall. The internal diameter of the artery was measured using two perpendicular lines which crossed the lumen of the artery. The internal diameter was described as the shortest (ID_{short}) and longest (ID_{Long}) distance from one adluminal side of the internal elastic lamina to another crossing the arterial lumen. (Figure 4.10). Equations 4.3, 4.4, 4.5 and 4.6 used to calculate the outer surface area, externa diameter, tunica media thickness and tunica media to lumen ratio.

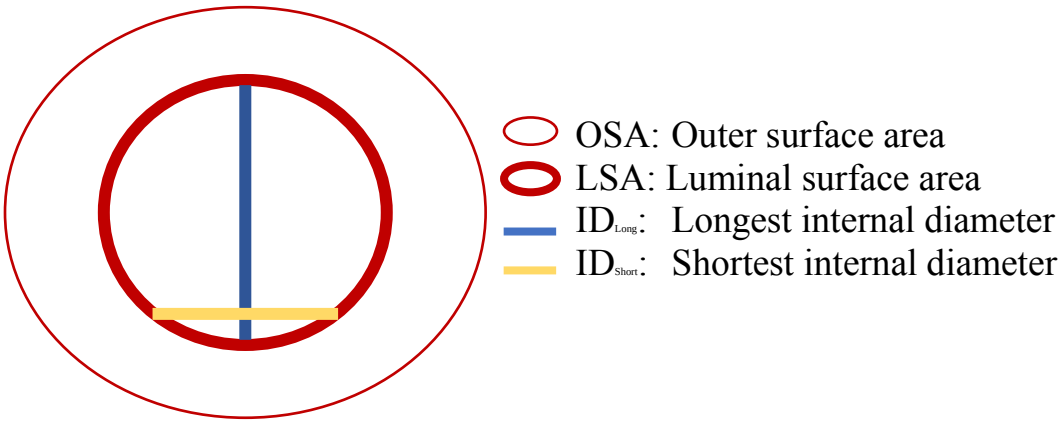

Figure 4.10: Schematic diagram describing the measurements completed on the arcuate arteries. The outer and luminal surface area (red thin and bold circles respectively) as well as the internal diameter short (beige) and long (blue) were determined using the Zen (2012) software. Modified from the description by Reddi *et al*. (2001).

$$OSA = (OSA_{tot} - OSA_{lum}) \times \left(\frac{ID_{short}}{ID_{Long}}\right)$$

Equation 4.3: Outer surface area of the arcuate artery Reddi *et al*. (2001).

$$ED = 2 \times (CSA \times (\frac{\frac{ID_{short}}{ID_{long}}}{\pi})^{\frac{1}{2}}$$

Equation 4.4: External diameter of the arcuate artery Reddi *et al*. (2001).

$$Media\ thickness = \frac{(ED - ID_{short})}{2}$$

Equation 4.5: Tunica media thickness Reddi *et al*. (2001).

$$Media{:}\ lumen\ ratio = \frac{\frac{(ED - ID_{short})}{2}}{ID_{short}}$$

Equation 4.6: Tunica media to lumen ratio of the arcuate artery Reddi *et al*. (2001).

4.8 HISTOPATHOLOGY EVALUATION OF THE PANCREAS LIVER AND KIDNEY

A veterinary histopathologist (Dr. Rick Last, VetDiagnostix) was consulted to confirm the pathology in the pancreas, liver and kidney. The pathologist was blinded to the treatment groups to ensure an unbiased assessment of the tissue was conducted. Table 4.3 describes the pathology evaluated by the veterinary histopathologist

Table 4.3 Pathology evaluated by the veterinary histopathologist of the pancreas, liver and kidney.

Organ	Pancreas	Liver	Kidney
Pathology evaluated	Peripancreatic lymph nodes	Hydropic degeneration	Renal tubular nephrosis
	Mononuclear cell infiltration	Vacuolar degeneration	Oedema
	Oedema	Hepatocyte swelling	Proteinaceous casts
	Congestion	Haematopoiesis	Congestion
		mononuclear cell infiltration	
		sinusoidal dilation	
		Kupffer cell proliferation	
		Central vein duplication & dilation	
		Capillary canal formation	

The non-alcoholic fatty liver disease (NAFLD) Activity Score (NAS) was used to grade and score the liver (Kleiner *et al.*, 2005). This is an accredited system used to assess steatosis, fibrosis, inflammation, hepatocyte changes and provide a diagnostic tissue score. Haematoxylin and eosin sections were used for standard evaluation and Masson's trichrome to assist the evaluation of liver fibrosis.

Five scorers evaluated the entire tissue section per animal using the NAS score. To ensure each scorer scored animals from each of the four study groups the animals were randomly selected based on tissue block numbers. The block numbers were put in a random order, every second number selected and placed into five diverse groups for analysis. Each observer was provided with a grading sheet to accustom themselves with the scoring system one day prior to analysis. Using the grading sheet, each scorer assigned a score for steatosis, fibrosis, inflammation. and hepatocyte injury in the liver tissue (Table 4.4). These scores were used for inter- and intra-observer scores. In addition, the scores were compared to the evaluation given by a veterinary histopathologist. Once analysis was complete, data was organized according to the four study groups and means determined for statistical analysis.

Table 4.4: The non-alcoholic fatty liver disease activity score used to evaluate the liver tissue Adapted from Kleiner *et al.*, 2005.

Category	Detailed explanation per subcategory	Score
Steatosis		
Grade	5%	0
Low to medium evaluation of parenchymal fat involvement	5-33%	1
	>33-66%	2
	>66%	3
Location		
	Zone 3	0
	Zone 1	1
	Azonal	2
	Panacinar	3
Microvesicular steatosis		
Contiguous pattern	Not present	0
	Present	1
Fibrosis stage		
Predominant distribution pattern	None	0
	Perisinusoidal or periportal	1
	Mild, zone 3 perisinusoidal	1A
	moderate zone 3 perisinusoidal	1B
	portal/periportal	1C
	Perisinusoidal and portal/ periportal	2
	Bridging fibrosis	3
	Cirrhosis	4
Inflammation		
Lobular inflammation	No foci	0
	<2 foci per 200x field	1
	2-4 foci per 200x field	2
	>4 foci per 200x field	3
Microgranulomas		
(Macrophage aggregates)	absent	0
	present	1
Large lipogranulomas		
in portal areas or adjacent to central vein	Absent	0
	present	1
Portal inflammation		
in portal areas or adjacent to central vein	none to minimal	0
	greater than minimal	1
Liver cell injury		
Ballooning	None to rare	0
	Few balloon cells	1
	many cells/prominent ballooning	2

4.9 STATISTICAL ANALYSIS

Professor Martin Kidd from the Centre for Statistical Consultation, Department of Statistics and Actuarial Sciences at Stellenbosch University was consulted for statistical analysis. The data was organised in Microsoft Excel spreadsheets blinded according to tissue block number and then organized by study group post analysis. Statistical analysis was performed using the Statistica® version 13.2 software (Dell, 2014, United States of America).

The normality of the data was determined by plotting the values on a theoretical line graph to identify outliers. The slope of the line graph determined whether parametric or non-parametric tests were done. The data was represented as $\log_{10}$ transformations to improve the spread. Data in the present study was parametric.

Descriptive statistics were performed including: mean values, standard deviations, and standard errors calculated with a 95% confidence interval. The mean values were plotted on graphs. One- and two-way analysis of variance (ANOVA) tests were conducted between groups and treatments (diet and Afriplex GRT™, respectively). This test assumes that all means are equal (null hypothesis) and tests the variations between the groups. Statistical significance was confirmed when the null hypothesis was rejected with a p-value of less than 0.05 ($p \leq .05$). To determine the uniformity of variance, a Levene's test was performed by assuming all variances were equal. In contrast, when all variances were not assumed to be equal a Games Howell or weighted-means test was performed.

Lastly, to determine whether any trends were present a Fisher Least Significant Difference (LSD) post-hoc test was performed. The Fisher test indicates trends between variables at $LSD < .05$. Statistical analysis of the histopathology was conducted using two-way tables and Chi square tests.

CHAPTER FIVE:

RESULTS

The following section will provide graphical, descriptive and statistical evidence, on histomorphometrically measurable effects of Afriplex GRT™ and a HFD on the pancreas, liver and kidney in male Wistar rats studied for 16-weeks. Two-way ANOVA tests were used to compare the control diet (C- and GRT) and the HFD diet (HFD and HFD-GRT) fed groups. This helped to determine whether the dietary treatment had a significant effect on the morphometric parameters. In addition, two-way ANOVA tests were performed to compare Afriplex GRT™ treated (GRT and HFD-GRT) and untreated (C- and HFD) groups. This was performed to determine whether Afriplex GRT™ had any ameliorative effects on the histomorphometry of the pancreas liver and kidney.

5.1 THE EFFECT OF TREATMENT ON BODY MASS (BM) AND ORGAN MASS

The Afriplex GRT™ treated (GRT and HFD-GRT) groups had a significantly lower BM compared to the untreated (C- and HFD) groups ($p < .01$). Additionally, The HFD-GRT group showed lower BM than the HFD group (LSD =.021) with a mean decrease of 55 g (Figure 5.1 A) (Addendum O).

Pancreas mass expressed as a percentage of body mass (Figure 5.2 B) was significantly lower in the Afriplex GRT™ treated (GRT and HFD-GRT) groups in comparison to the untreated (C- and HFD) groups ($p = .045$). Furthermore, significantly lower pancreas mass was observed between the C and the HFD-GRT group ($p = .034$); (Addendum O).

Liver mass expressed as a percentage of body mass was significantly lighter in the Afriplex GRT™ treated (GRT and HFD-GRT) groups compared to the untreated (C- and HFD) groups ($p = .033$). Liver mass was significantly heavier in the HFD fed animals (HFD and HFD-GRT groups) compared to the control fed animals (C- and GRT groups); ($p = .033$). All study groups showed significant differences (all $p < .001$) (Figure 5.1 C); (Addendum O).

Kidney mass expressed as a percentage of body mass was significantly lower in the HFD fed animals (HFD and HFD-GRT groups) compared to the control fed animals (C- and GRT groups); ($p = .032$). The HFD and HFD-GRT groups had significantly lower kidney mass in comparison to the C-group ($p = .041$ and $p = .01$ respectively); (Figure 5.1 D); (Addendum O).

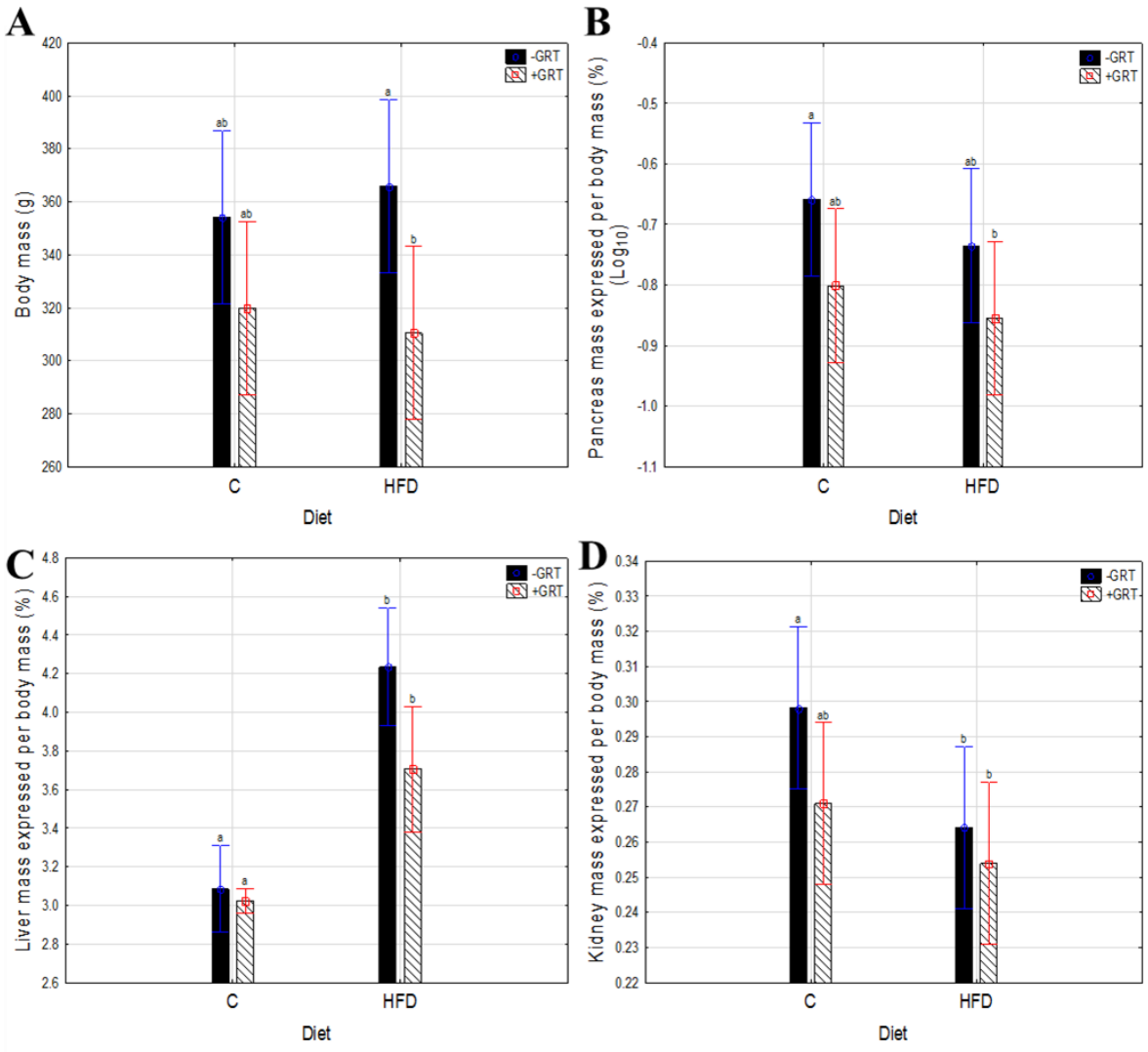

Figure 5.1: Final body mass and organ mass relative to body mass of the four study groups. Pancreas mass was expressed as a logarithmic transformation to make the data statistically normal. Significantly increased body and liver mass was observed in the HFD groups. A significant decrease in body and all three organ masses was seen in the HFD-GRT group. (C) control diet, (HFD) high-fat diet, (GRT) Afriplex GRT™ extract, (+) treated, (-) untreated. n=7 per group. Vertical bars denote 0.95 confidence intervals.

5.2 THE EFFECTS OF TREATMENT ON THE PANCREAS

Micrographs of the pancreatic islets using three staining techniques are shown in Figure 5.2. Pancreatic islets in the present study, were morphologically normal containing majority β-cells located centrally with a mantle of α-cells on the periphery. The exocrine portion of the pancreas, acini similarly showed normal morphology with centroacinar cells with lightly stained lumens and darker stained apical regions containing zymogen granules.

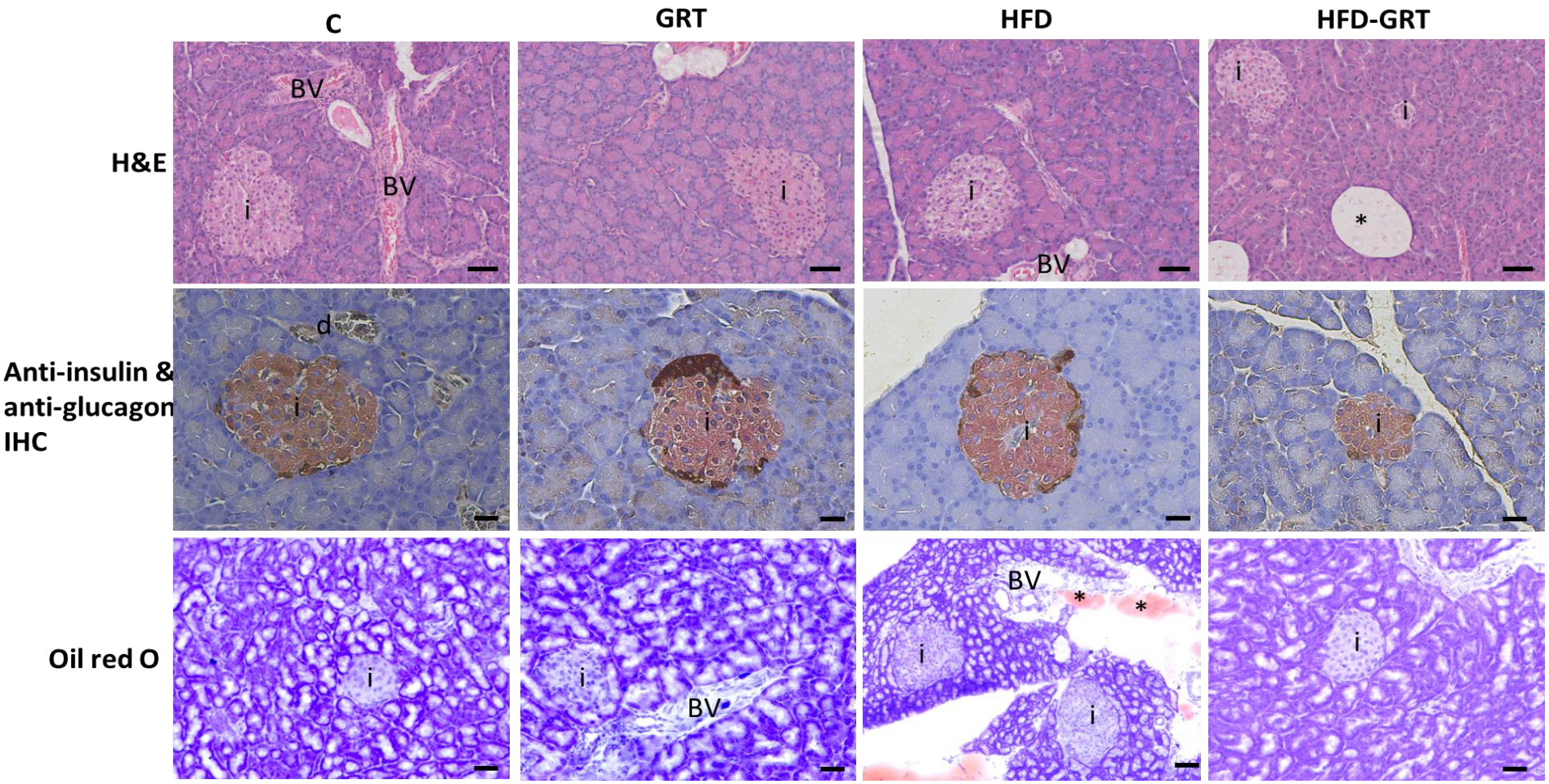

Figure 5.2*:* Histology of the pancreatic islets using three different techniques. Top row: H&E, Middle row: double antibody labelling with anti-glucagon (brown) and anti-insulin (pink) immunohistochemistry (IHC) and Bottom row: Oil red O. demonstrating lipids (red) in the HFD group, very little fat was observed in the HFD groups. H&E 400x magnification, IHC 200x magnification, Oil red O 100x magnification. (GRT) Afriplex GRT™, (HFD) High-fat diet, and (HFD-GRT) High-fat diet Afriplex GRT™ animals. Bar represents 500 µm. (BV) blood vessel, (i) pancreatic islet, (*) lipid droplets, (d) intercalated duct.

5.2.1 The effects of treatment on Pancreatic islets

The number, size and islets per reference tissue area were determined to investigate the effects of treatment on the pancreatic islets. Using absolute values, the total number of islets per study group was: C: 781, HFD: 609, GRT: 754 and HFD-GRT: 808. The size and number of islets per tissue reference area, was not significantly different across groups (Table 5.1). The mean islet size of 400 islets for each experimental group was significantly lower in the HFD fed animals (HFD and HFD-GRT groups) compared to the control fed animals (C- and GRT groups); ($p = .011$). Furthermore, the C- ($p = .076$), GRT ($p = .046$) and HFD ($p = .053$) groups had significantly larger islets than the HFD-GRT group (Figure 5.3).

Table 5.1: Pancreatic islets expressed per reference tissue area. No significant differences were observed across groups. Data is expressed as mean ± standard error of the mean (SEM).

	C	GRT	HFD	HFD-GRT
Islets area (µm^2) per tissue section area (µm^2) (%)	0.019±0.004	0.053±0.028	0.038±0.013	0.024±0.004
Islet number per tissue section area in mm^2	0.85±0.11	1.29±0.18	1.40±0.11	1.91±0.75

(C) control animals, (GRT), Afriplex GRT™ animals, (HFD) High-fat diet animals and (HFD-GRT) High-fat diet Afriplex GRT™ animals.

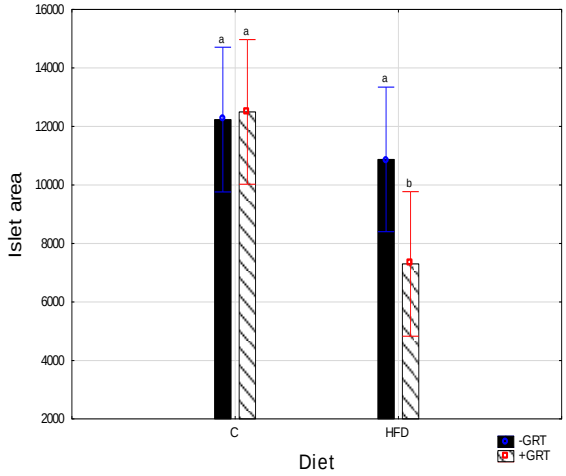

Figure 5.3: Pancreatic islet size. Mean islet area (µm^2).Islet area was significantly reduced in the HFD-GRT group in comparison to the C-group. (C) control diet, (HFD) high-fat diet, (GRT) Afriplex GRT™ extract, (+) treated, (-) untreated. n=7 per group. Vertical bars denote 0.95 confidence intervals.

The volume of islets per 1000 µm^2 of pancreatic tissue was not significantly different in dietary and Afriplex GRT™ treatments or across the study groups. (Figure 5.4 A & B). Level two had significantly more islets than level one and three. The HFD group (level two) had significantly more islets than the other study groups (across levels) (Figure 5.4 B).

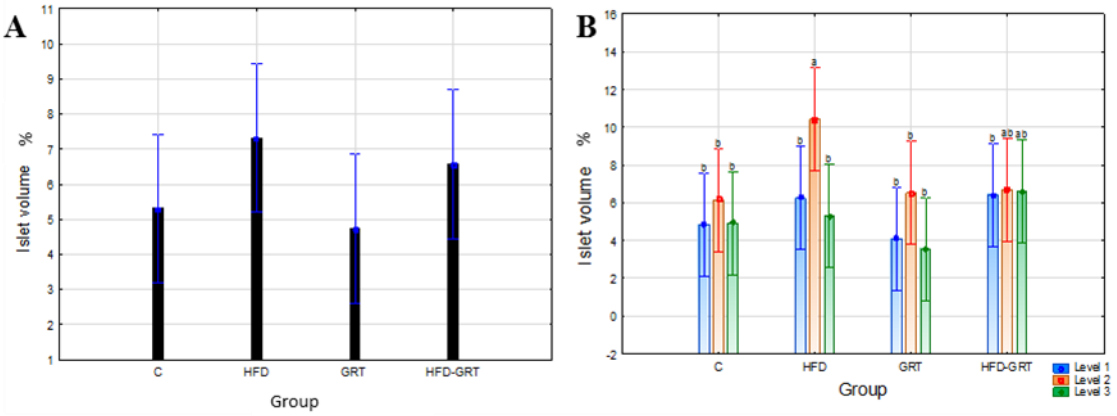

Figure 5.4: Pancreatic islet volume. Islet volume did not differ significantly across groups. Significantly more islets were present in the HFD group level 2 in comparison to many of the other groups however this could be related to the amount of tissue area. "Levels " refer to tissue section one, two and three (Section 4.6.3). (C) control diet, (HFD) high-fat diet, (GRT) Afriplex GRT™ extract, (+) treated, (-) untreated. n=7 per group. Vertical bars denote 0.95 confidence intervals.

5.2.2 Pancreatic islet α-cells and β-cell area

The α-cells were not significantly different across the four experimental study groups. The percentage of α- and β-cells did not differ across groups either. When α- and β-cells areas were expressed as a percentage of islet area no significant differences were observed. Lastly, α-cells were expressed as a percentage of β-cells, no differences were seen between groups (Table 5.2).

Table 5.2: Pancreatic islet α- and β-cells areas. No significant differences were found when comparing groups or treatments. Data is expressed as mean ± standard error of the mean (SEM).

Area (μm^2)	C	GRT	HFD	HFD-GRT
α-cells	1031.28±140.87	877.39±222.68	1102.43±142.87	648.44±107.39
Percentage of α-cells	12.83±1.21	12.84±1.22	13.52±1.46	15.69±1.55
Percentage of β-cells	72.91±3.82	69.72±2.34	74.81±1.51	69.47±3.72
Percentage of α-cells per islet area	8.58±0.67	8.59±1.32	8.23±1.22	9.22±1.05
Percentage of β-cells per islet area	52.83±3.07	49.87±3.05	52.64±2.35	46.23±4.00
Percentage of α-cells per β-cells	16.43±1.51	17.19±3.09	17.21±3.13	20.53±2.46

(C) control animals, (GRT), Afriplex GRT™ treated animals, (HFD) High-fat diet fed animals and (HFD-GRT) High-fat diet Afriplex GRT™ treated animals.

Pancreatic β-cells area (μm^2) was significantly decreased in the HFD-GRT group in comparison to the C- ($p = .008$) and GRT groups ($p = .009$); (Figure 5.5). In addition, the area of β-cells was significantly reduced in the HFD fed groups (HFD and HFD-GRT) compared to the control fed groups (C- and GRT) ($p = .01$).

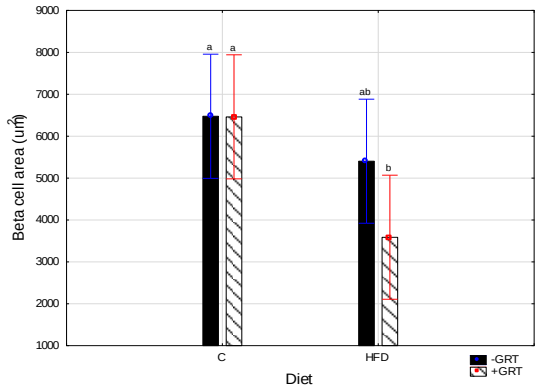

Figure 5.4: Pancreatic islets β-cells area of 400 Islets per group. β-cells area was significantly decreased in the HFD-GRT in comparison to the C- and GRT groups. (C) control diet, (HFD) high-fat diet, (GRT) Afriplex GRT™ extract, (+) treated, (-) untreated. n=7 per group. Vertical bars denote 0.95 confidence intervals.

5.3 THE EFFECT OF TREATMENT ON THE MORPHOMETRY OF THE LIVER

5.3.1 Volume of steatosis

When analysing the H&E stained livers, the mean volume of steatosis was significantly lower in the Afriplex GRT™ treated groups (GRT and HFD-GRT) in comparison to the untreated groups (C- and HFD) ($p = .02$). The HFD fed groups (HFD and HFD-GRT) had significantly more steatosis than the C-group (both $p < .001$) (Figure 5.5 A). A decreased volume of steatosis in the GRT compared to the HFD-GRT groups was observed (both $p < .001$). Analysis of the Oil red O stained tissue showed a significant increase in steatosis in the HFD and HFD-GRT groups compared to the C- and GRT groups ($p = .04$);(Figure 5.5 B). However, the addition of Afriplex GRT™ did not significantly reduce steatosis in the HFD-GRT group.

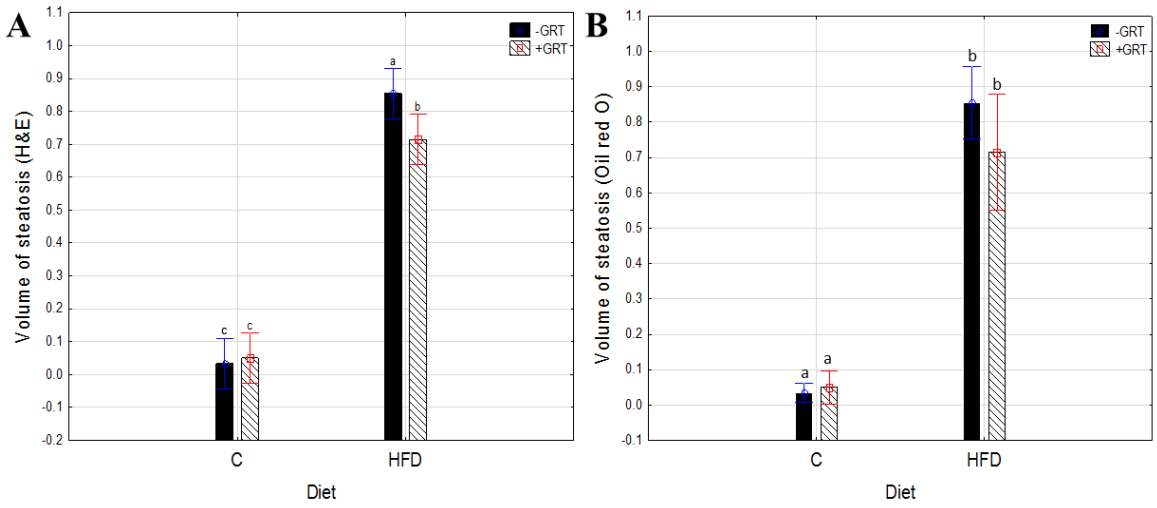

Figure 5.5: Volume of steatosis on the H&E (n=7 per group) (A) and Oil red O (n=5 per group) stained liver tissue (B). (C) control diet, (HFD) high-fat diet, (GRT) Afriplex GRT™ extract, (+) treated, (-) untreated. Vertical bars denote 0.95 confidence intervals.

5.3.2 Image processing

Image processing was used to determine the area of steatosis (converted to a percentage). In the H&E stained tissue steatosis was significantly higher in the HFD fed groups (HFD and HFD-GRT groups) in comparison to the control diet fed groups (C- and GRT groups); ($p < .01$). (Figure 5.6 A & Figure 5.7). The resultant hepatic tissue area was significantly reduced in the HFD and HFD-GRT groups in comparison to the C- and GRT groups ($p = .029$). Hepatic tissue was significantly lower in the HFD-GRT group in comparison to the C-group ($p = .045$) (Figure5.6 B & Figure 5.7).

The Oil red O tissue showed significantly less lipid deposits in the Afriplex GRT™ treated groups (GRT and HFD-GRT) in comparison to the untreated groups (C- and HFD); (p = .037). In contrast, significantly more lipid deposits were observed in the HFD fed groups (HFD and HFD-GRT) in comparison to the control fed groups (C- and GRT); (p < .001); (Figure 5.6 C & Figure 5.7). Hepatic tissue area was significantly lower in the HFD fed groups (HFD and HFD-GRT) in comparison to the control fed groups (C- and GRT); (p < .001); (Figure 5.6 D & Figure 5.7). The Afriplex GRT™ treated groups (GRT and HFD-GRT) showed significantly increased tissue area than the untreated groups (C- and HFD); (p = .038).

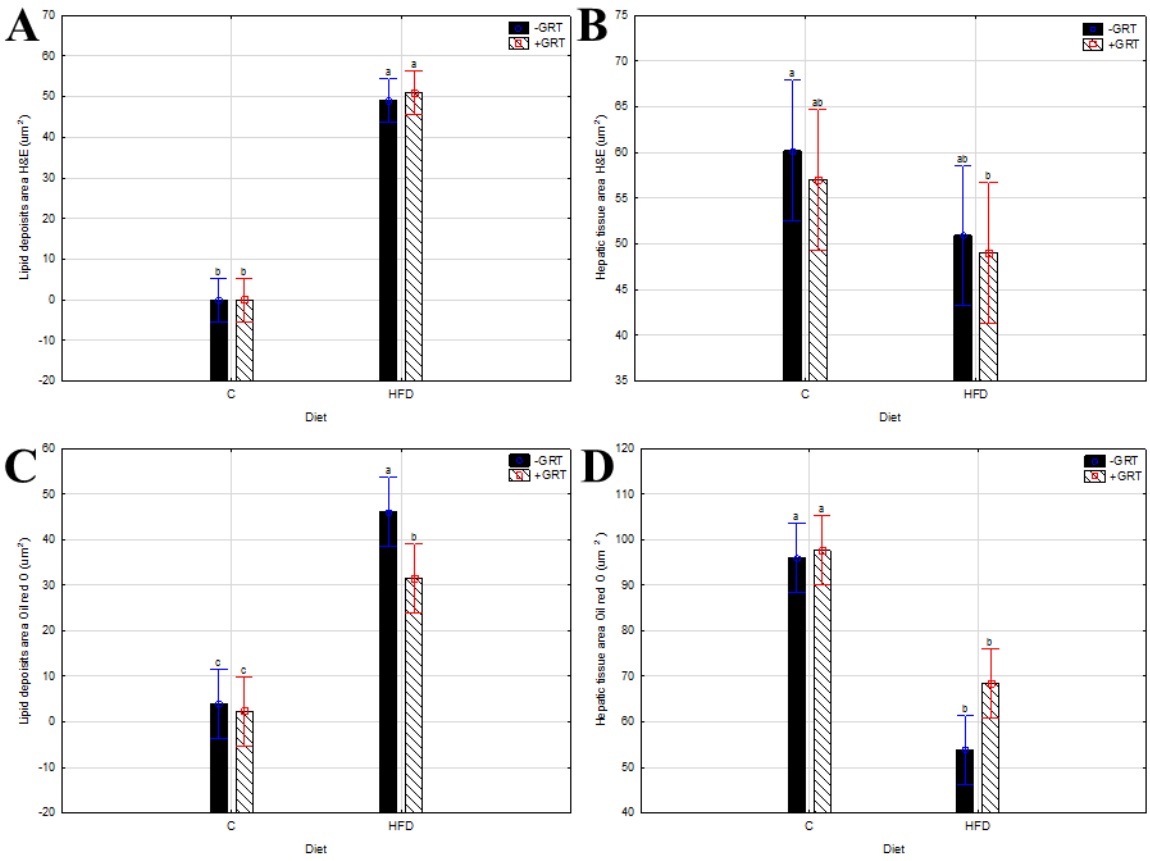

Figure 5.6: Area of lipid deposits (A & C) and hepatic tissue (B & D) area in the H&E (n=7 per group) and Oil red O (n=5 per group) stained tissue. Two-way ANOVA, Games Howell post-hoc test. (C) control diet, (HFD) high-fat diet, (GRT) Afriplex GRT™ extract, (+) treated, (-) untreated. n=7 per group. Vertical bars denote 0.95 confidence intervals.

Micrographs histologically showing the differences between the groups are indicated in figure 5.7.

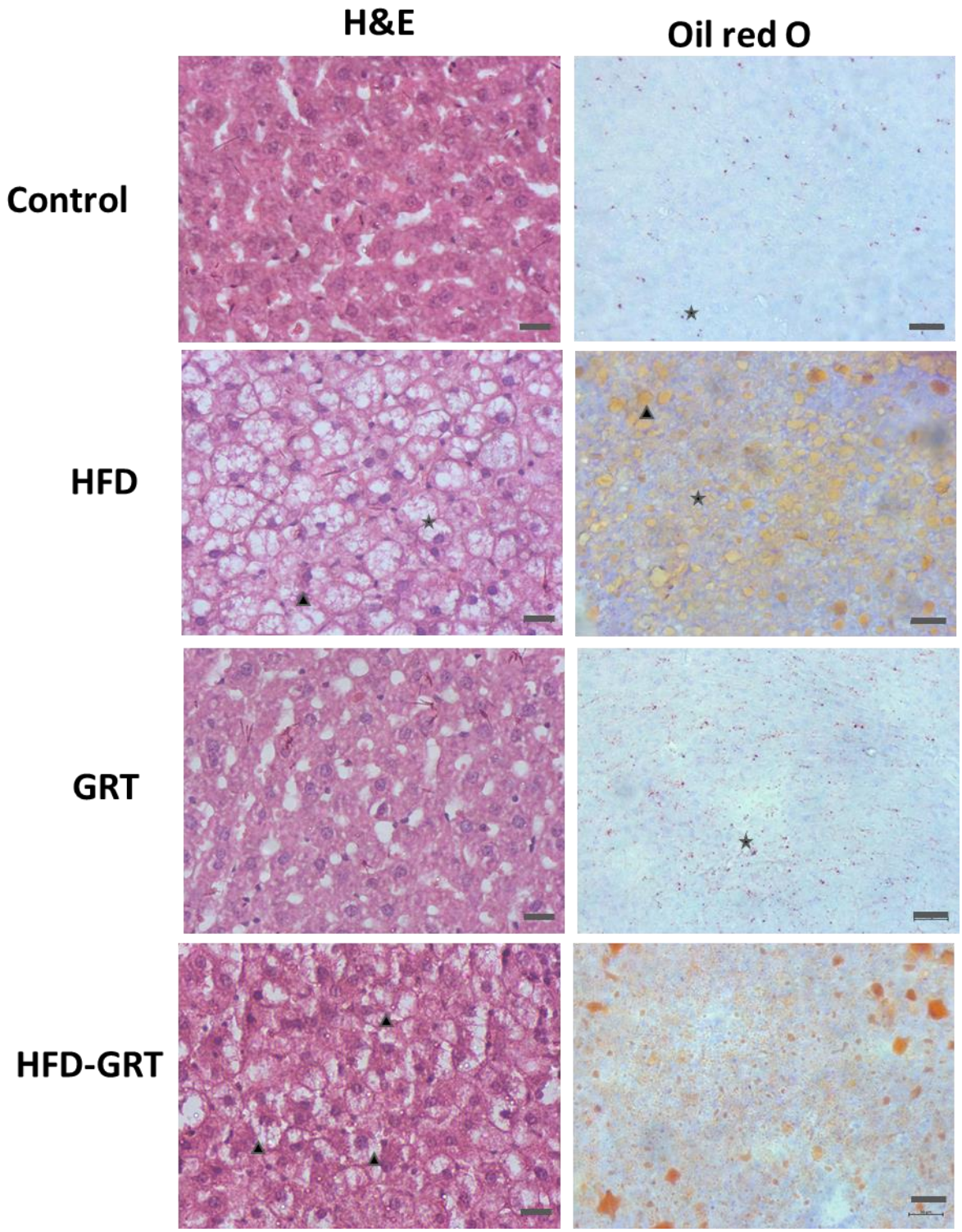

Figure 5.7: Liver tissue stained with H&E and Oil red O for morphometric measurements. C- and GRT group show normal morphology (H&E) with fatty deposits of less than 5%of the tissue. The HFD and HFD-GRT groups show fatty infiltration in both groups with the HFD group having ballooned hepatocytes (star) as well as micro (arrow head) and macrovesicular steatosis (star). H&E 200x (Bar= 50µm), and oil red O stain 100x magnification (bar=100µm). (C) control, (GRT), Afriplex GRT™, (HFD) High-fat diet and (HFD-GRT) High-fat diet Afriplex GRT™ animals.

5.4 THE EFFECTS OF TREATMENT ON THE KIDNEY

Kidney glomeruli and Bowman's capsule size (μm^2), proximal convoluted tubules and arcuate artery area, diameter and radius were determined for the various parameters measured. No significant differences were observed in the diameter and radii of the various structures measured (Addendum O, Table 20). Figure 5.8. illustrates the kidney glomeruli, Bowman's capsules, and proximal convoluted tubules of the four study groups stained with H&E and periodic acid Schiff (PAS) stain. No distinct difference in renal corpuscle or PCT morphology was present between the four study groups.

5.4.1 Glomeruli and Bowman's capsule morphometry

The size of the glomerulus and Bowman's capsule was not significantly different across groups (Table 5.3). By subtracting the Bowman's capsule and glomerular areas the renal space was determined. The HFD-GRT group showed a trend of smaller renal spaces in comparison to the C-group (LSD =.048) however, no statistically significant differences were observed.

Table 5.3: Size and diameter (μm²) of the glomerulus, Bowman's capsule and renal space. The renal space was smaller in the HFD-GRT group in comparison to the C-group (trend) however no significant differences were found in the size of glomeruli, Bowman's capsule or renal space. Mean ± Standard error of the mean (SEM).

	C	GRT	HFD	HFD-GRT
Glomeruli				
Area (μm²)	7749.39±605.65	7272.31±658.53	7196.69±871.90	6303.47±571.61
Diameter	97.818±3.879	94.303±4.338	92.683±6.789	87.568±4.094
Bowman's capsule				
Area (μm²)	10661.39±1415.71	8996.26±993.57	8848.55±1112.01	7610.39±744.40
Diameter	114.03±7.57	104.15±6.60	102.39±8.12	96.07±4.82
Renal space				
Area (μm²)	**2912.01±906.95^{a}**	1723.95±414.53^{ab}	1762.78±331.06^{ab}	**1318.14±277.68^{b}**

Differing letters indicate significant differences, letters that are shared indicate no significant difference. (C) control, (GRT), Afriplex GRT™, (HFD) High-fat diet and (HFD-GRT) High-fat diet Afriplex GRT™ animals.

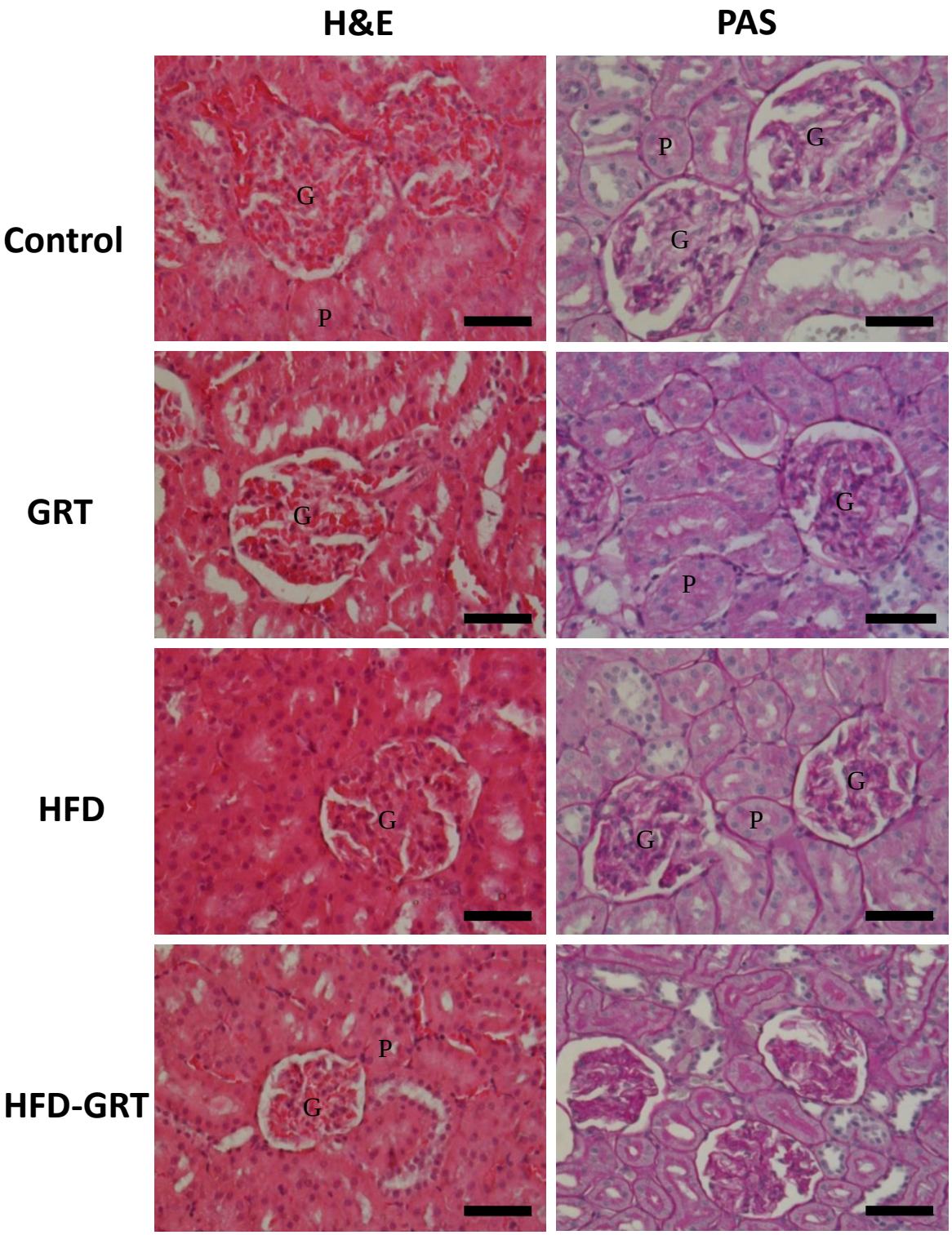

Figure 5.8: Kidney was stained with H&E for pathological evaluation and with periodic acid Schiff (PAS) stain to highlight the PCT brush border. No marked differences in morphology were seen between groups. Glomeruli (G), proximal convoluted tubules (P).(GRT), Afriplex GRT™, (HFD) High-fat diet and (HFD-GRT) High-fat diet Afriplex GRT™ treated animals. Bar represents 500 µm.

5.4.2 Proximal convoluted tubules

A non-significant trend between the HFD-GRT group in comparison to the C-group, with the former showing smaller PCT outer surface areas (LSD =.048). No significant differences were found in the outer surface, luminal surface or the tubule wall areas between the four study groups (Table 5.4).

Table 5.4: Morphometric parameters of the proximal convoluted tubules. A decreasing trend was observed in the HFD-GRT group in comparison to the C-group in PCT outer surface area. No significant differences were observed in the outer, luminal surface, tubule wall area or diameter. Data is expressed as mean ± standard error of the mean (SEM).

Areas & diameters (μm²)	C	GRT	HFD	HFD-GRT
Outer surface area	**2766.99±377.85^{a}**	2334.46±238.49^{ab}	2375.12±303.16^{ab}	**1941.00±155.33^{b}**
Outer diameter	56.80±3.59	52.64±2.79	52.37±3.83	48.10±1.87
Luminal surface area	525.06±87.72	523.21±51.17	410.61±58.58	382.78±43.80
Luminal diameter	23.63±2.14	23.63±0.83	21.63±1.83	19.86±1.25
Wall area	2241.94±299.03	1811.25±221.64	1964.51±246.81	1558.22±145.90
Wall diameter	33.18±1.77	29.01±2.737	30.73±2.18	28.23±1.95

Differing letters indicate trends, letters that are shared indicate no trends. Control (C), Afriplex GRT™ (GRT), High-fat diet (HFD) and High-fat diet Afriplex GRT™ (HFD-GRT) treated animals.

5.4.3 Arcuate arteries

The arcuate arteries outer and luminal surface areas, as well as the media to lumen ratio were determined (Table 5.5). The tunica media to lumen ratio differed between the HFD and GRT groups (LSD = .026) even though neither differed from the control. No significant differences were found in outer surface area, luminal surface area or media to lumen ratio.

Table 5.5: Morphometric parameters of the arcuate artery comparing the four study groups. A trend of smaller media to lumen ratio was observed in the HFD-GRT group in comparison to the C-group although no significant differences were observed in any of the parameters measured. Data is expressed as mean ± standard error of the mean (SEM).

Areas & diameters (μm²)	C	GRT	HFD	HFD-GRT
Outer surface area	5134.345±717.59	5967.046±847.08	4939.648±710.17	5026.925±767.13
Internal diameter	39.25±3.26	39.62±3.42	42.63±4.38	37.71±3.60
Luminal surface area	2127.30±319.40	2186.17±354.17	2074.92±411.26	1864.43±370.53
External diameter	600.67±91.94	605.82±89.29	496.64±62.04	448.00±85.91
Media area	1084.44±134.36	1219.22±188.019	897.882±88.10	886.89±153.24
Media thickness	290.44±44.75	293.31±115.68	238.03±29.97	216.04
Media: Lumen ratio	11.88±0.73^{ab}	**13.2±0.75^{a}**	**10.79±0.64^{b}**	11.46±0.75^{ab}

Differing letters indicate trends, letters that are shared indicate no trend. Control (C), Afriplex GRT™ (GRT), High-fat diet (HFD) and (High-fat diet Afriplex GRT™ HFD-GRT) treated animals.

5.5 MORPHOLOGY AND PATHOLOGY OF THE PANCREAS, LIVER AND KIDNEY.

The pancreas, liver and kidney (H&E) were sent to a veterinary histopathologist blinded to the allocation of study groups and treatments for analysis. A summary of the pathologist's examination is provided in Addendum M. Additionally, the liver was scored using the NAS score (Kleiner *et al.*, 2005) by five scorers. Evaluation of the liver by the NAS scorers and the histopathologist were compared.

5.5.1 Pancreas

The histopathologist noted the presence of active lymph nodes in the peripancreatic fat in the control and HFD groups more often than in the GRT and HFD-GRT groups ($X^2 = 5.3317$, $p = .021$) (Figure 5.9). A necrotic lesion was noted in a single GRT animal (one out of seven animals, 1/7); however, no additional lesions were found in any other group. Additionally, increased intra- and interlobular steatosis lesions were present in the HFD and HFD-GRT animals in comparison to the control and GRT groups. This was confirmed with the Oil red O stain (Figure 5.9). The acinar cells of the exocrine portion were normal. Mild periductal mononuclear cell infiltration was observed in the GRT (1/7) and HFD groups (2/7) however

this was not significant. A summary of the histopathologists findings is available in Addendum O Table 21.

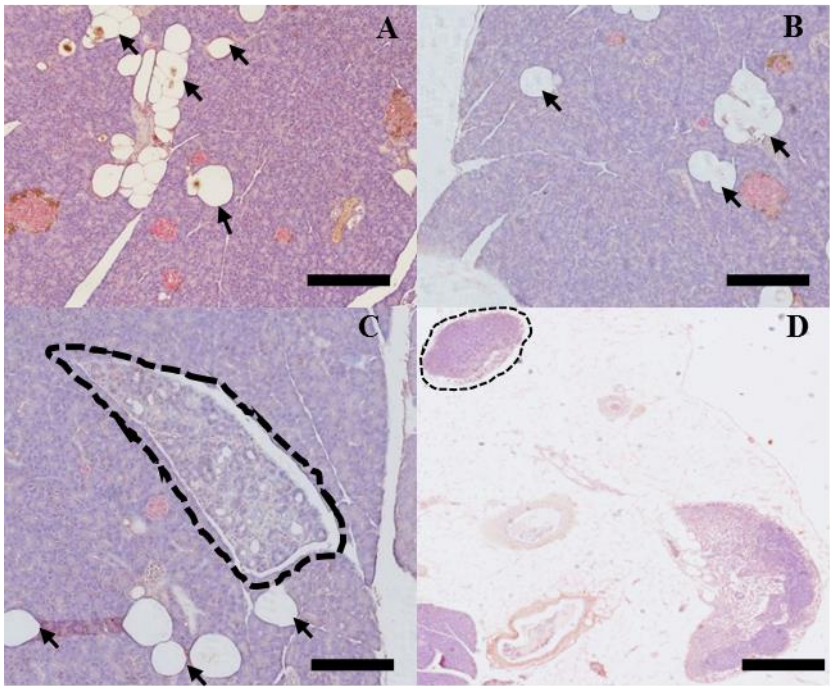

Figure 5.9: Pathology observed in the pancreas. (A) HFD group and (B) HFD-GRT group steatosis lesions (black arrows), (C) necrotic lesion observed in single animal (HFD-GRT animal) (as indicated by the dashed lines) and (D) peripancreatic fat active lymph nodules (as indicated by the dashed lines). All images 100X magnification. Bar represents 500um.

5.5.2 Liver

5.5.2.1 Non-alcoholic fatty liver disease (NAFLD) Activity Score

This score evaluates steatosis, fibrosis and inflammation, hepatocyte pathology and assigns a diagnostic classification. Significantly increased values in the grade of steatosis (Figure 5.10 A), microvesicular steatosis (Figure 5.10 B), and hepatocyte swelling (Figure 5.10 C) were found between groups. The presence of inflammation around the portal and lobular regions was increased in the HFD and HFD-GRT groups. The type of inflammatory foci, microgranulomas or lipogranulomas was also significantly increased. A summary of the steatosis and inflammatory lesions observed is shown in Figure 10 A-D.

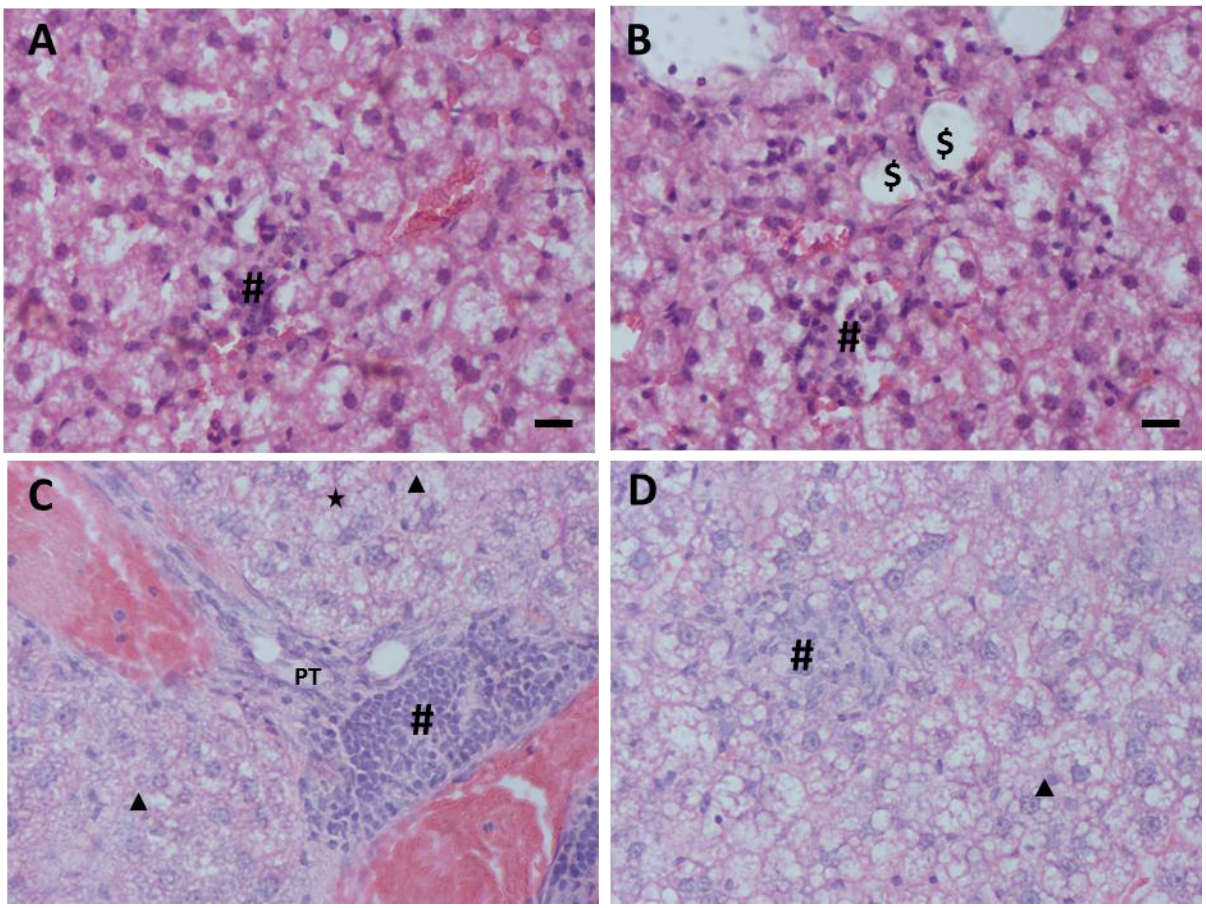

Figure5.10 **Pathological lesions observed in the livers of HFD fed animals as evaluated by the Non-alcoholic fatty liver disease activity score (NAS).** A)Hepatocytes with fat nitration and a microgranuloma of inflammatory cells. B) Microgranuloma and macrovesicular fatty infiltration in hepatocyte. C) Portal inflammation around the portal triad. D) Lipogranuloma with many hepatocytes with microvesicular steatosis and hepatocyte ballooning close by. CV:central vein; PT: portal triad; $: macrovesicular steatosis; star: microvesicular steatosis; #: inflammatory foci; arrow head: ballooned hepatocytes; arrows: glycogen deposits.

5.5.2.2 Steatosis

The HFD and HFD-GRT groups showed a significantly higher percentage of steatosis (grade 2 or 3) in comparison to the control and GRT groups (grade 0) ($p < .01$). There was no difference between the control and GRT groups in terms of percentage of steatosis, however both groups differed from the HFD and HFD-GRT groups respectively (both $p < .01$); (Figure 5.11 A). Microvesicular steatosis was significantly higher in the HFD and HFD-GRT groups (in comparison to the control and GRT groups ($X^2 = 34.59$, $p < .01$, $df = 3$) (Figure 5.11 B). Furthermore, the GRT group (1/7) had statistically more microvesicular steatosis than the control (0/7) ($p = .005$). Ballooning of hepatocytes was significantly higher in the HFD and

HFD-GRT groups (13/14) in comparison to the control and GRT groups (0/14, $p < .01$) (Figure 5.11 C). No significant differences were observed in location of steatosis.

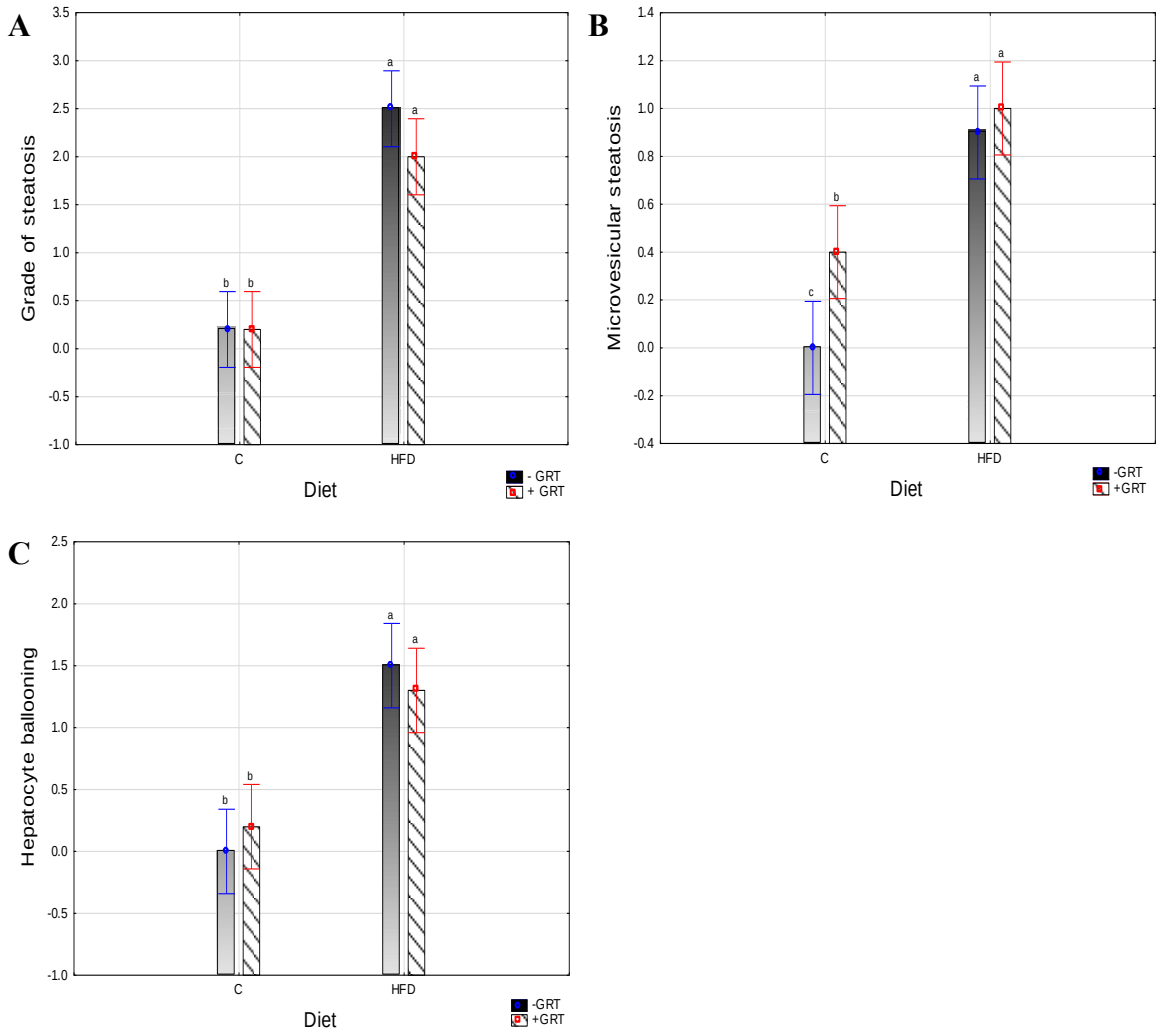

Figure 5.11: Liver pathology was evaluated using the non-alcoholic fatty liver disease activity score (NAS): (A) percentage of steatosis, (B) microvesicular steatosis and (C) hepatocyte ballooning. Vertical bars denote 0.95 confidence intervals. (GRT) Afriplex GRT™ extract, (+) treated, (-) untreated. n=7 per group. Differing letters indicate significant differences, letters that are shared indicate no significant difference.

5.5.2.3 Fibrosis

Using the NAS score, fibrosis was only observed in three animals, one animal each from the control, HFD and HFD-GRT groups (3/28). No additional fibrosis was scored and thus no trends or statistical significance was determined.

5.5.2.4 Inflammation

More inflammatory foci were observed in the region of the portal triads than within the lobes of the liver. Inflammatory foci were observed around the portal areas in the HFD and HFD-GRT groups (8/14) than the control and GRT groups (3/14); (Chi-square = 13.46, $p < .01$, df = 3);(Table 5.6). The HFD-GRT group (3/7) showed significantly less portal inflammation than the HFD group (5/7). Inflammatory portal lesions were observed in the GRT (2/7) and the C-group (1/7). Lobular inflammation differed significantly between the control and HFD fed groups ($p < .01$). Microgranulomas were present in the HFD (50%), GRT (30%) and HFD-GRT (60%) groups. More microgranulomas were observed in the HFD and HFD-GRT groups than the control and GRT groups ($X^2 = 12.26$, $p = .02$, df = 3). No lipogranulomas were observed in the control or GRT groups. In contrast, significantly more foci were present HFD and HFD-GRT groups (5/7 and 4/7 respectively) in comparison to the control and GRT groups (both 0/7) (Chi-square = 15.33, $p < .01$, df = 3);(Table 5.6).

Table 5.6: Inflammatory parameters scored using the non-alcoholic fatty liver disease activity score (NAS). The presence of inflammatory lesions in the various study groups expressed as percentages per group.

Percentage (%)	C	GRT	HFD	HFD-GRT
Lobular inflammation	**0^{a}**	**5^{a}**	**17^{b}**	**17^{b}**
Portal inflammation	**10^{a}**	20^{ab}	**80^{c}**	**50^{bc}**
Microgranulomas	**0^{a}**	30^{ab}	**50^{b}**	**60^{b}**
Lipogranulomas	**0^{a}**	**0^{a}**	**50^{b}**	**40^{b}**

Differing letters indicate significant differences, letters that are shared indicate no significant difference.

5.5.2.5 Interobserver reliability NAS score

Six observers including the scores given by the histopathologist were compared. The agreement between scorers $\kappa = 0.43$, which concludes that moderate agreement was observed between observers.

5.5.3 Liver architecture (structural integrity)

Collagen type-3 fibres (Reticulin) form the structural network in the liver whereas collagen type-1 fibres are usually associated with fibrotic change. Structural architecture was evaluated using the Gordon and Sweet's reticulin impregnation technique while fibrotic changes were evaluated using the Masson's Trichrome technique (Refer to Figure 5.12). The HFD group showed extensive hepatocyte ballooning and sinusoidal invasion with very few reticulin fibres

present (< 5%) apart from around the central vein and portal tracts. With Afriplex GRT™ treatment, the HFD-GRT group showed a reticulin network with less fragmentation and semi-complete fibres (> 60%). The HFD-GRT reticulin architecture resembled the C-group apart from some deviations associated with hepatocyte ballooning and steatosis in the central region (zone 3). The C- and GRT group livers were indistinguishable, both showing a normal architectural profile with little to no reticulin fibres fragmentation (Figure 5.12). Fibrotic changes were present in a few animals (3/28) and no pattern could be determined (Figure 5.12)

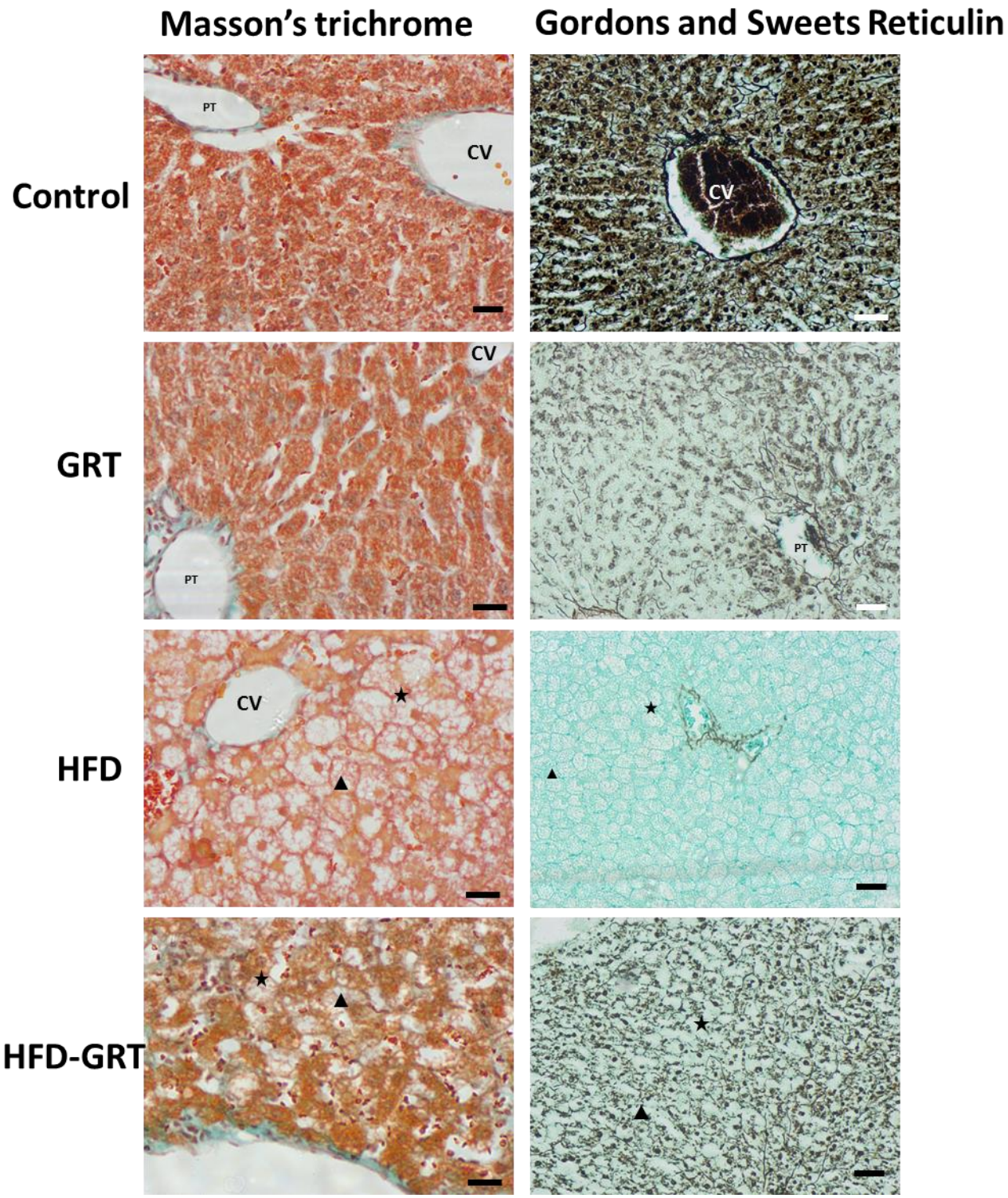

Figure 5.12 **Liver tissue stained with Masson's trichrome and Gordon and Sweet's Reticulin stain for pathological evaluation**. Fibrotic changes were sporadic, and no pattern was found. Reticulin architecture was substantially affected by HFD exposure however, the HFD-GRT group showed less fragmentation than HFD group. Masson's trichrome 200x (Bar= 50µm), and G&S reticulin 100x magnification (bar=100µm). (C) control, (GRT), Afriplex GRT™, (HFD) High-fat diet and (HFD-GRT) High-fat diet Afriplex GRT™ animals.5.5.2.6 Histopathologist

Significant lipid vacuole degeneration was reported by the histopathologist in the HFD and HFD-GRT groups than the control and GRT groups ($p < .01$). No other statistically significant differences were found observed. A summary of the histopathologists findings is available in Addendum O Table 21.

5.5.4 Kidney

5.5.4.1 Pathology review and Histopathologists findings

The kidney was evaluated for renal tubular nephrosis, intratubular oedema, proteinaceous luminal material and congestion. No significant differences were found. A summary of the histopathologists findings is available in Addendum O Table 21.

5.6 SUMMARY

In the present study, significantly decreased body mass in the HFD-GRT compared to the HFD group was observed. Pancreas, liver and kidney mass significantly decreased in the HFD-GRT group compared to the C-group. Pancreatic islets size, α- and β-cells area decreased in the HFD-GRT group compared to the C-group. Increased volume and area of steatosis was observed in the HFD groups compared to control diet fed groups. In terms of pathology increased grade of steatosis, presence of microvesicular steatosis, hepatocyte ballooning and inflammation in the liver of the HFD group. A trend, smaller media-to-lumen ratio in the HFD compared to the GRT group was observed.

In contrast, Afriplex GRT™ significantly reduced BM, liver mass, volume of steatosis (both H&E and Oil red O), decreased kidney mass, decreased active peripancreatic lymph nodes. Smaller renal spaces and proximal convoluted tubules were observed in Afriplex GRT™ treated groups however these were only trends.

CHAPTER SIX:

DISCUSSION

The anti-obesity effects of fermented rooibos (Beltran 2011; Sanderson 2014), and its polyphenolic compounds (Jung *et al.,* 2013; Mathijs *et al.,* 2014; Liu *et al.,* 2015; Son *et al.,* 2013) have been described. Afriplex GRT™ is a laboratory standardized unfermented (green) rooibos extract which has a high aspalathin content (12.8%) (Beelders *et al.,* 2012). Limited studies have evaluated unfermented green rooibos extracts as the development of this form of rooibos was only established in 1990 (Vilano *et al.,* 2010; Joubert & de Beer, 2011; Muller *et al.,* 2012; Mazibuko *et al.,* 2013; Kamakura *et al.,* 2015; Mazibuko *et al.,* 2015; Kroukamp, 2018; Maqeda, 2018). There is disagreement with regards to the use of individual rooibos polyphenols (Snijman *et al.,* 2007; Kawano *et al.,* 2009; Perold *et al.,* 2009) compared to complete rooibos extracts, as the latter may be more effective due to the synergistic effects produced by the combination of polyphenols in extracts (Canda *et al.,* 2014; Joubert & de Beer, 2011; Muller *et al.,* 2017). In the present study, an aspalathin-rich unfermented extract was used to evaluate the synergistic effects of a complete extract in an obese rat model. As previous extracts and pharmaceuticals can be unpalatable, a jelly block medium was used. The effectiveness of the Afriplex GRT™, an unfermented rooibos extract in the present study, could be related to the jelly medium by which it was administered to animals. A few authors have previously used jelly blocks as a medium to administer different drug and polyphenol treatments (Lilies *et al.,* 1997, Chellan *et al.,* 2008, Huisamen *et al.,* 2013, Symington *et al.,* 2017). The use of jelly mediums may be so effective because of compliance and precise dose control which it ensures (Huisamen *et al.,* 2013). A disadvantage of the jelly blocks is the additional sugar content. In the present study, animals each received a single jelly block containing the Afriplex GRT™ or placebo jelly blocks to control the sugar content received by each animal.

Dietary, pharmaceutical and genetic adaptations are frequently used to produce obese animal models which replicate the conditions seen in humans (Buettner *et al.,* 2007). High-fat diets (HFD) promote hyperglycaemia, insulin resistance and compromise β-cell function (Buettner *et al.,* 2007), induce hepatic steatosis, increase body and organ mass (Beltran-Debon *et al.,* 2011) and promotes glomerulopathy and tubular injury (Altunkaynak *et al.,* 2008) in various rodent models. The HFD in the present study, was readily consumed by the animals seemingly because of how sweet and moist the diet was. As rats have been shown to like sweet tasting things (Chellan *et al.,* 2008), the addition of fructose in the present study's HFD may have prompted animals to consume more food. Lenoir *et al*. (2007) reported that consumption of diets high in sugar is motivated by the sweetened taste. As the HFD had a higher moisture

content, these animals subsequently drank less water and showed increased food intake in comparison to the control-diet fed groups (C and GRT groups) (Maqeda, 2018). This resulted in increased water intake in the control fed groups in comparison to the HFD fed groups.

As the present study formed part of a larger project testing Afriplex GRT™ in a HFD fed model some interesting results from the larger project pertaining to the present study are briefly discussed. The studies completed found that Afriplex GRT™ improved oral glucose tolerance, improved whole-body insulin resistance and enhanced mitochondrial function (Kroukamp, 2018). Whereas in the study conducted by Maqeda, (2018) hypertension decreased, vascular function, the liver antioxidant profile, and glucose metabolism improved in the HFD-GRT animals. Both studies reported decreased body, liver and intraperitoneal fat masses as well as serum leptin levels in the HFD-GRT animals. Therefore, the present study, wanted to confirm whether the ameliorative adaptations in the HFD-GRT animals were observed in the histology and morphometry of the pancreas, liver and kidney.

6.1 BODY AND ORGAN MASS

In animal models, a HFD is frequently associated with an increase in body mass (BM) (Noeman *et al.,* 2011; Park *et al.,* 2012; Schultz *et al.,* 2013; Anyakudo *et al.,* 2015; Fraulob *et al.,* 2010) as was seen in the HFD group of the present study. Beltran *et al.* (2010) reported a decreased BM in control and HFD (40% fat) fed animals treated with a fermented rooibos extract for 14-weeks. Similarly, in the present study, significantly lowered BM was seen in the Afriplex GRT™ groups (GRT and HFD-GRT) treated for 16-weeks. However, controversy exist in the literature regarding the effects of rooibos and rooibos polyphenols on BM (Jung *et al.,* 2013; Liu *et al.,* 2015). Quercetin, a component of Afriplex GRT™ (0.57%), effectively decreased BM gain in C57BL/6J mice fed an HFD for nine-weeks (Jung *et al.,* 2013). Whereas in ApoE mice fed an HFD for 24-weeks, quercetin had no effect on BM, liver mass or the serum lipid profile (Liu *et al.,* 2015). The latter study had a longer treatment period and different animal model than Jung *et al*. (2013) which could explain the discrepancy between studies as similar HFD and quercetin suppliers were used. As the present study, used an extract containing quercetin, our findings agree with that of Jung *et al*. (2013), the action of quercetin in Afriplex GRT™ may have effects on BM of male Wistar rats fed a HFD for 16-weeks. Many studies reported no effect on BM with various rooibos extracts and polyphenols in various animal models. These included (Z)-2-(β-D-glucopyranosyloxy)-3-phenylpropenoic acid (PPAG) (Mathijs *et al.,* 2014) aspalathin or green rooibos (Watanabe *et al.,* 2014), a 2% and 5%

unfermented rooibos extract (Opuwari & Monsees, 2013; Monsees & Opuwari, 2016) or fermented rooibos extracts (Smith & Swart, 2016). Baba *et al*. (2009) and Canda *et al*. (2014) reported no significant changes in BM in animals fed various rooibos supplements, including unfermented rooibos treatments in animals on a control diet. Furthermore, an aspalathin-enriched green rooibos extract had no effect on BM in male Fisher rats fed a control diet for 28 days however over 90 days a significant decrease in liver and body mass was observed (Van der Merwe *et al.*, 2015). As decreased BM was observed in the HFD-GRT group in the present study, Afriplex GRT™ may have potential as a therapeutic agent against diet-induced obesity.

In the present study, pancreatic mass was expressed as a percentage of body mass to normalize any changes in tissue mass to the whole animal. Even though exposure to an HFD is associated with an increase in pancreas mass (Carter *et al.*, 2014; Fraulob *et al.*, 2010; Anyakudo & Omotayo, 2015, Yagahashi *et al.*, 2016), pancreatic mass in the present study was not significantly increased by the HFD. Similarly, He *et al*. (2010) showed no change in pancreas mass associated with an HFD when the diet contained 60% calories from fat. In contrast, to fermented rooibos (Beltran-Debon *et al.*, 2011), pancreas mass in the present study was significantly decreased in the GRT and HFD-GRT groups. The decreased organ mass in the HFD-GRT group could relate to decreased intraperitoneal fat mass reported in the same animals as in the present study (Maqeda, 2018). The decrease in intraperitoneal fat mass suggests less adipose tissue, overall. The decreased adipose tissue mass could be related to restoration of specific cell signalling molecules which may be linked to aspalathin. Aspalathin is hypothesized to increase adenosine monophosphate protein kinase (AMPK) and protein kinase B (PKB) during glucose metabolism and translocation into cells (Muller *et al.*, 2012; Son *et al.*, 2013; Kamakura *et al.*, 2015). In the present study, as Afriplex GRT™ contains 12% aspalathin it may have increased AMPK and PKB signalling resulting in reduced ectopic fat deposition and tissue mass.

In obese humans and rats, the liver may act as ectopic fat storage which results in increased liver mass. Fraulob *et al*. (2015) and He *et al*. (2010) both reported an increase in liver mass in C57BL/6J mice fed an HFD. Similarly, in the present study, an increase in liver mass was observed in the HFD fed animals. However, in the HFD-GRT animals' liver mass was significantly decreased compared to the HFD group. Few articles agree that rooibos and its extracts effectively decrease liver mass (Beltran-Debon *et al.*, 2011; Jung *et al.*, 2013) however some extracts have shown increased or negligible effects on liver mass (Opuwari & Monsees,

2013; Canda *et al.*, 2014; Monsees & Opuwari, 2016). In agreement with the present study, a decrease in liver mass was reported in control and HFD fed mice treated with a fermented rooibos extract (Beltran-Debon *et al.*, 2010) and quercetin (Jung *et al.*, 2013). As the Afriplex GRT™ extract used in the present study contained quercetin, the decreased liver mass seen by Jung *et al.*(2013) is similar to what was observed here. In contrast, increased liver mass was observed with a 2% and 5% unfermented rooibos solution in female Wistar rats (Monsees & Opuwari, 2016). Whereas a 2% unfermented solution had no effect on liver mass in male Wistar rats fed a standard rat chow diet (Canda *et al.*, 2014). Similarly, Opuwari and Monsees (2013) reported no effect on liver mass (absolute or relative to BM) in male Wistar rats with either a 2% or 5% unfermented rooibos extract.

In contrast to the liver mass, the animals in the present study showed a decrease in kidney mass in the HFD fed animals (HFD and HFD-GRT). Increased renal mass was reported in rats fed an HFD (60% and 45% fat respectively) for six-weeks (Crinigan *et al.*, 2015) and 52-weeks (Van Der Heijden *et al.*, 2015) respectively. In diabetic individuals, decreased renal mass is common and is associated with renal disease progression (Tobar *et al.*, 2013). Therefore, the decreased kidney mass in the present study may indicate diabetic related changes in the kidney. This is supported by changes in glucose tolerance in the HFD group confirmed by Maqeda (2018) and Kroukamp (2018). In the present study, a substantial decrease in kidney mass was seen in the Afriplex GRT™ treated groups. In contrast, a 2% and 5% unfermented rooibos extract showed no effect on kidney mass in female rats on a control diet (Monsees & Opuwari, 2016) whereas in male rats 5% fermented and unfermented rooibos extracts respectively, significantly decreased kidney mass relative to BM (Opuwari & Monsees, 2013). In the HFD-GRT group, decreased renal mass could indicate increased glomerular capillary pressure and possible diabetic changes which indicates renal disease progression. Therefore, the changes in renal mass in the HFD-GRT group may have illustrated an antagonistic interaction between Afriplex GRT™ and the HFD as well as differences in moisture content in the diets; however, further studies will need to confirm this.

Pancreas, liver and kidney mass were decreased with Afriplex GRT™ treatment in control and HFD fed animals (GRT and HFD-GRT groups respectively). The decrease in organ mass in the present study could be related to the inhibitory action of aspalathin and quercetin on adipogenesis and adipocyte metabolism *in vitro* (Sanderson *et al.*, 2014) and *in vivo* (HFD fed rats) (Moon *et al.*, 2013). Thus, the decrease in body and organ mass may be related to

inhibition of adipogenesis by aspalathin and/or quercetin components of the Afriplex GRT™ extract studied here.

6.2 PANCREATIC MORPHOMETRY, MORPHOLOGY AND PATHOLOGY

As pancreatic islets are the functional units of the endocrine pancreas, increased islet areas in the GRT group suggest increased hormone secretion from the pancreas especially insulin (Kim *et al.,* 2009). However, smaller islets are associated with increased insulin, as was seen in the HFD-GRT group. Furthermore, the HFD-GRT group had increased islet numbers and islets per section area were observed. Thus, two opposing theories can be proposed namely islet neogenesis or lipotoxicity. As larger islets were present in the GRT group in comparison to the C-group, islet (β-cells) neogenesis may have occurred (Sasaki *et al.,* 2018). Neogenesis postnatal in rats has been reported and is associated with pancreatic hormone-positive cells budding from the pancreatic duct epithelium (Bonner-Weir *et al.,* 2012). Lipotoxicity has been associated with a HFD, however, in the present study the increased islets per section area and marginally decreased islet, α- and β-cell areas were not sufficient to say lipotoxicity was present. However, in the HFD-GRT group, as the islet and β-cell areas were significantly decreased this suggests lipotoxicity occurred. In the HFD-GRT animals, improved glucose tolerance was suggested based on the oral glucose tolerance tests (Maqeda, 2018). Thus, the effect physiologically was reflected histologically on the pancreatic islets.

As α-cell area fell within the range of 12-15% in the present study, this is well within the normal range of 10-15% for rodents (Steiner *et al.,* 2010). Animals fed an HFD usually present with increased β-cell areas (Oliveira *et al.,* 2014, Falcoa *et al.,* 2016). Oliveira *et al.* (2014) saw no change in islet and β-cell areas in HFD treatment lasting for 30 days. However, when mice were fed the diet for 60 days a significant increase in islet areas, β-cell areas and islets per section area in male C57BL6/J0Unib mice was observed. In contrast, in the present study, no significant changes were observed in β-cell areas and islets per section area in the HFD group in comparison to the C-group. A component of Afriplex GRT™ namely PPAG, has been associated with increased β-cell mass in animals treated with an HFD (Mathijs *et al.,* 2014) and in response to streptozotocin (STZ) in Balb/c mice (Himpe *et al.,* 2016). In contrast, the HFD-GRT group in the present study, had smaller islets (and β-cell areas) which may indicate that this diet was more noxious due to the addition of fructose. Fructose does not activate the pancreatic β-cells (Elliot *et al.,* 2002). The lack of a stimulus to β-cells disrupts the insulin signalling pathway (Schultz *et al.,* 2013) and therefore afferent signals which control food

intake and weight gain are not activated (Meisser *et al.*, 2007). In the present study, the HFD animals had fewer β-cells than the control animals and this may be linked to the lack of β-cell activation by fructose in the HFD.

Pathology within the pancreas was minimal apart from the presence of pancreatic steatosis and active lymph nodes in the HFD groups. Pancreatic steatosis was confirmed with Oil red O staining on frozen sections and has similarly been reported in other HFD models (He *et al.*, 2010; Carter *et al.*, 2014; Fraulob *et al.*, 2010). In the present study, inter- and intralobular steatosis was noted in the all four study groups, with the HFD and HFD-GRT groups presenting with excess ectopic fat deposition within the pancreatic lobules and periodically near the pancreatic islets. The presence of active lymph nodes was significantly less in the GRT and HFD-GRT groups. This could be linked to the anti-inflammatory properties associated with rooibos (Baba *et al.*, 2009; Ajuwon *et al.*, 2013; Canda *et al.*, 2014).

6.3 LIVER MORPHOMETRY, MORPHOLOGY & PATHOLOGY

Schultz (2013) and Catta-pretta (2011) both reported an increase in the volume and area of steatosis in male C57BL/6J mice fed a HFD in comparison to the control fed groups. In agreement with the fore mentioned studies, the volume and area of steatosis was increased in the HFD fed groups in the present study. For the assessment of steatosis analysis of the Oil red O stained tissue is regarded as more accurate than that of H&E stained tissue (Levene *et al.*, 2012, Schultz *et al.*, 2013). However, as H&E stained tissue is more readily available than frozen tissue it can easily be compared retrospectively (Levene *et al.*, 2013). Although, future studies assessing steatosis should aim to obtain frozen tissue as this is the most accurate technique.

In the present study, both micro-and macrovesicular steatosis were present while the latter was more common in the HFD groups. Steatosis in the HFD-GRT animals showed microvesicular steatosis which indicates a possible restorative effect associated with rooibos. Various studies have evaluated the presence of these steatosis lesions within the liver of rats fed a HFD (Beltran-Debon *et al.*, 2010; Park *et al.*, 2012; Fraulob *et al.*, 2010). Beltran *et al.* (2010) showed the decrease of hepatic steatosis with a fermented rooibos extract which may explain the reduced steatosis in the HFD-GRT group in the present study. A decrease in the grade of steatosis and the degree of hepatocyte ballooning in the HFD-GRT was observed in comparison to the HFD group. This indicates a healthier profile and a possible restorative effect of Afriplex

GRT™ in HFD animals. This is further prompted by the presence of more microvesicular than macrovesicular steatosis in the HFD-GRT group as the former can be reversed.

In the present study, portal inflammation and lipogranulomas were reduced in the HFD-GRT group, however increased inflammatory lesions were observed in the GRT group suggesting that GRT may stimulate an inflammatory response. As the animals in the present study had characteristics of obesity they were predisposed to oxidative stress and inflammation (Noeman *et al.,* 2011). Rooibos and its extracts have shown anti-inflammatory potential (Scholms *et al.,* 2012; Baba *et al.,* 2009). The increased inflammatory lesions observed in the GRT group in the present study are contrary to the effects of fermented rooibos which have shown to decrease inflammatory cytokines levels in control fed male Wistar rats (Smith & Swart, 2016). The marginally increased inflammatory lesions in the GRT group may be related to the large number of antioxidants (polyphenols) contained in rooibos and its extracts. Baba *et al.* (2009) reported increased tissue inflammation associated with antioxidants (SOD) levels in rooibos treated rats and related this to the increased number of flavonoids found in rooibos.

In the present study, evaluation of the Gordon and Sweet's reticulin stain, showed less fragmentation in structural architecture reticulin fibres in the HFD-GRT in comparison to the HFD group. The improvement in structural integrity can be related to reduced steatosis in the HFD-GRT group in comparison to the HFD group. Similarly, Singhi *et al.* (2012) reported improved reticulin architecture in areas where less steatosis was present in human studies. As rooibos and its extracts have been suggested as antilipidemic agents (Beltran *et al.,* 2011; Sanderson *et al.,* 2014; Jung *et al.,* 2013) the decreased steatosis and hepatocyte ballooning in the HFD-GRT group, may have put less strain on the reticulin network resulting in in improved morphology. In terms of fibrosis, only three animals presented with fibrosis, an essential marker for progression of fatty liver disease. However, as the liver is a regenerative organ, the lack of fibrosis at the end of experimentation suggests reversal and or prevention of fibrotic change as a result of Afriplex GRT. Whether Afriplex GRT™ can effectively reduce steatosis and inflammatory conditions including fibrotic changes (not seen in the present study) requires further investigation.

6.4 KIDNEY MORPHOMETRY, MORPHOLOGY AND PATHOLOGY

Marked renal structural remodelling including glomerulosclerosis and tubular injury (Altunkaynak *et al.,* 2008) is associated with diet-induced obesity yet in the present study

extensive renal corpuscle pathology was not observed. Furthermore, in the present study, the glomerular surface area was not significantly increased by an HFD. Contrastingly, glomerular surface area was increased in mice fed a HFD for 12-weeks and further glomerulomegaly was observed in the same animals at 16-weeks (Ruggiero *et al.*, 2011). In the present study, the HFD was assigned for 16-weeks however the glomerular and Bowman's capsule areas and diameters were decreased in the HFD group. In addition, no glomerular pathology was noted. The lack of changes in the present study are contrary to the literature as well as findings in the liver and pancreas where the effects of fructose contained in the HFD produced some detrimental effects.

Decreased glomerular and Bowman's capsule size was noted in the Afriplex GRT™. Pereira. (2017) studied the renal corpuscle (glomeruli and Bowman's capsule) and proximal convoluted tubules of rats supplemented with a 2% fermented rooibos extract. No significant effects were determined although larger glomerular and Bowman's capsule areas and diameters were reported in the rooibos treated rats. Similarly, in the present study, no significant changes were observed in glomerular and Bowman's capsule areas and diameters. In control fed female Wistar rats treated with a 5% fermented rooibos extract no deviations in kidney morphology were observed however an increased creatinine level was present (Monsees & Opuwari, 2016). As no kidney function tests were performed, no conclusion can be determined on whether Afriplex GRT™ is detrimental on the kidney.

The renal space, proximal convoluted tubules (PCT) and arcuate arteries were not significantly altered in the present study. In non-diabetic obese individuals, the renal space is increased, which may be a consequence of glomerular hyperfiltration (Tobar *et al.*, 2013). Similar to the effects on renal mass the effects seen in the renal space, PCTs and arcuate arteries in the HFD-GRT group may indicate synergistic or antagonistic effects of Afriplex GRT™ and an HFD.

In sustained hypertension a morphological increase in both arterial media-to-lumen ratio and wall thickness is expected (Laurent, 1995). In contrast, in the present study, a trend of smaller media-to lumen ratio in the HFD group in comparison to the GRT group was observed. As neither group was significantly different from the C-group, the arcuate arteries were not morphologically adapted by the HFD or Afriplex GRT™ treatment. In the HFD animals in the present study, hypertension was confirmed by increased mean systolic, diastolic, arterial pressure, and increased aortic ring tension all of which were improved in the HFD-GRT

animals (Maqeda, 2018). Previously, anti-hypertensive characteristics of rooibos *in vivo* and *in vitro* have been suggested.(Person *et al.*, 2010) Therefore, Afriplex GRT™ may possess promising effects on hypertension not reflected on the histomorphometry of the arcuate artery.

Contrary to the literature, glomerulopathy such as focal segmental glomerulosclerosis or glomerulomegaly which are commonly seen in rats fed an HFD (Tobar *et al.*, 2013) was not observed in the present study. Stemmer *et al.* (2012) reported the presence of proteinaceous cast, monocyte infiltration, slightly basophilic tubules, glomerulosclerosis and basement membrane thickening in male Wistar rats. Gai *et al.* (2014) reported increased fibrosis, glomerular pathology and interstitial fibrosis in C57/BJ mice fed an HFD of 20-weeks. Lastly, glomerulomegaly with the absence of albuminuria and podocyte loss was observed in mice fed an HFD (Wicks *et al.*, 2016).

Thus, the decrease in kidney mass and parts of the nephron suggest overall that Afriplex GRT™ treatment may negatively affect the kidney. However, with an increased study period alternate results may have been observed. Kidney function tests such as the urine albumin-creatinine ratio and serum creatinine values would explain if histomorphometric effects of Afriplex GRT™ related to changes in kidney function as well. The mild histomorphometric and minimal pathology observed in the present study contradicts the effects known to occur in conjunction with an HFD.

CHAPTER SEVEN:

CONCLUSION

In conclusion, this study demonstrates that Afriplex GRT™ may possess anti-obesity properties as demonstrated by the significant decrease in body mass as well as liver mass in the HFD fed animals. Further study is required to investigate the mechanism of action that Afriplex GRT™ has on pancreas and kidney mass and to determine whether the decrease in mass in the control fed GRT group was harmful.

This study postulates that neogenesis or lipotoxicity were present in the pancreata of HFD-GRT group due to the presence of increased islet numbers and islets per section area in the same group. As the GRT group showed increased islet and β-cell areas, this may have indicated proliferation of the pancreatic islets. However, as the HFD group had decreased islet numbers and marginally decreased islet and β-cell areas, the addition of fructose to the diet may be toxic to pancreatic islets as was seen in the literature. Therefore, in the HFD-GRT group, the addition of antioxidants by Afriplex GRT™, may have reduced oxidative stress and lipotoxicity induced by the HFD. This allowed more islets to be present and improved glucose tolerance of the same animals studied presently. The changes observed require further investigation of β-cell proliferation, function, apoptosis as well as determination of pancreatic lipases.

As Afriplex GRT™ successfully decreased liver mass, the volume and area of steatosis, it may be promising as a hepatoprotective supplement against obesity associated non-alcoholic fatty liver disease (NAFLD). Reduced steatosis, inflammation and improved architecture in the liver further promote this product as an anti-obesity agent in the liver. In the present study, fibrosis was only observed sporadically suggesting reversal of NAFLD. As liver tissue was only evaluated at the end of the 16-week study period, changes seen during the study period cannot be confirmed, including the presence of fibrosis. Additional staining with Sirius red instead of Masson's trichrome could assist detection of minute fibrotic changes. Therefore, a study period with periodic investigation of tissue over a longer study period may detect NASH changes associated with a HFD and better illustrate the ameliorative effects of Afriplex GRT™ on NAFLD.

In the kidney Afriplex GRT™ decreased kidney mass, components of the renal corpuscle (glomerular and Bowman's capsule), proximal convoluted tubules and arcuate arteries. Whether these affects were negative cannot be substantiated as kidney function tests were not performed namely albumin and creatinine levels.

Thus, Afriplex GRT™ may possess observable ameliorative effects on the histomorphometry of the liver. Whether the changes on the pancreas and kidney were ameliorative is inconclusive. However, in the pancreas Afriplex GRT™ may improve pancreatic islet numbers leading to improved glucose tolerance as seen physiologically. Additional tests of the pancreas and kidney are required to be able to substantiate the effects seen in the present study and further elaborate on the effects of Afriplex GRT™. Afriplex GRT™ reduced pathology in the pancreas and liver as shown by decreased steatosis and hepatocyte ballooning in the liver as well as the presence of active lymph nodes in the pancreas and inflammatory foci in the liver, respectively.

The use of green rooibos as a natural supplement drug is possible. Afriplex GRT™ is available as a powder and therefore addition of it to food and liquids is possible. Green rooibos is also available in many supermarkets however, the effects of green rooibos at cup of tea strength may not be as effective. The use of Afriplex GRT™ as an anti-steatotic agent along with healthy eating (dieting) may be effective in weight loss. In the present study, Afriplex GRT™ reduced body mass (organ and intraperitoneal fat mass) suggests a promising effect for many wanting to lose body mass. In obesity, the problem is regaining the body mass after losing it. Afriplex GRT™ may be effective for these patients as in the present study (HFD-GRT group) no toxic effects were reported. Three studies have confirmed hepatotoxicity with excess consumption of rooibos and therefore chronic consumption should be done with caution and in conjunction with a dietician or medical professional**.** The effectiveness of this extract in the present study calls for further study in other animal models and possible clinical trials.

Limitations and future studies

Afriplex GRT™ is a stable powder unfermented rooibos extract however, future researchers should determine whether the polyphenol content was affected by the jelly medium used in this study. As ameliorative effects were observed in this study the polyphenol levels were sufficient to produce effects on tissue histomorphology. Although understanding of why this medium was effective may improve other vehicles of treatment and the translation of this medium into a product.

To ensure efficient use of animals, tissue was shared with the Division of Medical Physiology, Stellenbosch University. This affected the amount of pancreatic tissue available for histomorphometry. Future research should aim to study a specific portion of the pancreas as

changes in the distribution of islets differs in different regions of the pancreas. Pancreatic studies should also determine pancreatic β-cell mass, function, the presence of apoptotic markers and pancreatic lipases expression. As this will help explain changes observed in the HFD-GRT group. As the pancreas has very few endogenous antioxidants, evaluation of the antioxidants profile in the HFD-GRT animals may explain how Afriplex GRT™ improved glucose tolerance.

The study-period employed in the present study, caused increased body and liver mass as well as hepatic steatosis (signs of obesity). However, study of these changes at periodic intervals e.g. 4, 8, 12 and 16 -weeks or over a longer period may determine whether fibrotic changes had taken place in the liver (as it is regenerative) and were absent as tissue samples were only taken at the endpoint of the study. Furthermore, staining with Sirius red may assist detection of minute fibrotic changes. Afriplex GRT™ significantly reduced steatosis in the liver, determination of the liver lipid profile (very-low density lipoproteins, low density lipoproteins, high density lipoproteins) will detect deviations in the type of lipids present in the different groups. In addition, study of the inflammatory cytokines will explain the immune systems role in the function of Afriplex GRT™.

For the kidney, plasma albumin-creatinine ratio and serum creatinine levels should be performed to determine kidney function. Changes in the histomorphometry are inconclusive as statistical power was not sufficient due to the small sample number. The addition of these functional (blood) tests as well as the investigation of endogenous antioxidants will indicate whether Afriplex GRT™ has a protective effect on the kidney. The addition of the Cavalieri principle to estimate glomerular volume may provide more details on the glomeruli and whether Afriplex GRT™ induced a protective effect in HFD fed animals. A longer study time period may allow the effects of the HFD and Afriplex GRT™ to be seen on a histological level.

REFERENCES

Abdollahi M., Ranjbar A., Shadnia S., Shekoufeh N. and Rezaie A., Pesticide and oxidative stress: a review. *Medical Science Monitor* 2004;10:141-147.

Ajuwon, O.R., Katengua-Thamahane, E., van Rooyen, J., Oguntibeju, O.O. & Marnewick, J.L. 2013. Protective effects of rooibos (*Aspalathus linearis*) and/or red palm oil (*Elaeis guineensis*) supplementation on tert-butyl hydroperoxide-induced oxidative hepatotoxicity in Wistar rats. *Evidence-Based Complementary and Alternative Medicine*, 2013(1):1-19.

Ajuwon, O.R., Oguntibeju, O.O. & Marnewick, J.L. 2016. Hepatic, renal and endogenous antioxidant status modulatory effects of chronic co-supplementation of rooibos (*Aspalathus linearis*) and red palm oil (*Elaeis guineensis*) in male Wistar rats. *African Journal of Traditional, Complementary and Alternative Medicines*, 13(3):1-15.

Alhoshani, A.R., Hafez, M.M., Husain, S., Al-sheikh, A.M., Alotaibi, M.R., Al Rejaie, S.S., Alshammari, M.A., Almutairi, M.M. & Al-Shabanah, O.A. 2017. Protective effect of rutin supplementation against cisplatin-induced Nephrotoxicity in rats. *BMC nephrology*, 18(1):194.

Altunkaynak, M.E., Özbek, E., Altunkaynak, B.Z., Can, İ., Unal, D. & Unal, B. 2008. The effects of high-fat diet on the renal structure and morphometric parametric of kidneys in rats. *Journal of Anatomy*, 212(6):845-852.

Anyakudo, M.M.C. & Omotayo, P. 2015. Effects of high dietary fat intake on biochemical variables and pancreas histoarchitecture in diabetic rats. *Journal of Human Nutrition and Food Science*, 3(1):1-6.

Baba, H., Ohtsuka, Y., Haruna, H., Lee, T., Nagata, S., Maeda, M., Yamashiro, Y. & Shimizu, T. 2009. Studies of anti-inflammatory effects of Rooibos tea in rats. *Pediatrics International*, 51(5):700-704.

Baker, H.J., Lindsey, J.R. & Wesibroth, S.H. (eds.). 2013. *The laboratory rat: biology and diseases* (Vol. 1). New York: Elsevier.

Bancroft, J.D. and Gamble, M. eds., 2008. *Theory and practice of histological techniques*. Elsevier Health Sciences.

Beelders, T., Sigge, G.O., Joubert, E., de Beer, D. & de Villiers, A. 2012. Kinetic optimisation of the reversed phase liquid chromatographic separation of rooibos tea (*Aspalathus linearis*) phenolics on conventional high-performance liquid chromatographic instrumentation. *Journal of Chromatography A*, 1219:128-139.

Beltrán-Debón, R., Rull, A., Rodríguez-Sanabria, F., Iswaldi, I., Herranz-López, M., Aragonès, G., Camps, J., Alonso-Villaverde, C., Menéndez, J.A., Micol, V. & Segura-Carretero, A. 2011. Continuous administration of polyphenols from aqueous rooibos (*Aspalathus linearis*) extract ameliorates dietary-induced metabolic disturbances in hyperlipidaemic mice. *Phytomedicine*, 18(5):414-424.

Bonner-Weir, S., Guo, L., Li, W.C., Ouziel-Yahalom, L., Lysy, P.A., Weir, G.C. & Sharma, A. 2012. Islet neogenesis: a possible pathway for beta-cell replenishment: a review. *The Review of Diabetic Studies*, 9(4):407.

Bowles, S., Joubert, E., de Beer, D., Louw, J., Brunschwig, C., Njoroge, M., Lawrence, N., Wiesner, L., Chibale, K. & Muller, C. 2017. Intestinal transport characteristics and metabolism of C-glucosyl dihydrochalcone, aspalathin: a review. *Molecules*, 22(4):554.

Breiter, T., Laue, C., Kressel, G., Gröll, S., Engelhardt, U.H. & Hahn, A. 2011. Bioavailability and antioxidant potential of rooibos flavonoids in humans following the consumption of different rooibos formulations. *Food Chemistry*, 128(2):338-347.

Brown, M.S. & Goldstein, J.L. 1986. A receptor-mediated pathway for cholesterol homeostasis. *Science*, 232(4746):34-47.

Brunt, E.M., Kleiner, D.E., Wilson, L.A., Belt, P. and Neuschwander-Tetri, B.A., 2011. Nonalcoholic fatty liver disease (NAFLD) activity score and the histopathologic diagnosis in NAFLD: distinct clinicopathologic meanings. Hepatology, 53(3), pp.810-820.

Buettner, R., Parhofer, K.G., Woenckhaus, M., Wrede, C.E., Kunz-Schughart, L.A., Schölmerich, J. & Bollheimer, L.C. 2006. Defining high-fat-diet rat models: metabolic and molecular effects of different fat types: a review. *Journal of Molecular Endocrinology*, 36(3):485-501.

Buettner, R., Schölmerich, J. & Bollheimer, L.C. 2007. High-fat diets: modelling the metabolic disorders of human obesity in rodents: a review. *Obesity*, 15(4):798-808.

Burton, G.J. and Jauniaux, E., 2011. Oxidative stress: a review. *Best practice & research Clinical obstetrics & gynaecology*, *25*(3): 287-299.

Campbell, S.A. & Hoffman, B.G. 2016. Chromatin regulators in pancreas development and diabetes. *Trends in Endocrinology and Metabolism*, 27(3):142-152.

Canda, B.D., Oguntibeju, O.O. & Marnewick, J.L. 2014. Effects of consumption of rooibos (*Aspalathus linearis*) and a rooibos-derived commercial supplement on hepatic tissue injury by tert-butyl hydroperoxide in Wistar rats. *Oxidative Medicine and Cellular Longevity*, 2014:1-9.

Carter, R., Mouralidarane, A., Soeda, J., Ray, S., Pombo, J., Saraswati, R., Novelli, M., Fusai, G., Rappa, F., Saracino, C. & Pazienza, V. 2014. Non-alcoholic fatty pancreas disease pathogenesis: a role for developmental programming and altered circadian rhythms. *PLoS One*, 9(3):e89505.

Catta-Preta, M., Mendonca, L.S., Fraulob-Aquino, J., Aguila, M.B. & Mandarim-de-Lacerda, C.A. 2011. A critical analysis of three quantitative methods of assessment of hepatic steatosis in liver biopsies. *Virchows Archiv*, 459(5):477.

Chellan, N., De Beer, D., Muller, C., Joubert, E. & Louw, J. 2008. A toxicological assessment of *Athrixia phylicoides* aqueous extract following sub-chronic ingestion in a rat model. *Human and Experimental Toxicology*, 27(11):819-825.

Choi, S., Choi, Y., Choi, Y., Kim, S., Jang, J. & Park, T. 2013. Piperine reverses high fat diet-induced hepatic steatosis and insulin resistance in mice. *Food chemistry*, 141(4):3627-3635.

Cohen, B., Novick, D. & Rubenstein, M. 1996. Modulation of insulin activities by leptin. The American Association for the Advancement of Science, 274(5290):1185-1188.

Courts, F. & Williamson, G. 2009. The C-glucosyl flavonoid, aspalathin, is absorbed, methylated and glucuronidated intact in humans. *Molecular Nutrition Food Research*, 53:1104-1111.

Courts, F.L. & Williamson, G. 2015. The occurrence, fate and biological activities of C-glycosyl flavonoids in the human diet. *Critical Reviews in Food Science and Nutrition*, 55(10):1352-1367.

Crinigan, C. 2015. Effect of a short-term high fat diet on kidney morphology and function. Unpublished masters thesis. Arizona: Arizona State University.

De Beer, D., Miller, N. & Joubert, E. 2017. Production of dihydrochalcone-rich green rooibos (*Aspalathus linearis*) extract taking into account seasonal and batch-to-batch variation in phenolic composition of plant material. *South African Journal of Botany*, 110:138-143.

Della Corte, C., Mosca, A., Majo, F., Lucidi, V., Panera, N., Giglioni, E., Monti, L., Stronati, L., Alisi, A. & Nobili, V. 2015. Nonalcoholic fatty pancreas disease and nonalcoholic fatty liver disease: more than ectopic fat. *Clinical Endocrinology*, 83(5):656-662.

Dludla, P.V., Muller, C.J.F., Louw, J., Joubert, E., Salie, R., Opoku, A.R. & Johnson, R. 2014. The cardioprotective effect of an aqueous extract of fermented rooibos (*Aspalathus linearis*) on cultured cardiomyocytes derived from diabetic rats. *Phytomedicine*, 21(5):595-601.

Donath, M.Y., Gross, D.J., Cerasi, E. & Kaiser, N. 1999. Hyperglycaemia-induced beta-cell apoptosis in pancreatic islets of *Psammomys obesus* during development of diabetes. *Diabetes*, 48(4):738-744.

Ekonoyan, G. 2011. Obesity and chronic kidney disease: a review. *Nefrologia*, 31(4):397-403.

El Akoum, S., Lamontagne, V., Cloutier, I. & Tanguay, J.F. 2011. Nature of fatty acids in high fat diets differentially delineates obesity-linked metabolic syndrome components in male and female C57BL/6J mice. *Diabetology and Metabolic Syndrome*, 3(1):34.

Elayat, A., El-Naggar, M. & Tahir, M. 1995. An immunocytochemical and morphometric study of the rat pancreatic islets. *Journal of Anatomy*, 186:629-637.

Elliott, S.S., Keim, N.L., Stern, J.S., Teff, K. & Havel, P.J. 2002. Fructose, weight gain, and the insulin resistance syndrome: a review. *The American Journal of Clinical Nutrition*, 76(5):911-922.

Engels, M., Wang, C., Matoso, A., Maidan, E. & Wands, J. 2013. Tea not tincture hepatotoxicity associated with rooibos herbal tea. *ACG Case Reports Journal*, 1(1):58.

Falcão, V.T.F., Maschio, D.A., de Fontes, C.C., Oliveira, R.B., Santos-Silva, J.C., Almeida, A.C.S., Vanzela, E.C., Cartaxo, M.T., Carvalho, C.P. & Collares-Buzato, C.B. 2016. Reduced insulin secretion function is associated with pancreatic islet redistribution of cell adhesion molecules (CAMs) in diabetic mice after prolonged high-fat diet. *Histochemistry and Cell Biology*, 146(1):13-31.

Farrell, G.C. & Larter, C.Z. 2006. Nonalcoholic fatty liver disease: from steatosis to cirrhosis: a review. *Hepatology*, 43(1):99-112.

Favero, G., Lonati, C., Giugno, L., Castrezzati, S., Rodella, L.F. and Rezzani, R., 2013. Obesity-related dysfunction of the aorta and prevention by melatonin treatment in ob/ob mice. *Acta histochemica*, *115*(8):783-788.

Fraulob, J.C., Ogg-Diamantino, R., Fernandes-Santos, C., Aguila, M.B. & Mandarim-de-Lacerda, C.A. 2010. A mouse model of metabolic syndrome: insulin resistance, fatty liver and non-alcoholic fatty pancreas disease (NAFPD) in C57BL/6 mice fed a high fat diet. *Journal of Clinical Biochemistry and Nutrition*, 46(3):212-223.

Gai, Z., Hiller, C., Chin, S.H., Hofstetter, L., Stieger, B., Konrad, D. & Kullak-Ublick, G.A. 2014. Uninephrectomy augments the effects of high fat diet induced obesity on gene expression in mouse kidney. *Biochimica et Biophysica Acta (BBA)-Molecular Basis of Disease*, 1842(9):1870-1878.

Greene, E. 1955. *Anatomy of the rat*. New York: Hafner publishing co.

Gupta, S. 2000. Hepatic polyploidy and liver growth control. *Seminars In Cancer Biology*, 10(3):161-171.

Hall, J., Brands, M., Henegar, J. & Shek, E. 1998. Abnormal kidney function as a cause and a consequence of obesity hypertension: a review. *Clinical and Experimental Pharmacology and Physiology*, 25:58-64.

Hanhineva, K., Törrönen, R., Bondia-Pons, I., Pekkinen, J., Kolehmainen, M., Mykkänen, H. and Poutanen, K., 2010. Impact of dietary polyphenols on carbohydrate metabolism. *International journal of molecular sciences*, 11(4),1365-1402.

He, M., Su, H., Gao, W., Johansson, S.M., Liu, Q., Wu, X., Liao, J., Young, A.A., Bartfai, T. & Wang, M.W. 2010. Reversal of obesity and insulin resistance by a non-peptidic glucagon-like peptide-1 receptor agonist in diet-induced obese mice. *PLoS One*, 5(12):e14205.

Himpe, E., Cunha, D.A., Song, I., Bugliani, M., Marchetti, P., Cnop, M. & Bouwens, L. 2016. Phenylpropenoic acid glucoside from rooibos protects pancreatic beta cells against cell death induced by acute injury. *PLoS One*, 11(6):1-13.

Huang, M., du Plessis, J., du Preez, J., Hamman, J. & Viljoen, A. 2008. Transport of aspalathin, a rooibos tea flavonoid, across the skin and intestinal epithelium. *Phytotherapy Research*, 22(5):699-704.

Hübsch, Z., van Vuuren, S.F. & van Zyl, R.L. 2014. Can rooibos (*Aspalathus linearis*) tea have an effect on conventional antimicrobial therapies? *South African Journal of Botany*, 93:148-156.

Huisamen, B., George, C., Genade, S. & Dietrich, D. 2013. Cardioprotective and anti-hypertensive effects of Prosopis glandulosa in rat models of pre-diabetes. *Cardiovascular Journal of Africa*, 24(2):10.

Jang, H. 2017. *High-fat diets for diet-induced obesity (DIO) models*: a review. New Jersey: Research diets incorporated.

Jesus, A.R., Vila-Viçosa, D., Machuqueiro, M., Marques, A.P., Dore, T.M. and Rauter, A.P., 2017. Targeting type 2 diabetes with C-glucosyl dihydrochalcones as selective sodium glucose co-transporter 2 (SGLT2) inhibitors: synthesis and biological evaluation. *Journal of medicinal chemistry*, *60*(2), pp.568-579.

Joubert, E. 1996. HPLC quantification of the dihydrochalcones, aspalathin and nothofagin in rooibos tea (*Aspalathus linearis*) as affected by processing. *Food Chemistry*, 55:403-411.

Joubert, E., Winterton, P., Britz, T. & Ferreira, D. 2004. Superoxide anion and α, α-diphenyl-beta-picrylhydrazyl radical scavenging capacity of rooibos (*Aspalathus linearis*) aqueous extracts, crude phenolic fractions, tannin and flavonoids. *Food Research International*, 37:133-138.

Joubert, E., Gelderblom, W., Louw, A. & de Beer, D. 2008. South African herbal teas: *Aspalathus linearis*, Cyclopia spp. & Athrixia phylicoides- A review. *Journal of Ethnopharmacology*, 119:376-412.

Joubert, E. & de Beer, D. 2011. Rooibos (*Aspalathus linearis*) beyond the farm gate: From herbal tea to potential phytopharmaceutical: a review. *South African Journal of Botany*, 77:869-886.

Jung, C.H., Cho, I., Ahn, J., Jeon, T.I. & Ha, T.Y. 2013. Quercetin reduces high-fat diet-induced fat accumulation in the liver by regulating lipid metabolism genes. *Phytotherapy Research*, 27(1):139-143.

Kamakura, R., Son, M.J., de Beer, D., Joubert, E., Miura, Y. & Yagasaki, K. 2015. Antidiabetic effect of green rooibos (*Aspalathus linearis*) extract in cultured cells and type 2 diabetic model KK-A y mice. *Cytotechnology*, 67(4):699-710.

Kawano, A., Nakamura, H., Hata, S.I., Minakawa, M., Miura, Y. & Yagasaki, K. 2009. Hypoglycaemic effect of aspalathin, a rooibos tea component from *Aspalathus linearis*, in type 2 diabetic model db/db mice. *Phytomedicine*, 16(5):437-443.

Kierszenbaum, A.L. & Tres, L. 2015. *Histology and Cell Biology: An Introduction to Pathology E-Book*. Phillidelpia: Elsevier Health Sciences.

Kim, A., Miller, K., Jo, J., Kilimnik, G., Wojcik, P. and Hara, M., 2009. Islet architecture: A comparative study: a review. *Islets*, *1*(2), pp.129-136.

Kleiner, D.E., Brunt, E.M., van Natta, M., Behling, C., Contos, M.J., Cummings, O.W., Ferrell, L.D., Liu, Y.C., Torbenson, M.S., Unalp-Arida, A. & Yeh, M. 2005. Design and validation of a histological scoring system for non-alcoholic fatty liver disease. *Hepatology*, 41(6):1313-1321.

Kotzé, P.C. 2015. Islet composition and architecture in streptozotocin-induced diabetic rat following pancreatic duct ligation. Unpublished masters thesis. Stellenbosch: Stellenbosch University.

Krafczyk, N. & Glomb, M. 2008. Characterization of phenolic compounds in rooibos tea. *Journal of Agricultural and Food chemistry*, 56:3368-3376.

Krafczyk, N., Heinrich, T., Porzel, A. & Glomb, M. 2009. Oxidation of the dihydrochalcone aspalathin leads to dimerization. *Journal of Agricultural and Food Chemistry*, 57:6838-6843.

Kreuz, S., Joubert, E., Waldmann, K.H. & Ternes, W. 2008. Aspalathin, a flavonoid in *Aspalathus linearis* (rooibos), is absorbed by the pig intestine as a C-glycoside. *Nutrition Research*, 690-701.

Kroukamp, M. 2018. The effect of chronic ingestion of Afriplex GRT™ on myocardial insulin resistance and mitochondrial function–a preclinical study. Unpublished masters thesis. Stellenbosch: Stellenbosch University.

Lannes, W.R., Miranda, A.C.D., Souza-Mello, V.D., Barbosa-da-Silva, S., Aguila, M.B. & Mandarim-de-Lacerda, C.A. 2015. La Lipogénesis Hepática y la Beta-Oxidación están Alteradas en las Crías de Madres Alimentadas con una Dieta Alta en Grasas en las Dos Primeras Generaciones (F1 y F2). *International Journal of Morphology*, 33(4):1510-1517.

Lee, J.S., Jun, D.W., Kim, E.K., Jeon, H.J., Nam, H.H. & Saeed, W.K. 2015. Histologic and metabolic derangement in high-fat, high-fructose, and combination diet animal models. *The Scientific World Journal*, 2015:1-9.

Lee, W. & Bae, J.P. 2015. Anti-inflammatory effects of aspalathin and nothofagin from rooibos (*Aspalathus linearis*) in vitro and in vivo. *Inflammation*, 38:1502-1516.

Lenoir, M., Serre, F., Cantin, L. & Ahmed, S.H. 2007. Intense sweetness surpasses cocaine reward. *PLoS One*, 2(8):1-10.

Levene, A.P., Kudo, H., Armstrong, M.J., Thursz, M.R., Gedroyc, W.M., Anstee, Q.M. & Goldin, R.D. 2012. Quantifying hepatic steatosis–more than meets the eye. *Histopathology*, 60(6):971-981.

Liles, J.H., Flecknell, P.A., Roughan, J. & Cruz-Madorran, I. 1998. Influence of oral buprenorphine, oral naltrexone or morphine on the effects of laparotomy in the rat. *Laboratory Animals*, 32(2):149-161.

Liu, L., Chao, G., Yao, P. & Gong, Z. 2015. Quercetin alleviates high-fat diet induced oxidized low-density lipoprotein accumulation in the liver: Implication for autophagy regulation. *BioMed Research International*, 2015:1-9.

Lozano, I., van der Werf, R., Bietiger, W., Seyfritz, E., Peronet, C., Pinget, M., Jeandidier, N., Maillard, E., Marchioni, E., Sigrist, S. & Dal, S. 2016. High-fructose and high-fat diet-induced disorders in rats: impact on diabetes risk, hepatic and vascular complications. *Nutrition and Metabolism*, 13(1):15.

Malarkey, D.E., Johnson, K., Ryan, L., Boorman, G. and Maronpot, R.R., 2005. New insights into functional aspects of liver morphology: a review. *Toxicologic pathology*, 33(1):27-34.

Manach, C., Williamson, G., Morand, C., Scalbert, A. & Rémésy, C. 2005. Bioavailability and bioefficacy of polyphenols in humans: a review. I. Review of 97 bioavailability studies. *The American Journal of Clinical Nutrition*, 81(1):230-242.

Maqeda, Z. 2018. Investigating the modulating effects of Afriplex GRT Extract on vascular function and antioxidant status in obese Wistar rat. Unpublished masters thesis. Stellenbosch: Stellenbosch University.

Marnewick, J.L., Joubert, E., Swart, P., van der Westhuizen, F. & Gelderblom, W.C. 2003. Modulation of hepatic drug metabolizing enzymes and oxidative status by rooibos (*Aspalathus linearis*) and honeybush (*Cyclopia intermedia*), green and black (*Camellia sinensis*) teas in rats. *Journal of Agricultural and Food Chemistry*, 51(27):8113-8119.

Marnewick, J.L., Rautenbach, F., Venter, I., Neethling, H., Blackhurst, D.M., Wolmarans, P. & Macharia, M. 2011. Effects of rooibos (*Aspalathus linearis*) on oxidative stress and biochemical parameters in adults at risk for cardiovascular disease. *Journal of Ethnopharmacology*, 133(1):46-52.

Marnewick, J. 2014. Antioxidant properties of rooibos (*Aspalathus linearis*)-*in vitro* and *in vivo* evidence. In I. Laher (ed.). *Systems biology of free radicals and antioxidants*. Berlin: Springer: 4083-4104.

Mathijs, I., Da Cunha, D.A., Himpe, E., Ladriere, L., Chellan, N., Roux, C.R., Joubert, E., Muller, C., Cnop, M., Louw, J. & Bouwens, L. 2014. Phenylpropenoic acid glucoside augments pancreatic beta cell mass in high-fat diet-fed mice and protects beta cells from ER stress-induced apoptosis. *Molecular Nutrition and Food Research*, 58(10):1980-1990.

Mazibuko, S.E., Muller, C.J.F., Joubert, E., de Beer, D., Johnson, R., Opoku, A.R. & Louw, J. 2013. Amelioration of palmitate-induced insulin resistance in C2C12 muscle cells by rooibos (*Aspalathus linearis*). *Phytomedicine*, 20(10):813-819.

Mazibuko, S.E., Joubert, E., Johnson, R., Louw, J., Opoku, A.R. & Muller, C.J. 2015. Aspalathin improves glucose and lipid metabolism in 3T3-L1 adipocytes exposed to palmitate. *Molecular Nutrition and Food Research*, 59(11):2199-2208.

Mehlem, A., Hagberg, C.E., Muhl, L., Eriksson, U. & Falkevall, A. 2013. Imaging of neutral lipids by Oil red O for analysing the metabolic status in health and disease. *Nature Protocols*, 8(6):1149.

Messier, C., Whately, K., Liang, J., Du, L. & Puissant, D. 2007. The effects of a high-fat, high-fructose, and combination diet on learning, weight, and glucose regulation in C57BL/6 mice: a review. *Behavioural Brain Research*, 178(1):139-145.

Monsees, T. & Opuwari, C. 2016. Effects of rooibos (*Aspalathus linearis*) on the female rat reproductive tract and liver and kidney functions in vivo. *South African Journal of Botany*, 110:208-215.

Morton, J. 1983. Rooibos tea, *Aspalathus linearis*, a caffeinless, low-tannin beverage: a review. *Economic Botany*, 37(2):164-173.

Muller, C.J.F., Joubert, E., de Beer, D., Sanderson, M., Malherbe, C.J., Fey, S.J. & Louw, J. 2012. Acute assessment of an aspalathin-enriched green rooibos (*Aspalathus linearis*) extract with hypoglycaemic potential. *Phytomedicine*, 20(1):32-39.

Muller, C.J., Joubert, E., Pheiffer, C., Ghoor, S., Sanderson, M., Chellan, N., Fey, S.J. & Louw, J. 2013. Z-2-(β-d-glucopyranosyloxy) -3-phenylpropenoic acid, an α-hydroxy acid from rooibos (*Aspalathus linearis*) with hypoglycaemic activity. (2012). *Molecular Nutrition and Food Research*, 57(12):2216-2222.

Muller, C.J., Malherbe, C.J., Chellan, N., Yagasaki, K., Miura, Y. & Joubert, E. 2018. Potential of rooibos, its major C-glucosyl flavonoids, and Z-2-(β-D-glucopyranosyloxy)-3-phenylpropenoic acid in prevention of metabolic syndrome: a review. (2017). *Critical Reviews in Food Science and Nutrition*, 58(2):227-246.

Netter, F. H., Hansen, J. T., & Lambert, D. R. (2005). Netter's clinical anatomy. Carlstadt, N.J., Icon Learning Systems.Noeman, S.A., Hamooda, H.E. & Baalash, A.A. 2011. Biochemical study of oxidative stress markers in the liver, kidney and heart of high fat diet induced obesity in rats. *Diabetology and Metabolic Syndrome*, 3(1):17.

Nolan, C.J., Damm, P. & Prentki, M. 2011. Type 2 diabetes across generations: from pathophysiology to prevention and management: a review. *The Lancet*, 378(9786):169-181.

Obesity and Overweight. 2018. [Online]. Available: http://www.who.int/en/news-room/fact-sheets/detail/obesity-and-overweight. [2017, May 22].

Oliveira, R.B.D., Carvalho, C.P.D.F., Polo, C.C., Dorighello, G.D.G., Boschero, A.C., Oliveira, H.C.D. and Collares-Buzato, C.B., 2014. Impaired compensatory beta-cell function and growth in response to high-fat diet in LDL receptor knockout mice. *International journal of experimental pathology*, *95*(4), 296-308.

Opuwari, C. & Monsees, T. 2013. In vivo effects of *Aspalathus linearis* (rooibos) on male rat reproductive functions. *Andrologia*, 46(8):867-877.

Organization for Economic Cooperation and Development (OECD). (2017). Obesity Update, 2017.

Ou, H.Y., Wang, C.Y., Yang, Y.C., Chen, M.F. & Chang, C.J. 2013. The association between non-alcoholic fatty pancreas disease and diabetes. *PLoS One*, 8(5):1-9.

Pantsi, W.G., Marnewick, J.L., Esterhuyse, A.J., Rautenbach, F. & van Rooyen, J. 2011. Rooibos (*Aspalathus linearis*) offers cardiac protection against ischaemia/reperfusion in the isolated perfused rat heart. *Phytomedicine*, 18(14):1220-1228.

Park, E.J., Lee, J.H., Yu, G.Y., He, G., Ali, S.R., Holzer, R.G., Österreicher, C.H., Takahashi, H. & Karin, M. 2010. Dietary and genetic obesity promote liver inflammation and tumorigenesis by enhancing IL-6 and TNF expression. *Cell*, 140(2):197-208.

Park, S., Park, N.Y., Valacchi, G. & Lim, Y. 2012. Calorie restriction with a high-fat diet effectively attenuated inflammatory response and oxidative stress-related markers in obese tissues of high-fat diet fed rats. *Mediators of Inflammation*, 2012:1-11.

Pellizon, M. & Ricci, M. 2018. The common use of improper control diets in diet-induced metabolic disease research confounds data interpretation: the fibre factor. *Nutrition and Metabolism*, 15(3):1-6.

Pereira, D.L., 2017. The effects of Rooibos (*Aspalathus linearis*) supplementation on the pancreas, liver, and kidney of male Wistar rats following antiretroviral treatment. Unpublished masters thesis. Stellenbosch: Stellenbosch University.

Perold, H. 2009. The influence of rooibos (*Aspalathus linearis*) on adrenal steroidogenic P450 enzymes. Unpublished masters thesis. Stellenbosch: Stellenbosch University.

Persson, I.A.L., Persson, K., Hägg, S. and Andersson, R.G., 2011. Effects of cocoa extract and dark chocolate on angiotensin-converting enzyme and nitric oxide in human endothelial cells and healthy volunteers–a nutrigenomics perspective. *Journal of cardiovascular pharmacology*, 57(1):44-50.

Petrova, A., 2009. Modulation of ultraviolet light-induced skin carcinogenesis by extracts of rooibos and honeybush using a mouse model: elucidating possible protective mechanisms. Unpublished masters thesis. Cape Town: Cape Peninsula University of Technology.

Pizzino, G., Irrera, N., Cucinotta, M., Pallio, G., Mannino, F., Arcoraci, V., Squadrito, F., Altavilla, D. & Bitto, A. 2017. Oxidative stress: harms and benefits for human health: a review. *Oxidative Medicine and Cellular Longevity*, 2017:1-13.

Quesada, I., Todorova, M.G. and Soria, B., 2006. Different metabolic responses in α-, β-, and δ-cells of the islet of Langerhans monitored by redox confocal microscopy. *Biophysical journal*, 90(7), 2641-2650.

Rahal, A., Kumar, A., Singh, V., Yadav, B., Tiwari, R., Chakraborty, S. & Dhama, K. 2014. Oxidative stress, prooxidants, and antioxidants: the interplay: a review. *BioMed Research International*, 1-19.

Reaven, G, Abbasi, F. and McLaughlin, T., 2004. Obesity, insulin resistance, and cardiovascular disease. *Recent progress in hormone research*, *59*, 207-224.

Reddi, A.S., Nimmagadda, V.R. & Arora, R. 2001. Effect of antihypertensive therapy on renal artery structure in type 2 diabetic rats with hypertension. *Hypertension*, 37(5):1273-1278.

Riccillo, F.L., Bracamonte, M.I., Console, G.M. and Gómez Dumm, C.L.A., 2004. Histomorphological and quantitative immunohistochemical changes in the rat pancreas during aging. *Biocell*, *28*(2), pp.127-134.

Ritchie, S.A. & Connell, J.M.C. 2007. The link between abdominal obesity, metabolic syndrome and cardiovascular disease: a review. *Nutrition, Metabolism and Cardiovascular Diseases*. 17(4):319–326.

Roberts, C.K. & Sindhu, K.K. 2009. *Oxidative stress and metabolic syndrome* : a review. Life Sciences, 84(21-22):705-712.

Rodríguez-Sanabria, F., Rull, A., Aragonès, G., Beltrán-Debón, R., Alonso-Villaverde, C., Camps, J. & Joven, J. 2010. Differential response of two models of genetically modified mice fed with high fat and cholesterol diets: relationship to the study of non-alcoholic steatohepatitis. *Molecular and Cellular Biochemistry*, 343(1-2):59-66.

Rogers, P.J., Hogenkamp, P.S., De Graaf, C., Higgs, S., Lluch, A., Ness, A.R., Penfold, C., Perry, R., Putz, P., Yeomans, M.R. & Mela, D.J. 2016. Does low-energy sweetener consumption affect energy intake and body weight? A systematic review, including meta-analyses, of the evidence from human and animal studies. *International Journal of Obesity*, 40(3):381.

Ruggiero, C., Ehrenshaft, M., Cleland, E. & Stadler, K. 2011. High-fat diet induces an initial adaptation of mitochondrial bioenergetics in the kidney despite evident oxidative stress and mitochondrial ROS production. *American Journal of Physiology-Endocrinology and Metabolism*, 300(6):1047-1058.

Sakuraba, H., Mizukami, H., Yagihashi, N., Wada, R., Hanyu, C. & Yagihashi, S. 2002. Reduced beta-cell mass and expression of oxidative stress-related DNA damage in the islet of Japanese Type II diabetic patients. *Diabetologia*, 45(1):85-96.

Sanderson, M., Mazibuko, S.E., Joubert, E., de Beer, D., Johnson, R., Pheiffer, C., Louw, J. & Muller, C.J. 2014. Effects of fermented rooibos (*Aspalathus linearis*) on adipocyte differentiation. *Phytomedicine*, 21(2):109-117.

Sasaki, M., Nishida, N. & Shimada, M. 2018. A Beneficial Role of Rooibos in Diabetes Mellitus: A Systematic Review and Meta-Analysis. *Molecules*, 23(4):839.

Saxena, R. 2010. Special stains in interpretation of liver biopsies. *Connection, Technical Articles*, 1:92-103.

Schloms, L., Storbeck, K.H., Swart, P., Gelderblom, W.C. and Swart, A.C., 2012. The influence of *Aspalathus linearis* (Rooibos) and dihydrochalcones on adrenal steroidogenesis: Quantification of steroid intermediates and end products in H295R cells. *The Journal of steroid biochemistry and molecular biology*, *128*(3-5): 128-138.

Schultz, A., Neil, D., Aguila, M.B. & Mandarim-de-Lacerda, C.A. 2013. Hepatic adverse effects of fructose consumption independent of overweight/obesity. *International Journal of Molecular Sciences*, 14(11):73-86.

Schulz, H., Joubert, E. & Schütze, W. 2003. Quantification of quality parameters for reliable evaluation of green rooibos (*Aspalathus linearis*). *European Food Research and Technology*, 216(6):539-543.

Sezik, E., Aslan, M., Yesilada, E. & Ito, S. 2015. Hypoglycaemic activity of *Gentiana olivieri* and isolation of the active constituent through bioassay direct fractionation techniques. *Life Science*, 76:1223-1238.

Sherwood, L. 2009. *Human physiology: From cells to systems*. 7th edition. USA: Brooks/Cole Publishing.

Shindo, Y. & Kato, K. 1991. Effect of rooibos tea on some dermatological diseases. Unpublished paper delivered at the International symposium on tea science, 26-29 August, Japan.

Shi, H., Yang, G., Zheng, T., Wang, J., Li, L., Liang, Y., Xie, C., Yin, D., Sun, B., Sun, J. and Wang, H., 2015. A preliminary study of ALPPS procedure in a rat model. *Scientific reports*, 5, 17567.

Singhi, A.D., Jain, D., Kakar, S., Wu, T.T., Yeh, M.M. & Torbenson, M. 2012. Reticulin loss in benign fatty liver: an important diagnostic pitfall when considering a diagnosis of hepatocellular carcinoma. *The American Journal of Surgical Pathology*, 36(5):710-715.

Sinsalo, M., Enkovaara, A.L. & Kivisto, K. 2010. Possible hepatotoxic effect of rooibos tea: a case report. *European Journal of pharmacology*, 66:427-428.

Slavin, B.G., Zarow, C., Warden, C.H. & Fisler, J.S. 2010. Histological, immunocytochemical, and morphometrical analyses of pancreatic islets in the BSB mouse model of obesity. *The Anatomical Record: Advances in Integrative Anatomy and Evolutionary Biology*, 293(1):108-116.

Smith, C. and Swart, A.C., 2016. Rooibos (*Aspalathus linearis*) facilitates an anti-inflammatory state, modulating IL-6 and IL-10 while not inhibiting the acute glucocorticoid response to a mild novel stressor in vivo. *Journal of Functional Foods*, *27:* 42-54.

Snijman, P.W., Swanevelder, S., Joubert, E., Green, I.R. & Gelderblom, W.C. 2007. The antimutagenic activity of the major flavonoids of rooibos (*Aspalathus linearis*): Some dose–response effects on mutagen activation–flavonoid interactions. *Mutation Research/Genetic Toxicology and Environmental Mutagenesis*, 631(2):111-123.

Son, M., Minakawa, M., Miura, Y. & Yagasaki, K. 2013. Aspalathin improves hyperglycaemia and glucose tolerance in obese ob./ob mice. *European Journal of Nutrition*, 52:1607-1619.

South African demographics survey. (2016). [Online]. Available: http://www.statssa.gov.za/?page_id=6634 [2018, May 14].

Stalmach, A., Mullen, W., Pecorari, M., Serafini, M. & Crozier, A. 2009. Bioavailability of C-linked dihydrochalcone and flavanone glucosides in humans following ingestion of unfermented and fermented rooibos teas. *Journal of Agricultural and Food Chemistry*, 57(15):7104-7111.

Steiner, J., Kim, A., Miller, K. & Hara, M. 2010. Pancreatic islet plasticity: interspecies comparison of islet architecture and composition: a review. *Islets*, 2(3):135-145.

Stemmer, K., Perez-Tilve, D., Ananthakrishnan, G., Bort, A., Seeley, R.J., Tschöp, M.H., Dietrich, D.R. & Pfluger, P.T. 2012. High-fat-diet-induced obesity causes an inflammatory and tumour-promoting microenvironment in the rat kidney. *Disease Models and Mechanisms*:dmm-009407.

Symington, B., Mapanga, R.F., Norton, G.R. & Essop, M.F. 2017. Resveratrol co-treatment attenuates the effects of HIV protease inhibitors on rat body weight and enhances cardiac mitochondrial respiration. *PLoS One*, 12(1):1-13.

The Heart and Stroke Foundation South Africa, 2016. [Online]. Available: http://www.heartfoundation.co.za/wp-content/uploads/2017/10/CVD-Stats-Reference-Document-2016-FOR-MEDIA-1.pdf. [2018, August 25]

Tobar, A., Ori, Y., Benchetrit, S., Milo, G., Herman-Edelstein, M., Zingerman, B., Lev, N., Gafter, U. & Chagnac, A. 2013. Proximal tubular hypertrophy and enlarged glomerular and proximal tubular urinary space in obese subjects with proteinuria. *PLoS One*, 8(9):e75547.

Ulicna, O., Greksak, M., Vancova, O., Zlatos, L., Galbavy, S., Bosek, P., Nakano, M. 2003. Hepatoprotective effect of rooibos tea (*Aspalathus linearis*) on CCL4-induced liver damage in rats. *Physiology Research*, 52:461-466.

Ulicna, O., Vancova, O., Bozek, P. & Carsky, J. 2006. Rooibos tea (*Aspalathus linearis*) partially prevents oxidative stress in streptozotocin-induced diabetic rats. *Physiological Research*, 55(2):157-164.

Ulicna, O., Vancova, O., Waczulikova, I., Bozek, P., Janega, P., Babál, P., Liskova, S. & Greksák, M. 2008. Does rooibos tea (*Aspalathus linearis*) support regeneration of rat liver after intoxication by carbon tetrachloride? *General Physiology and Biophysics*, 27(3):179-186.

Van der Heijden, R.A., Bijzet, J., Meijers, W.C., Yakala, G.K., Kleemann, R., Nguyen, T.Q., de Boer, R.A., Schalkwijk, C.G., Hazenberg, B.P., Tietge, U.J. & Heeringa, P. 2015. Obesity-induced chronic inflammation in high fat diet challenged C57BL/6J mice is associated with acceleration of age-dependent renal amyloidosis. *Scientific Reports*, 5:16474.

Van der Merwe, J.D., de Beer, D., Joubert, E. & Gelderblom, W.C. 2015. Short-term and sub-chronic dietary exposure to aspalathin-enriched green rooibos (*Aspalathus linearis*) extract affects rat liver function and antioxidant status. *Molecules*, 20(12):22674-22690.

Villaño, D., Pecorari, M., Testa, M.F., Raguzzini, A., Stalmach, A., Crozier, A., Tubili, C. & Serafini, M. 2010. Unfermented and fermented rooibos teas (*Aspalathus linearis*) increase plasma total antioxidant capacity in healthy humans. *Food Chemistry*, 123(3):679-683.

Wang L, Shuangni Yu, & Chan AWH. (2016). Pathology of Non-Alcoholic Fatty Liver Disease. *International Journal of Digestive Diseases*, 2(1). doi:10.4172/2472-1891.100014.

Warden, C. & Fisler, J. 2008. Comparisons of diets used in animal models of high fat feeding: a review. *Cell Metabolism*, 7(4):1-3.

Wedler, J., Daubitz, T., Schlotterbeck, G. & and Betterweck, V. 2014. *In vitro* anti-inflammatory and wound healing potential of a *Phyllostachys edulis* leaf extract- Identification of isoorietin as an active compound. *Planta Medica*, 80:1678-1684.

Wicks, S.E., Nguyen, T.T., Breaux, C., Kruger, C. & Stadler, K. 2016. Diet-induced obesity and kidney disease–In search of a susceptible mouse model. *Biochimie*, 124:65-73.

Williams, J.A. 2016. Regulation of Normal and Adaptive Pancreatic Growth: a review. Pancreapedia: Exocrine Pancreas Knowledge Base, 1-22. DOI: 10.3998/panc.2017.02.

Xia, N. & Li, H. 2016. The role of perivascular adipose tissue in obesity-induced vascular dysfunction: a review. *British Journal of Pharmacology*, 1(1):1-18.

Yagihashi, S. 2016. Diabetes and pancreas size, does it matter? *Journal of Diabetes Investigation*, 8(4):413-415.

Young, B., Woodford, P. & O'Dowd, G. 2013. *Wheater's Functional Histology E-Book: A Text and Colour Atlas*. Philadelphia: Elsevier Health Sciences.

Yu, T.Y. & Wang, C.Y. 2017. Impact of non-alcoholic fatty pancreas disease on glucose metabolism. *Journal of Diabetes Investigation*,1-13.

Zacharia, C. & Whitlatch, H. 2013. Rooibos herbal tea linked to hepatotoxicity and severe hypercholesteremia. Unpublished paper delivered at the Endocrine Society's 95th Annual Meeting and Expo, 15-18 June, San Francisco.

Zaitoun, A.M., Al Mardini, H., Awad, S., Ukabam, S., Makadisi, S. & Record, C.O. 2001. Quantitative assessment of fibrosis and steatosis in liver biopsies from patients with chronic hepatitis C. *Journal of Clinical Pathology*, 54(6):461-465.

ADDENDA

Addendum A: Outputs

Layman, J; Chellan, N; Huisamen, B; Kotzé, SH. 2018. The effect of Afriplex GRT™ on the histomorphology of the pancreas of high-fat diet fed rats. 62nd Annual Academic Year day, 29th August 2018, Stellenbosch University. Cape Town.

Addendum B: Materials

Table 1: Materials used in study.

Materials	**Company**
Animal feeds	
Rodent breeder feed (Control feed)	*Nutritionhub* (Pty) Ltd, Stellenbosch, South Africa
High-fat diet	
Rodent breeder feed 390 g	*Nutritionhub* (Pty) Ltd, Stellenbosch, South Africa
Condense milk	*Nestle™*
Cholesterol 10 g	*Merck*
Holsum cooking fat 400 g	*Animal Unit*
Casein 100 g	*Merck*
Boiling water 200 ml	-
Fructose 100 g	*Merck*
Afriplex GRT™ supplement	
Afriplex GRT™ extract powder	776295-36-4, *Afriplex* (Pty) Ltd
Jelly	Moirs
Gelatin	
Harvesting	
Blue top collection tubes	-
Gloves	-
Plastic Eppendorf tubes 1 mL	-
Scalpel	-
Scissors	-
Tweezers	-
Weighing boats	-
Electronic scale	-
Zip lock bags	-
Histology	
Aqueous mounting media	Kimix
Cover slips (24 x 32 mm)	-
Cover slips (24 x 50 mm)	-
Clear nail varnish	-
Double frosted glass microscope slides	Kimix, Cat: 7107
Embedding cassettes	SPL Lifesciences (Pty) Ltd Cas: 400600
Low profile microtome blades	Leica microsystems (Pty) Ltd, Germany
Paraffin wax (Embedding wax)	Leica Microsystems (Pty) Ltd Cat: 39602012
Plastic specimen jaws	SPL Lifesciences (Pty) Ltd Cas: 400600

Materials	**Company**
Positively charged microscope slides	Merck- (Pty) Ltd Cat no: S001
Moisture chamber	-
Reagents	
10% Formaldehyde	Merck (Pty) Ltd Cat: 47608
Acid Fuschin	Merck- (Pty) Ltd
Dextrin from potatoes starch	9004-53-9, Merck Chemicals, (Pty), Ltd
DPX mounting media	Associated Chemical Enterprises Batch: 30773
Eosin Yellowish	SAAR218600DC, Merck Chemicals (Pty) Ltd., Gauteng, South Africa
EnVision™ G/2 Double stain system, Rabbit/mouse (DAB+/Permanent red	K5361, *Dako*, Denmark, Inc
Ethanol 99%	Merck- Cas: 64-17-5
Ferrous sulphate	Merck- Cas: 127-03-55
Glacial Acetic acid	Merck- Cas: 10005706
Hydrogen Peroxide	Merck (Pty) Ltd, Modderfontein, Gauteng
Mayer's Haematoxylin	SAAR282201LC; Merck Chemicals (Pty), Ltd Gauteng
Monoclonal Anti-insulin	K5355, *Dako*, North America, Inc
Normal Goat Serum	-
Normal Horse Serum	-
Orange G	Merck Cas: 1936-15-8
Oil red O solution (0.2% isopropanol)	Merck chemicals (Pty), Ltd. 01391,
Oxalic acid	BDH Chemical Ltd Cat: 10174
Phosphate Buffer solution	Merck Cas: P5358
Periodic acid	Merck Cas: P7875
Phosphotungstic acid	Merck Cas: P4006
Polyclonal Anti-glucagon	*Dako*, North America, Inc. A0564,
Ponceau de xylidine	Merck- P2395
Potassium permanganate	BDH Chemicals, Cat: 10217
Schiff reagent	Science World Batch: 08-01-127
Silver nitrate	Merch chemicals Pty, Ltd Cat: 576 50 40 DC
Sodium hydroxide	Merck Cas: 8045
Strong ammonia (25%)	Merck Chemicals, Pty Ltd Wadeville, Gauteng
Sulfuric acid	Merck Cas: 339741
Tris Buffer solution	Merck Cas: T5912
Vector Laboratories ABC Kit	Vector Laboratories PK6100
Vector Laboratories ABC AP alkaline phosphatase mouse IgM kit	Vector Laboratories Ak-5010
Xylene	Merck Cas: 214736

Materials	**Company**
Histology machinery	
Axiocam 105	Carl Zeiss, AG, Oberkom, Germany
Embedding table	Leica EG 116 Embedder (SMM *instruments.* Johannesburg
Incubator	Model IH-150; Gallenkamp
Gilson pipettes 10, 100, 200 and 1000 µL	
Leica CM1850 UV Cryostat microtome	SMM instruments,
Leica Autostainer XL	Leica ST 5010; Serial number 1732/02.2007
Leica RM 2125 rotary microtome	Cat no. 045737989, SMM instruments, Germany
Nikon Eclipse T*i* Automated scanning microscope	*Nikon Instruments Inc*. Walt Whitman Road Melville. New York
Nikon Microscope camera	Nikon Digital Sight DS-Fic. *Nikon corporation*. Japan
Incubator (Oven)	Model: M53C. serial number 9513249
Tissue processor	Shandon Elliot Duplex Processor *OptoLaboratory*. Cape Town
Zeiss ® Axioskop 2 light microscope	Carl Zeiss, AG, Oberkom, Germany
Software used	
Nikon NIS Imaging Software v4.40	*Nikon Instruments Inc*. Copyright 1991-2015
ImageJ	*National institute of Health*
STEPanizer © stereology tool (2017) Version 1.8 jar	*Stephan Tschanz (2017)*
Statistica Version 13.2	Dell. 2014. USA
Zen (2012) blue edition Version 1.1.2.0 software	Carl Zeiss Microscopy. Oberkochen

Addendum C: Harvest procedure

Table 2: Description of tissue harvesting, storage and embedding.

Tissue	Method	Storage	Embedding
Pancreas	Once the pancreas was removed from its attachments in the abdominal cavity; it was weighed. The pancreas was halved, one portion was fixed in formalin and the other was snap frozen in liquid nitrogen	10% buffered formalin, screw cap container, room temperature Snap frozen in liquid nitrogen and stored in -80˚C freezer.	The excess fat was removed from the pancreas and the whole specimen was processed and embedded in wax blocks.
Liver	The liver was removed by severing its attachments in the abdomen. It was weighed, and the left lateral lobe was removed for processing to wax blocks. The middle lobe was excised for frozen liver sections.	10% buffered formalin, screw cap container, room temperature. Tissue was snap frozen in liquid nitrogen in zip lock packets and stored in -80˚C freezer.	Tissue was trimmed to fit into the cassette, processed and embedded in wax. Frozen tissue was cut, mounted with mounting media and allowed to freeze solid in liquid nitrogen before sectioning.
Kidney	The right kidney was removed from the animal and weighed. The kidney was cut in cross section and each half, halved once more so that four equal pieces were produced. The two middle halves were processed to wax blocks.	10% buffered formalin, screw cap container, room temperature.	Two halves of kidney were trimmed and placed in cassette for processing. The tissue was aligned in such a way that the inside of the kidney would be visible

Table 3: The location, number and stain used for the pancreas, liver and kidney.

Organ	Sample location	Fixative	Number of samples		Stains used
Pancreas		10% neutral buffered formalin	28	7 per group	H&E Anti-insulin and anti-glucagon labelling
		Liquid nitrogen	12	3 per group	Oil red O H&E
Liver	Left lateral lobe	10% neutral buffered formalin	28	7 per group	H&E Masson's Trichrome Gordon and Sweet's Reticulin impregnation
	Middle lobe	Liquid nitrogen	20	5 per group	Oil red O H&E
Kidney	Whole left kidney	10% neutral buffered formalin	28	7 per group	H&E Periodic acid Schiff

*

Addendum D: Green Rooibos supplement preparation and dosage calculation

Materials

- 5 ml Red jelly (Moir's)
- 10 ml Gelatin
- 35 ml water
- 600 mg aspalathin enriched green rooibos extract powder (Afriplex)

Methods

- Dissolve 4 g of strawberry jelly and 4 g of gelatine in 25 ml of boiling water
- Determine the dosage of Afriplex GRT™ per animal and add to mixture.
- Place the mixture on a magnetic stirrer to ensure it does not set.
- Use a repetitive pipet to transfer 1 ml of the mixture into an ice-block container and allow it to set.
- Keep the jelly blocks refrigerated in sealed containers protected from light.

Dosage (Adapted from Maqeda, 2018)

Each animal was given Afriplex GRT™ according to their average body mass per week. Each dose had a concentration of 60 mg per kg body mass per day.

For example:

If the rat weighed 275 g, their mass was multiplied by the concentration of Afriplex GRT™ (60 milligrams per kilogram body mass) and divided by 1000 (to cancel out the kilogram). This value was then multiplied by the total volume of Afriplex GRT™ required per week. The value in milligram per milliliter will be the amount to add to the jelly mixture

$$\frac{275\ g\ body\ mass\ of\ animal\ X\ 60\ mg\ Afriplex\ GRT(TM)}{1000} X\ 25\ ml$$

Addendum E: Afriplex GRT™ high performance liquid chromatography polyphenol analysis and certificate of analysis

Table 4: Afriplex GRT™ high performance liquid chromatography polyphenol analysis.

Nq: not quantifiable

[compound] (g compound/ 100 g Soluble Solids)	
Phenylpyruvic acid-2-Oglucoside (PPAG)	0.423265
Aspalathin	12.78348
Nothofagin	1.974419
Isoorientin	1.427281
Orientin	1.255839
Ferulic acid	nq
Vitexin	0.338513
Isovitexin	0.298022
Quercetin-3- robinobioside	1.040565
Hyperoside	0.398773
Rutin	0.496034
Isoquercitin	0.572251852

Afriplex PHARMACEUTICALS

CERTIFICATE OF ANALYSIS

Product Name: Afriplex GRT Extract
Product Code: CPE--03287
Product Batch Number: 730330
Product Manufacturing date: September 2015
Product Expiry Date: August 2017

CHARACTERISTIC	SPECIFICATION	RESULTS
Analytical parameters		
Definition	Needle-like leaves and fine stems	Conforms
Characteristics	Reddish brown fine powder. Aroma is typical to Rooibos	Conforms
Appearance	Appearance complies	Conforms
Identification (FT-IR)	≥ 95.00 %	First Reference
Loss on Drying	≤ 5.0 % (m/m)	2.2 % (m/m)
Bulk Density	0.20 - 0.45 g/ ml	0.32 g/ ml
Extract Yield	> 15 % (g/ 100g)	16.84 %
Soluble Solids content	> 2 % (g/ 100g)	2.12 %
Aspalathin Content	> 15 % (g/ 100g)	12.36 %
Pesticides	Meets Ph. Eur. requirements	Conforms
Heavy Metal parameters		
Heavy Metals	≤ 10 ppm	Conforms
Cadmium	≤ 1.0 ppm	< 0.01 ppm
Lead	≤ 3.0 ppm	0.07 ppm
Mercury	≤ 0.1 ppm	0.02 ppm
Arsenic	≤ 1.0 ppm	0.09 ppm
Microbial parameters		
Total aerobic count	< 2 000 cfu/ g	65 cfu/ g
Total combined yeast and mould count	< 100 cfu/ g	No growth
Escherichia coli	Absent/ g	No growth
Coliforms	Absent/ g	No growth
Salmonella	Absent/ 25 g	Absent

STORAGE REQUIREMENTS
Store in a cool dry place protected from temperature extremes and direct light.

PAARL, 23 September 2015

Quality Control Department

Figure 1: Certificate of analysis of Afriplex GRT™ extract.

Addendum F: Tissue processing

Methods

After 36-48 hours in neutral buffered formalin the tissue was processed using the Shannon Eliot Duplex automatic tissue processor (Opto Laboratory, Cape Town) for 12 hours according to the following protocol.

- Tissue was trimmed and placed into labelled plastic embedding cassettes with metal lids.
- Cassettes placed into processing basket and into the machine.

Table 5: Automated tissue processing protocol.

Step	Solution	Time (min)	Temperature (ºC)
1	70% Ethanol	30	40
2	80% Ethanol	30	40
3	95% Ethanol	45	40
4	95% Ethanol	45	40
5	100% Ethanol	45	40
6	100% Ethanol	45	40
7	100% Xylene	45	40
8	100% Xylene	45	40
9	Paraffin	30	58
10	Paraffin	30	58
11	Paraffin	30	58
12	Paraffin	30	58

Addendum G: Hematoxylin and eosin (H&E) staining procedure

The H&E stain was done using the Leica Autostainer XL (Leica ST5010, 1732/07.2007). The slides were placed into a plastic rack and then into the autostainer. A pre-programmed procedure was followed as shown below.

- Remove slides from the incubator
- Place slides into a plastic staining rack
- Place rack into autostainer
- Start the autostainer

Table 6: Automated H&E staining protocol using the Leica Autostainer XL.

Step	Solution	Time (minutes)	Repetitions
1	Xylene	10	2
2	Ethanol (99%)	5	2
3	Ethanol (96%)	2	1
4	Ethanol (70%)	2	1
5	Distilled water	5 sec	1
6	Hematoxylin	8	1
7	Running water	5	1
8	Ethanol (1% acid alcohol)	30 sec	1
9	Running water	1	1
10	Ammonia (0.2%)	45 sec	1
11	Running water	5	2
12	Ethanol (96%)	10 dips	1
13	Eosin	45 sec	1
14	Ethanol (96%)	5	2
15	Xylene	5	2

Addendum H: Double antibody labelling protocol

Double Antibody labelling was performed as per the protocol by the South African Medical Research Council Biomedical Research and Innovation Platform): **SOP No: ICC\B7-V01.**

Additionally, the following standard operating procedures were followed:

- ICC\B8-V01 Vectastain Kit
- ICC\B14-V01 0.05M Tris Buffered Saline pH7.2
- ICC\B9-V01 Biotinylated Mouse Anti-IgG
- ICC\B16-V01 Normal Goat Serum
- ICC\B17-V01 Normal Horse Serum
- ICC\B18-V01 0.1M Phosphate Buffered Saline pH7.2
- ICC\B20-V01 Polyclonal Anti-Glucagon
- ICC\B17-V01 Monoclonal Anti-Insulin
- ICC\B27-V01 Liquid DAB+ Substrate Chromagen System
- ICC\B26-V01 Envision G/2 System/AP, Rabbit/Mouse Kit

Table 7: List of reagents used for Double antibody labelling.

Reagents	**Quantity**
Polyclonal Anti-glucagon (rabbit) 1:100	1 µL anti-glucagon + 99 µL 0.1 M PBS = 100 µL/slide
Biotinylated Goat Anti-Rabbit IgG	11.25 µL made up to 2.5 mL 0.05 M TBS pH 7.2
Vectastain ABC Kit	5 mL distilled water + 1 drop A and 1 drop B
DAKO Liquid DAB+ Chromogen	1 mL substrate buffer + 1 drop DAB chromogen=100 µL/slide/10x
Monoclonal Anti-Insulin (mouse) 1:1 000	5 µL 1:50 anti-insulin + 95 µL 0.1 M PBS = 100 µL/slide
DAKO Envision Kit	
Rabbit/Mouse Link	100 µL/slide
AP Enzyme (ENHANCER)	100 µL/slide
Permanent Red Chromogen Substrate Working Solution	10 µL permanent red chromogen + 1 000 µL permanent red substrate buffer = 100 µL/slide (10 slides)

Table 8: Double antibody labelling protocol.

Double antibody labelling protocol: anti-glucagon and anti-insulin			
Step	**Description**	**Time (minutes)**	**Temperature**
1	Dewax sections through xylene and alcohol to water	-	RT
2	Rinse slides in staining jar with distilled water	-	RT
3	Block tissues for endogenous peroxidase with a 3% hydrogen peroxide (H2O2)	5	RT
4	Rinse slides with 0.05 M TBS pH 7.2	5	RT
5	Dry around the section		RT
6	Add 1:20 dilution of normal goat serum (NGS) to slides in a moisture chamber	20	RT
7	Blot excess serum	-	RT
8	Add 100 µL anti-glucagon primary antibody 1:100 to sections in a moisture chamber	30	RT
9	Jet wash with 0.05 M TBS pH 7.2 and rinse in staining jar in 0.05 M TBS pH 7.2	5	RT
	Make up Biotinylated Anti-Rabbit igg and Vectastain)	-	RT
10	Dry around sections and add Biotinylated Anti-Rabbit IgG 1:200 to slides in moisture chamber	30	RT
11	Jet wash with 0.05 M TBS pH 7.2 and rinse in staining jar in 0.05 M TBS pH 7.2	10	RT
12	Dry around sections and add Vectastain to slides in moisture chamber	60	RT
13	Jet wash slides with 0.05 M TBS pH 7.2 and rinse in 0.05 M TBS pH 7.2 in staining jar.	10	RT
14	Dry around sections and add Liquid DAB + Chromogen solution to slides on a rack over the sink	5	RT
15	Jet wash slides with distilled water and rinse with distilled water in a staining jar	5	RT
16	Rinse slides in 0.05 M TBS pH 7.2 in staining jar	5	RT
17	Dry around section and add normal horse serum (NHS) 1:20 to slides in a moisture chamber	20	RT
18	Blot excess serum	-	RT
19	Add 100 µL anti-insulin 1:10 000 to sections in moisture chamber	Overnight	4 ºC
20	Remove slides from the refrigerator and allow slides to reach room temperature	-	RT
21	Jet wash with 0.05 M TBS pH 7.2 and rinse in staining jar in 0.05 M TBS pH 7.2	5	RT
22	Dry around sections and add 100 µL Rabbit/Mouse (LINK) to slides in moisture chamber	30	RT
23	Jet wash with 0.05 M TBS pH 7.2 and rinse in staining jar in 0.05 M TBS pH 7.2	10	RT
24	Dry around sections and add 100 µL AP Enzyme (ENHANCER) to slides in moisture chamber	30	RT
25	Jet wash slides with 0.05 M TBS pH 7.2 and rinse in 0.05 M TBS pH 7.2 in staining jar.	10	RT

Step	**Description**	**Time (minutes)**	**Temperature**
26	Dry around sections and add Substrate Working Solution to slides on a rack Check progress under microscope. Carcinogenic wear gloves.	3-5	RT
27	Jet wash slides with distilled water and rinse in distilled water in staining jar	5	RT
28	Counterstain with haematoxylin	2-4	RT
29	Rinse well in tap water and leave to blue in tap water	30	RT
31	Dry completely on paper towel (section facing upwards)	-	RT
32	Mount slides in DPX	-	RT

Results	**Label**
α-cells	Brown
β-cells	Red/pink
Tissue	Blue/purple

Controls

Method control- Kidney tissue from a unrelated study (same fixative)

External control-pancreas tissue unrelated study

Internal control- pancreas tissue from control group

Addendum I: Oil red O staining procedure (adapted from Bancroft and Gamble., 2008)

Frozen liver and pancreas sections were stained with Oil red O stain to determine lipid accumulation. Oil red O demonstrates neutral lipids in fresh or frozen tissue and generally stains lipids orange-red (Saxena, 2010). Serial sections were prepared on positively charged microscope slides and stained with Oil Red O in dextrin for 20 minutes. Lastly, they were counterstained with 50% crystal violet for 1 minute. The Oil Red O stains makes it possible to identify lipid deposits in the tissue and the fatty accumulation may be quantified based on colour intensity using specialized morphometric techniques. Additionally, an H&E stain was done on frozen sections to assist in the identification and morphometry of the tissue. For optimum images, photographs need to be taken within 24-hours, but the stain is stable for up to three months.

Table 9: Solutions used for Oil red O staining procedure.

Solutions	Quantity
Oil Red O solution	
Oil red O	0.9 g
Absolute isopropyl alcohol	180 ml
Stir and leave overnight	
Dextrin solution	
Dextrin	1.2 g
Distilled water	120 ml
Working solution	
Oil Red O solution	180 ml
Dextrin solution	120 ml
Allow to stand for a day or more. Stable for months, filter before use.	

Table 10: Protocol used for Oil red O staining.

Step	**Description**	**Time (minutes)**	**Temperature**
1	Remove the slides from the refrigerator and rest to each room temperature	-	(-4 ºC) to (±25 ºC).
2	Pack the slides in a staining rack and stain in Oil Red O-Dextrin for	20	RT
3	Rinse the slides in running tap water until water is clear.	2-3	RT
4	Stain the slides in 50% Crystal violet	1	RT
5	Rinse the slides in running tap water until water is clear.	2-3	
6	Air dry the slides until most of the water has run off.		
7	Apply coverslips to the slides with aqueous mounting media		
8	Seal the edges of the coverslip with clear nail varnish and allow to dry.		
9	For optimum analysis slides should be analysed within 24-hours but this stain has been found to be stable ±3 months after which significant colour leaching is seen.		
10	Warning: Do not expose the slides to alcohol, xylene or DPX as it will leach out the Oil red O stain as it digests fat.		

Results of Oil red O	**Label**
Lipids	Orange-red
Nuclei and tissue	Blue purple

Furthermore, a manual H&E protocol was used on frozen tissue to assist morphological identification at the same tissue level. Tissue was mounted on positively charged microscope slides, fixed in 10% neutral buffered formalin (NBF) for 10 minutes and stained with haematoxylin for 10 minutes. The slides were rinsed and soaked in water. Subsequently, they were stained with eosin for two minutes. Lastly, the tissue was rehydrated to xylene and mounted with DPX.

Controls

Method control- liver tissue from unrelated study

External control -intraperitoneal fat attached to muscle

Internal control -tissue from control study group

Addendum J: Masson's trichrome

Masson's trichrome stain was performed to assess the degree of fibrosis within the liver.

Table 11: Masson's trichrome stain.

Solutions	Reagents	Quantity
Acetic acid water	Glacial acetic acid	2 ml
	Distilled water	1000 ml
Masson Fuchsin Ponceau-Orange G (MFPOG)(Stock solution)	Ponceau de Xylidine (Ponceau Red)	2 g
	Acid Fuchsin	1 g
	Orange-G	2 g
	Acetic acid water (Working solution)	300 ml
Working solution MFPOG	MFPOG	10 ml
	Acetic acid water	90 ml
Light Green solution 0.1%	Light Green	0.1 g
	Acetic acid water - 100 ml	100 ml
5% Phosphotungstic acid	Phosphotungstic acid	5 g
	Distilled water	100 ml

Table 12: Staining procedure for Masson's trichrome.

Step	**Description**	**Time (minutes)**
1	Deparaffinize sections (Xylene x2, graded alcohols 99, 96 & 70% twice each). Wash in tap water. Place in distilled water.	
2	Stain with Mayers Haematoxylin.	5
3	Place in tap water for 3 minutes until dark blue.	3
4	Rinse in distilled water.	
5	Stain the sections in Fuchsin Ponceau-orange G solution	15
6	Rinse in acetic acid water.	
7	Immerse in 5% phosphotungstic acid solution	5
8	Rinse in acetic acid water.	1
9	Stain in light green solution.	20
10	Treat with acetic acid water	5
11	Dehydrate as usual.	
12	Mount coverslip with DPX.	
	Results	**Label**
	Nuclei	Purple black
	Parenchyma	Orange red
	Collagen	Green blue

Controls

Method control- liver tissue unrelated study (same fixative)

External control skin

Internal control-tissue from control study group

Addendum K: Gordon and Sweet's silver impregnation protocol (Adapted from Bancroft & Gamble., 2008

The Gordon and Sweet's stain was used on liver tissue to evaluate the structural integrity.

Table 13: Gordon and Sweet's staining solutions

Solutions.	**Quantity**
Acidified Potassium permanganate XE	
0.5% Potassium permanganate	95 mL
3% Sulphuric acid	5 mL
Silver solution	
10% Aqueous silver solution	5 ml
Ammonia	Drop
3% sodium hydroxide	5 ml
Make up 5 mL of 10% aqueous silver nitrate. Add strong ammonia drop by drop until the precipitate is just dissolved. Add 5 mL of 3% sodium hydroxide. Then add strong ammonia drop by drop until the resulting precipitate is almost completely dissolved. Make up to 50 mL using distilled water then pour into a clean coplin staining jar. NOTE: If too much ammonia is added there is a great loss of sensitivity.	
2% aqueous oxalic acid	
Oxalic acid (analytical)	2 g
Distilled water	100 mL
Light green solution 0.1%	
Light green	0.1 g
Acetic acid water 0.2%	100 mL
4% aqueous iron alum	
Iron alum (Ferric ammonium sulphate)	4 g
10% formalin	
Formaldehyde 40 g/L	10 mL
Distilled water	90 mL
Sodium thiosulphate (HYPO)	
Sodium thiosulphate	2 g
Distilled water	100 mL

Table 14: Gordon and Sweet's staining procedure.

Step	**Description**	**Time (minutes)**	**Temperature**
1	Dewax tissues from xylene, through alcohols to water		RT
2	Oxidize in acidified potassium permanganate	3	RT
3	Rinse with distilled water		RT
4	Decolorize with 2 % oxalic acid	1	RT
5	Rinse with distilled water		RT
6	Mordant with 4 % iron alum	10	RT
7	Rinse with distilled water		RT
8	Impregnate in ammonical silver solution	11 seconds	RT
9	Rinse quickly with distilled water		RT
10	Reduce with 10 % aqueous formalin		RT
11	Wash with tap water	2	RT
12	Rinse in distilled water		RT
13	Fix 2 % aqueous sodium thiosulphate	2	RT
14	Wash with water	2	RT
15	Counterstain with light green solution	30 seconds	RT
16	Rehydrate with alcohols (5 dips each) to xylene (2 minutes) and coverslip with DPX		RT

Results	**Label**
Reticulin fibres	Black
Parenchyma	Green

Controls

External control -skin

Internal control- control tissue from the control study group

Addendum L: Periodic acid Schiff stain

Table 15: Periodic acid Schiff staining solutions.

Solutions.		**Quantity**
0.5% Periodic acid solution		
	Periodic acid	0.5 g
	Distilled water	100 mL
Schiff solution		Drop wise
Mayer's Haematoxylin		Counterstain

Table 16: Periodic acid Schiff staining protocol.

Step	**Description**	**Time (minutes)**	**Temperature**
1	Deparaffinize and hydrate to water		RT
2	Oxidize tin 0.5% periodic acid solution	5	RT
3	Rinse in distilled water		RT
4	Cover each section with Schiff reagent (tissue becomes light pink in colour)	15	RT
5	Wash in lukewarm water (tissue sections turn a dark pink colour)	5	RT
6	Wash tissue sections in running tap water	5	RT
7	Dehydrate and mount using DPX mounting medium		RT
Results:			**Stain**
Glycogen. mucin and basement membranes			Magenta
Nuclei			Purple
Cytoplasm			Pink

Schiff Reagent viability.

To test Schiff reagent, pour 10 mL of 37% formalin into a watch glass. Using a pasteurized plastic pipette add a few drops of Schiff reagent. Schiff will rapidly turn a red-purple colour if useable. If colour change happens over a longer period of time, this indicates a deteriorating Schiff reagent. The colour produced will be a dark blue-purple.

Controls

Method control- kidney from an unrelated study (same fixative)

External control Colon

Internal control- tissue from study control group

Addendum M: Macros produced to perform automated and semi-automated analysis of the tissues using ImageJ.

Pancreas

Pancreatic section area

```
run("RGB Stack");
//Trace whole Islet
waitForUser
run("Measure");
```

Islet, α- cell and B-cell areas

```
//Trace whole Islet
waitForUser
run("Measure");
run("RGB Stack");
//Measure alpha area
run("Threshold...");
waitForUser("set the threshold and press OK, or cancel to exit macro");
// pauses the execution and lets you access ImageJ manually
 // as long as you don't press OK, which resumes the macro execution
run("Measure");
//Measure beta cell area
//Trace beta cell area
run("Threshold...");
waitForUser("set the threshold and press OK, or cancel to exit macro");
run("Measure");
```

Liver

Image processing (Area of steatosis)

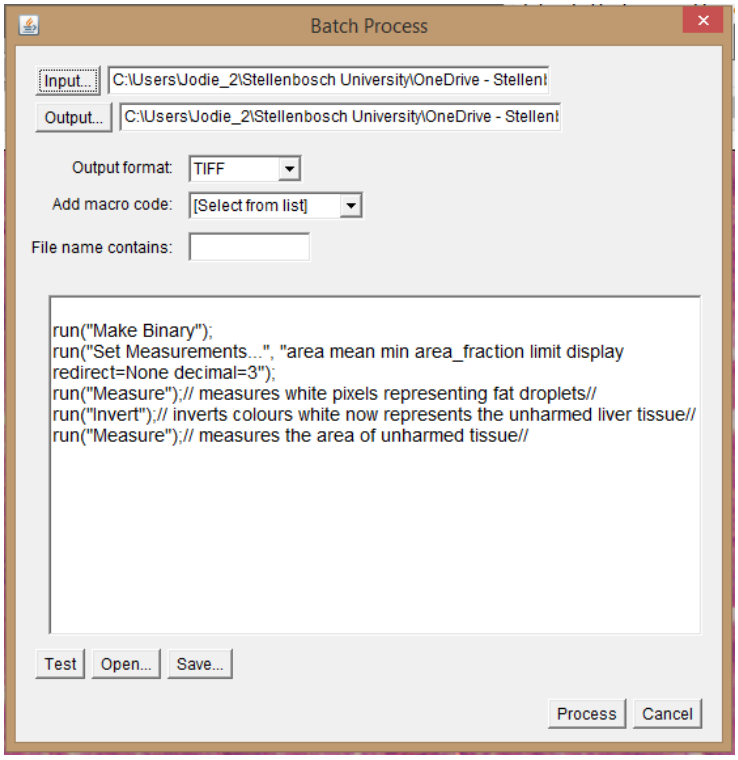

Addendum N: Randomization technique for the pancreas, liver and kidney

Pancreas

All pancreatic islets which were completely in view were analysed.

As tissue differences existed due to sharing of the tissue for molecular and physiological tests. To control for this, an equal number of pancreatic islets was analysed per group (n=400). Tod determine this, the data per animal was moved to a new Microsoft Excel spreadsheet. Pancreatic islets which lacked α- cells or B-cells were excluded. Thereafter, if groups had more than 400 islets, a random number generator was applied to each group. This was done by assigning numbers to each pancreatic islet which fell within the criteria. Fifty-seven numbers were randomly produced by the random number generator, selected and transferred to a new spreadsheet. Means were determined per group where after statistical analysis was performed.

Liver

- The liver tissue section was macroscopically divided into four regions by five parallel lines 4 mm apart (Figure 4.6).
- Three images per region were captured and stored in a single folder
- Randomly every second image was selected and moved to a new folder until 10 images per animal were selected.

Kidney

- Once the kidney was photographed using the Nikon system (Table 4.2) all images were stored in a single file.
- Images containing glomeruli were selected and moved to a new folder.
- Every fourth image was selected, and measurements of the glomeruli, Bowman's capsule and proximal convoluted tubules was completed.
- glomeruli were rejected if:
    - Not surrounded by three similar proximal convoluted tubules
    - Not completely in view (cut by image borders)

Addendum O: Supplementary statistical analysis

Table 17: Body and organ mass

Mean	C	GRT	HFD	HFD-GRT	One-way ANOVA	Two-way ANOVA
					p-value	p-value**
Body mass	354.21±19.76	319.71±7.95	365.86±20.02	310.43±12.12		
Pancreas mass	0.86±0.2	0.51±0.047	0.74±0.15	0.44±0.04		
Liver mass	10.93±0.68	9.65±0.17	15.47±0.97	11.51±0.64		
Kidney mass	1.05±0.05	0.87±0.02	0.95±0.03	0.79±0.04		

***Values based on a one-way ANOVA between groups**

****Values based on two-way ANOVA between treatment & diets**

Pancreas

Table 18: Supplementary statistical analysis of the pancreas (Mean ± standard error of the mean).

Mean	**C**	**GRT**	**HFD**	**HFD-GRT**	**Two-way ANOVA** **p-value****
Section area	69573594±4187661[a]	52941171±7561923[ab]	40938268±8439985[b]	33252298±4225573[b]	0.058(T) 0.012(D) 0.356 (D*T)
Islet area	12236.12 ±1588.94	12498.84 ±964.15	10875.19 ±959.11	7302.47±1168.88	0.18(T) 0.01(D) 0.12(D*T)
B-cell area	6475.97±974.27	6461.62±437.10	5403.25±494.20	3588.24±820.97	0.21(T) 0.01(D) 0.22(D*T)
α- cell area	1031.28±140.87	1102.43±222.68	887.39±142.62	648.44±107.39	0.62(T) 0.068(D) 0.355(D*T)
Islet volume level 1	4.84±1.97	4.11±1.19	6.24±4.18	6.42±2.74	p=.01
Islet volume level 2	6.16±3.26	6.53±3.41	10.43±8.08	6.71±2.28	p=0.69
Islet volume level 3	4.92±2.34	3.54±1.31	5.30±4.62	6.58±2.45	p=0.00
Islets area (μm^2) per tissue section area (μm^2) (%)	0.019±0.004	0.053±0.028	0.038±0.013	0.024±0.004	0.55(T) 0.75(D) 0.14(D*T)
Islet number per tissue section area in mm^2	0.85±0.11	1.29±0.18	1.40±0.11	1.91±0.75	0.24(T) 0.151(D) 0.934(D*T)
α-cells (%)	12.83±1.21	12.84±1.22	13.52±1.46	15.69±1.55	0.21(T) 0.43(D) 0.44(D*T)
β-cells (%)	72.91±3.82	69.72±2.34	74.81±1.51	69.47±3.72	0.21(T) 0.43(D) 0.44(D*T)

α-cells per islet area (%)	8.58±0.67	8.59±1.32	8.23±1.22	9.22±1.05	0.65(T) 0.90(D) 0.66(D*T)
β-cells per islet area (%)	52.83±3.07	49.87±3.05	52.64±2.35	46.23±4.00	0.55(T) 0.15(D) 0.60(D*T)
α-cells per β-cells (%)	16.43±1.51	17.19±3.09	17.21±3.13	20.53±2.46	0.44(T) 0.44(D) 0.63(D*T)

Supplementary data for the liver

Table 19: Supplementary statistical analysis of the liver

Mean	**C**	**GRT**	**HFD**	**HFD-GRT**	**p-value**
Volume of steatosis: fat points H&E	0.19±0.06	0.13±0.04	22.37±1.86	16.71±1.82	0.037(T) 0.000(D) 0.041(D*T)
Volume of steatosis H&E	0.05±0.048	0.003±0.001	0.62±0.052	0.46±0.050	0.02(T) 0.00(D) 0.22(D*T)
Volume of steatosis: fat points: Oil red O	1.24±0.34	1.82±0.61	30.77±1.33	25.74±2.12	0.11(T) 0.00(d) 0.046(D*T)
Volume of steatosis Oil red O	0.034±0.009	0.050±0.017	0.85±0.036	0.715±0.0589	0.11(T) 0.00(D) 0.045(D*T)
Sinusoid area Image processing	39.79±3.51	42.96±3.98	0±0	0±0	0.56(T) 0.00(D) 0.56(D*T)
Fat area Image processing	0±0	0±0	49.07±3.14	50.94±4.17	0.72(T) 0.00(D) 0.72(D*T)
Tissue area Image processing	60.20±3.51	57.04±3.98	50.93±3.14	49.06±4.17	0.51(T) 0.03(D) 0.86(D*T)
Fat area Image processing	4.06±1.10	2.38±0.96	46.10±4.38	31.52±5.497	0.038(T) 0.000(D) 0.090(D*T)
Tissue area Image processing	95.94±1.10	97.61±0.96	53.90±4.37	68.47±5.50	0.037(T) 0.000(D) 0.090(D*T)

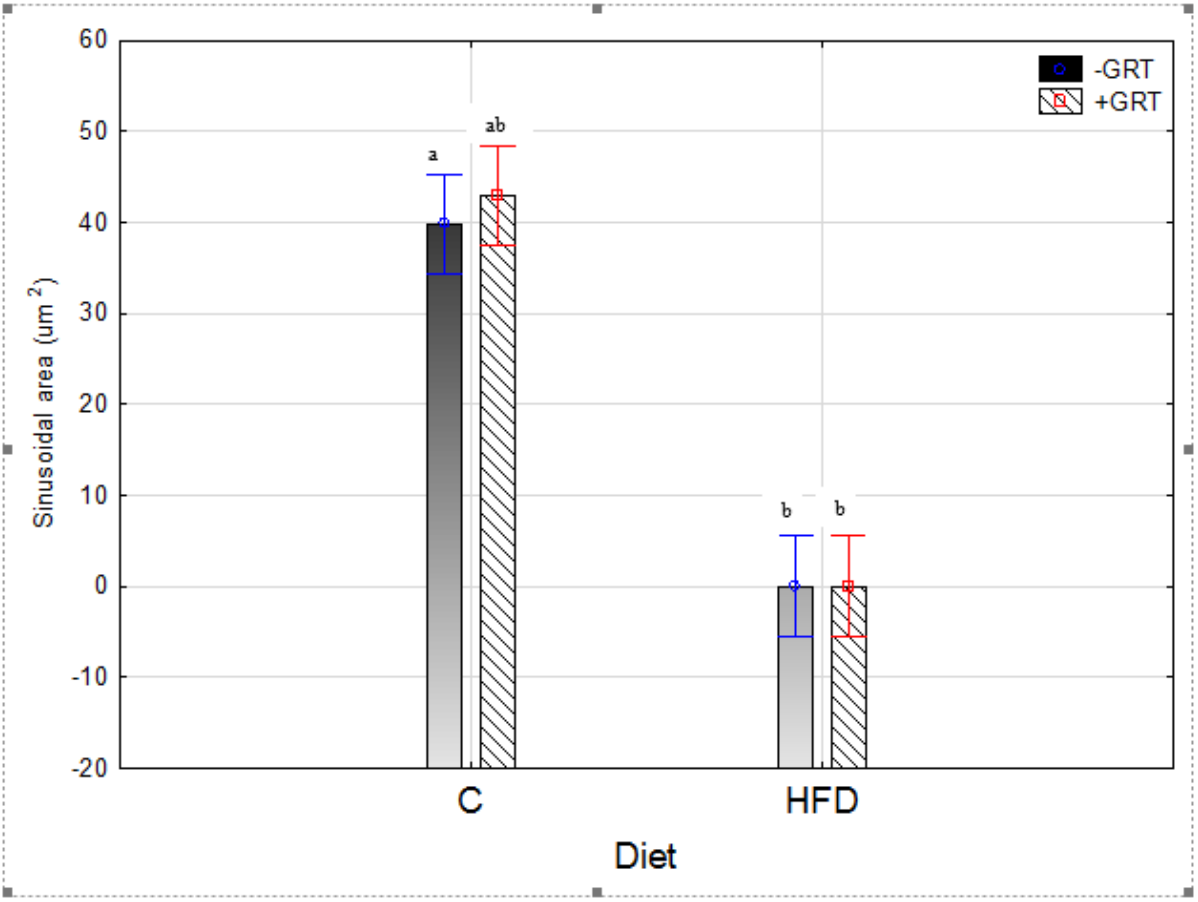

Figure 2: Liver sinusoidal area as determined using image processing.

On the H&E slides in the C- and GRT groups the sinusoid area is easily discernable as very little fat is present. The purpose of this graph is to account for the difference between tissue area and fat area which would be the sinusoidal area. Therefore, in the C- and GRT groups the sinusoids account for about 40-43% of the area while the hepatic tissue 60-67% accounts for the remainder.

Kidney

Table 20: Kidney supplementary data.

Mean	C	GRT	HFD	HFD-GRT	p-values
Glomerular area	7749.39±605.65	7272.31±658.53	7196.69±871.90	6303.47±571.61	0.33 0.28 0.76
Glomerular diameter	97.818±3.879	94.303±4.338	92.683±6.789	87.568±4.094	0.391 0.24 0.87
Glomerulus radius	48.91±1.94	47.15±2.17	47.08±3.59	44.15±2.23	0.37 0.36 0.82
Bowman's capsule area	10661.39±1415.71	8996.26±993.57	8848.55±1112.01	7610.39±744.40	0.20 0.16 0.85
Bowman's capsule diameter	114.03±7.57	104.15±6.60	102.39±8.12	96.07±4.82	0.241 0.16 0.79
Bowman's capsule radius	57.02±3.78	52.08±3.03	52.04±4.27	48.43±2.55	0.23 0.23 0.85
Renal space area	**2912.01±906.95**[a]	1723.95±414.53[ab]	1762.78±331.06[a b]	**1318.14±277.68**[b]	0.15 0.17 0.50
PCT outer area	**2766.99±377.85**[a]	2334.46±238.49[ab]	2375.12±303.16[a b]	**1941.00±155.33**[b]	0.14 0.17 0.99
PCT outer diameter	56.80±3.59	52.64±2.79	52.37±3.83	48.10±1.87	0.19 0.16 0.99
PCT outer radius	28.40±1.8	26.32±1.4	26.48±2.02	24.24±1.03	0.191 0.23 0.96
PCT luminal area	525.06±87.72	523.21±51.17	410.61±58.58	382.78±43.80	0.81 0.052 0.83
PCT luminal diameter	23.63±2.14	23.63±0.83	21.63±1.83	19.86±1.25	0.59 0.08 0.58
PCT luminal radius	11.76±1.05	11.82±0.42	10.85±0.93	10.02±0.64	0.63 0.10 0.57
PCT wall area	2241.94±299.03	1811.25±221.64	1964.51±246.81	1558.22±145.90	0.08 0.27 0.96
PCT wall diameter	33.18±1.77	29.01±2.737	30.73±2.18	28.23±1.95	0.14 0.47 0.71

Table 21: Histopathologist pancreas, liver and kidney evaluation.

		Pancreas						**Liver**										**Kidney**			
		Peripancreatic fat lymph nodule	Mononuclear cell infiltration	Interstitial interlobular oedema	Congestion	Exocrine and Endocrine **N**	Other	Hydropic degeneration/change	Hepatocyte swelling	Microvesicular vacuoles	Hematopoiesis	Vacuolar degeneration	Monocellular portal cell infiltration	Dilation of sinusoids-centriazonal	Proliferation of sinusoidal Kupffer cells	Dilation and duplication of central vein	Capillary canal formation	Renal tubular nephrosis	Intertubular oedema	Luminal proteinaceous material	Diffuse congestion
Control	Mean	1	0.333	0	0	0	0	1.7	0	0	0	0	0	0	1	1	1	1	0	0	1
	%	**1**	**33.33**	**0**	**0**	**33**	**0**	**33**	**0**	**0**	**0**	**0**	**0**	**0**	**100**	**100**	**67**	**33**	**0**	**0**	**100**
GRT	Mean	0	0.667	0	0	1	0	1.7	0	0	0	0	0	0.333	1	1	1	2	0	0	0.7
	%	**0**	**66.67**	**0**	**0**	**67**	**0**	**33**	**0**	**0**	**0**	**0**	**0**	**33.33**	**100**	**67**	**67**	**67**	**0**	**0**	**67**
HFD	Mean	0.67	0.333	0	0	1	0	4	1	0	1	0.667	0	0	0.67	0	0	2	0.67	0	1
	%	**66.67**	**33.33**	**33**	**0**	**67**	**0**	**80**	**67**	**0**	**100**	**66.67**	**0**	**0**	**66.67**	**33**	**0**	**67**	**66.67**	**0**	**100**
HFD-GRT	Mean	0.33	0.333	0	0	0	0	3	0	0	0.7	1	0	0	0	0	0	1	0	0	0.7
	%	**33.3**	**33.33**	**0**	**0**	**33**	**0**	**60**	**33**	**0**	**67**	**100**	**0**	**0**	**0**	**33**	**0**	**33**	**0**	**0**	**67**
p-value		**<0.05**	**n.s**	**n.s**	**n.s**	**n.s**	**n.s**	**<0.05**	**n.s**	**n.s**	**n.s**	**n.s**	**n.s**	**n.s**	**n.s**	**n.s**	**n.s**	**n.s**	**n.s**	**n.s**	**n.s**

*n.s= non-significant (statistically)

<0.05= statistically significant

Table 22: Non-alcoholic fatty liver disease activity score observers score sheet.

Study group	Scorer	Liver	Steatosis			Fibrosis	Inflammation				Hepatocyte ballooning
			Grade	Location	Microvesicular steatosis		Lobular	Microgranulomas	Large lipogranulomas	Portal	
Control	4	1363/16	0		0	0	0	0	0	0	0
	4	1381/16	0		0	0	0	0	0	0	0
	2	1537/16	0		0	0	0	0	0	0	0
	3	1557/16	0		0	0	0	0	0	0	0
	1	1533/16	0		0	0	0	0	0	0	0
	5	1541/16	0		0	0	0	0	0	0	0
	5	1385/16	0		0	1	1	0	0	1	0
GRT	1	1474/16	0		0	0	0	0	0	0	0
	4	1486/16	0		0	0	0	0	0	0	0
	2	1509/16	0		0	0	1	1	0	1	0
	1	1545/16	0		0	0	0	0	0	0	0
	2	1553/16	0		0	0	0	0	0	0	0
	2	1505/16	0	2	1	0	2	1	0	1	0
	4	1549/16	0		0	0	2	1	0	0	0
HFD	3	1330/16	3	2	1	0	3	1	1	1	2
	1	1338/16	2	2	1	0	2	0	1	1	2
	3	1396/16	1	2	1	0	0	0	0	0	0
	2	1521/16	3	3	1	0	2	1	1	1	2
	5	1529/16	3	2	1	1	2	1	1	1	2
	3	1400/16	3	2	1	0	3	1	0	0	2
	5	1525/16	2	2	1	0	0	1	1	1	1
HFD GRT	1	1513/17	2		1	0	2	0	1	0	1
	2	1478/16	3	3	1	0	3	1	1	1	2
	3	1517/16	2	1	1	0	2	1	0	0	2
	3	1569/16	1	1	1	0	1	1	0	0	1
	4	1466/16	3	2	1	0	2	1	1	1	2
	4	1561/16	3	2	1	0	1	1	1	0	2
	5	1565/16	2	2	1	1	3	1	0	1	1

*Observer number: Five observers including the investigator

Addendum P: Grading sheet provided to Non-alcoholic fatty liver disease scorers

NAS summary

Below is a summary of the main pathology topics you will score. Thereafter brief descriptions of each. Please read through thoroughly and if you have any questions please contact me.

Steatosis

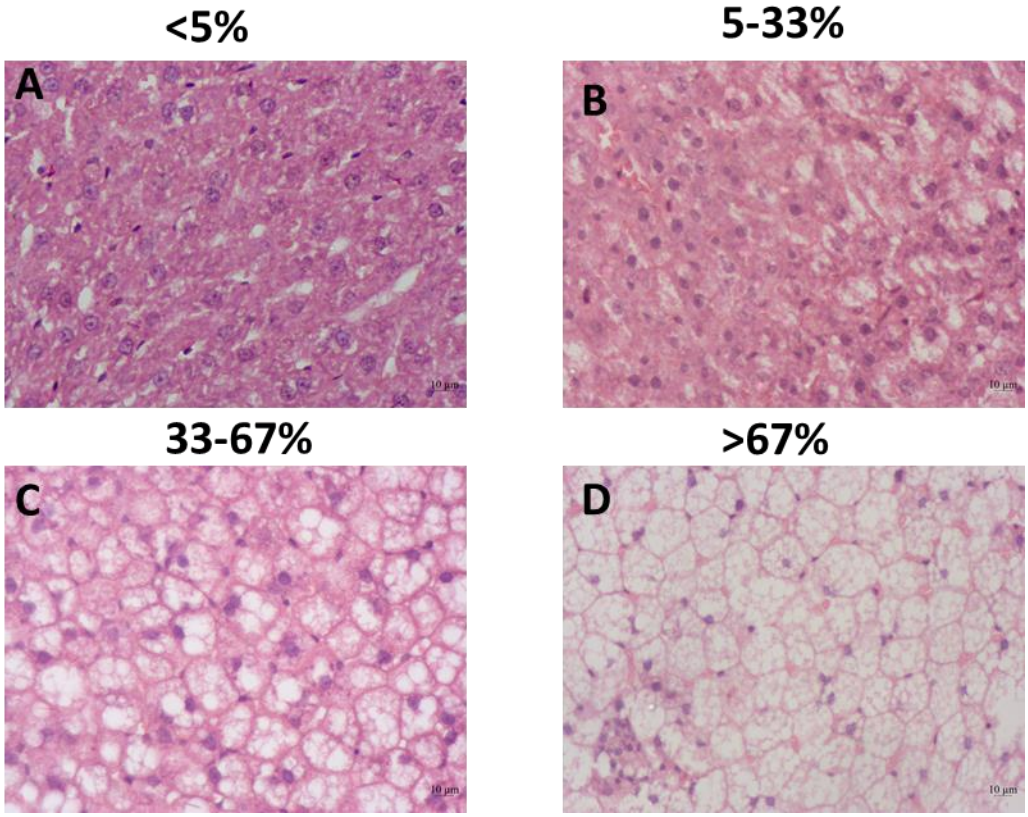

Figure 3: Non-alcoholic fatty liver disease activity score steatosis grading. A) normal fatty change. B) mild fatty change. C) moderate fatty change and D) severe fatty change. Micrography by Jodie Layman.

Grade: Starting at low magnification (4x) evaluate each animal e.g. 1385-16 from broader end to the tip of the tissue section for steatosis. Evaluate the tissue for small (microvesicular) and/or large (macrovesicular) vacuoles of fat in the grades described above and assign a score.

Location: Zone 3 (close to CV), Zone 1 (close to PT) and azonal (no distinct pattern).

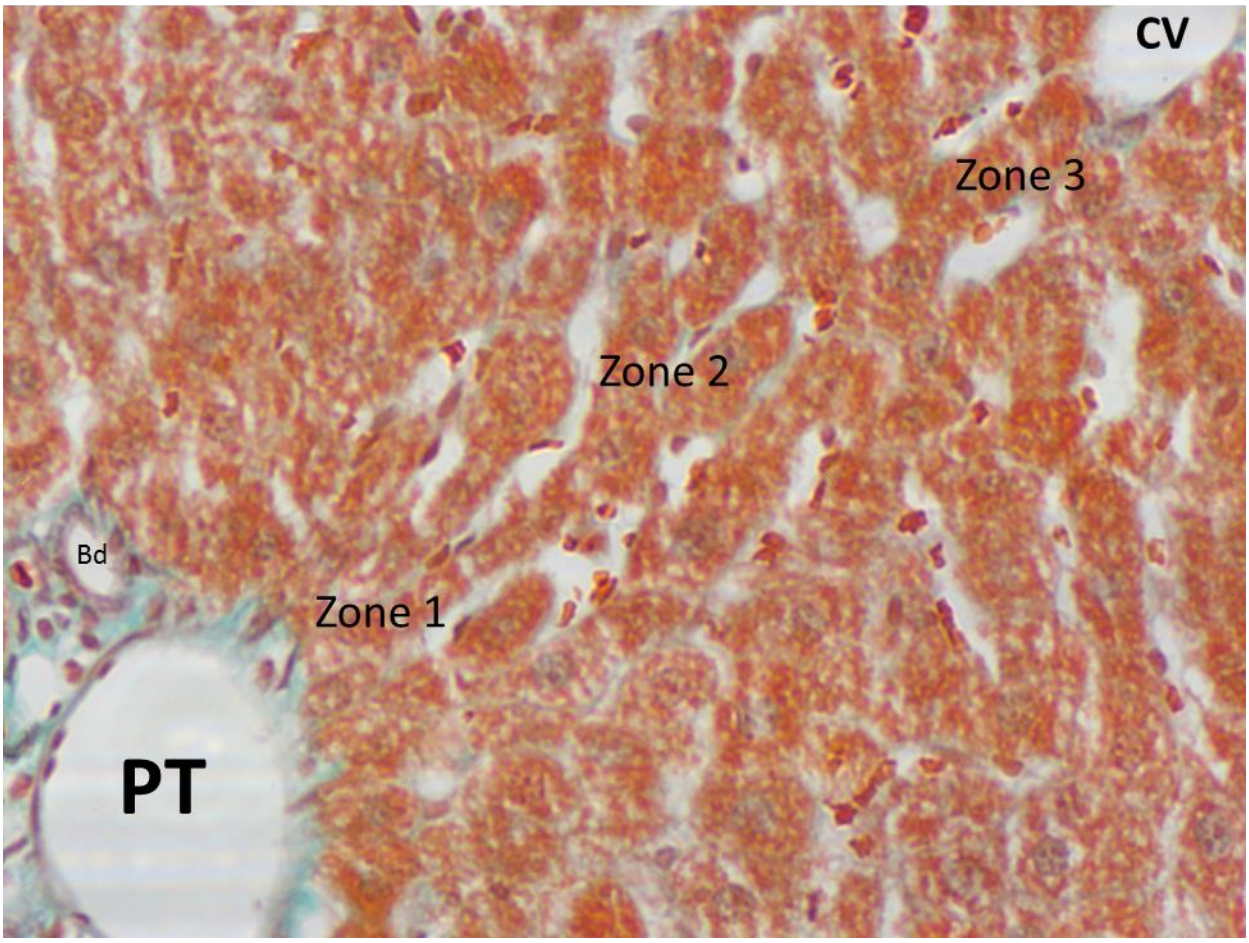

Figure 4: Non-alcoholic fatty liver disease activity score evaluating the location of steatosis. CV= central vein, PT= portal triad, consists of an artery, vein and bile duct form part of hepatic lobules, 1, 2, & 3 describe zones. Micrography by Jodie Layman

Microvesicular and Macrovesicular steatosis

Please describe the predominant area of steatosis: zone 3, zone 1 or azonal (no pattern)

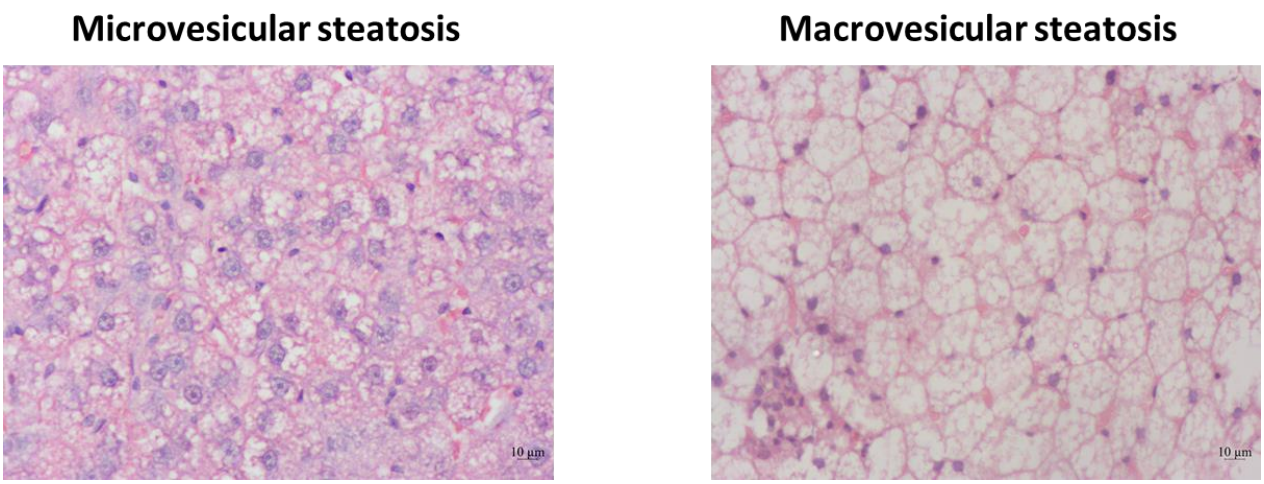

Figure 5: Non-alcoholic fatty liver disease activity score microvesicular steatosis evaluation. Both images show microvesicular steatosis, the figure on the left being less severe than the right. The figure on the right has been labeled macrovesicular as the nucleus has been displaced and would most likely become macrovesicular.

*Note some tissues present with a combination of the two. The score only wants to know if microvesicular was present or not.

Microvesicular steatosis- lipid vacuoles less than 15µm which do not displace the hepatocyte nucleus, which is usually centrally located in the cell.

Macrovesicular steatosis- lipid vacuoles which displace the nucleus and are larger than 15µm. When the many tiny microvesicular lesions break down to form one large vacuole.

Fibrosis

*Please use the Masson's trichrome stained slides of the same number to evaluate the tissue.

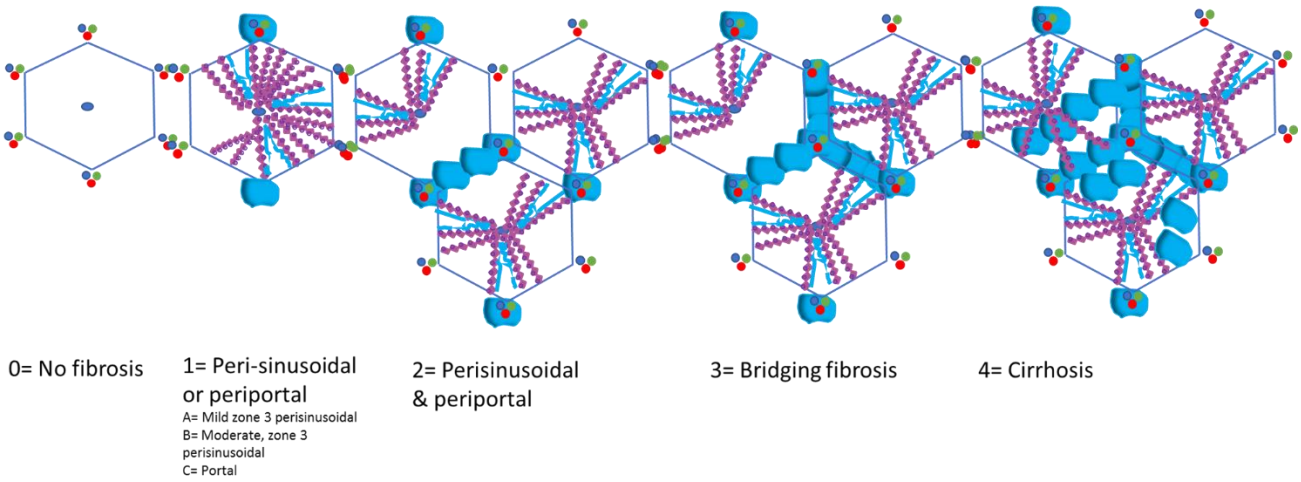

Figure 6: Stages of fibrosis. Illustration of fibrosis as graded by the NAS score. Portal triad=red, green navy, Hepatic lobules= blue polygon, radiating hepatocytes= pink, light blue=fibrotic lesions.

Categories

Look for teal blue staining in the following regions:

- Only Peri-sinusoidal **or** peri-portal- extensive blue staining around portal triads or in the sinusoids (blue lining along hepatocytes)
- Mild Zone 3 (around the central vein) and around the sinusoids
- Moderate staining involving zone 3 and around the sinusoids
- Only around the portal triads
- Perisinusoidal **and** periportal
- Bridging- fibrosis which forms continuous bands (not isolated around portal triads or sinusoids but joins together)
- Cirrhosis- blue staining throughout parenchyma of the liver

Inflammation

Lobular inflammation (Lobes of inflammation) (extra medullary haematopoiesis)

Overall assessment of all inflammatory foci (purple, rod shaped to rounded structures)

No foci	0
<2 foci per 200X field	1
2-4 foci per 200X field	2
>4 foci per 200X field	3

The following scoring grades are to define the types of inflammatory foci. Fat containing inflammatory foci (Lipogranulomas), congregates of pigmented (brown, red & purple) macrophages (Pigmented macrophages), collections of inflammatory cells only purple (Microgranulomas).

Microgranulomas (Small aggregates of macrophages)

Absent 0

Present 1

Large lipogranulomas (Usually in portal areas or adjacent to central veins)

Absent 0

Present 1

Portal inflammation (Assessed from low magnification)

None to minimal	0
Greater than minimal	1

*inflammatory foci around portal triads

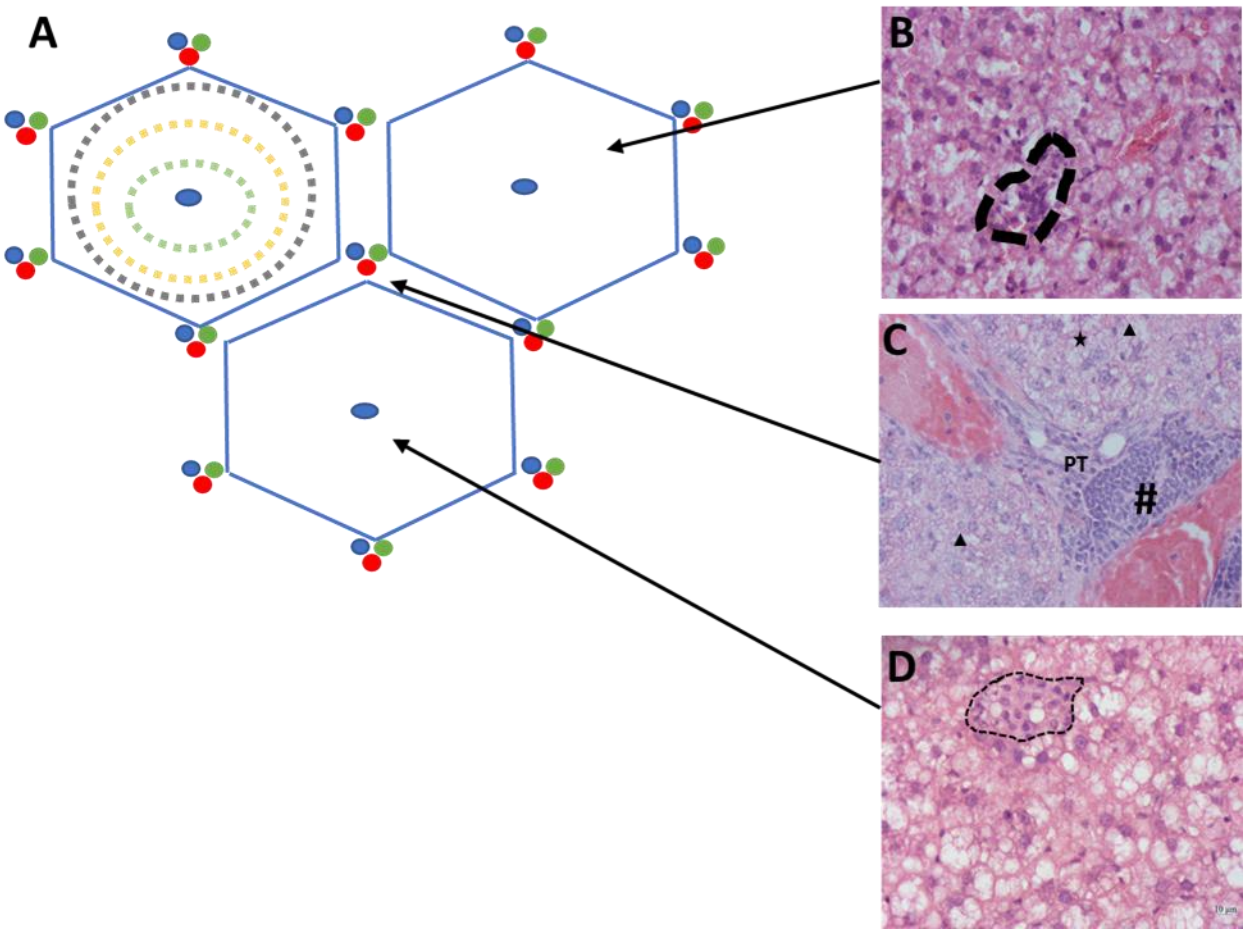

Figure 7: Inflammatory foci as evaluated by the NAS. A) An illustration of liver lobules showing the locations (zone one, two and three) as well as the type of inflmattory foci found in that region.

Liver cell injury

*This is specifically about the hepatocytes

Ballooning*

None	0
Few balloon cells	1
Many cells/prominent ballooning	2

*Look for cells that are swollen, possible nuclei displacement, lighter colour in the centre of cell compared to the cell border.

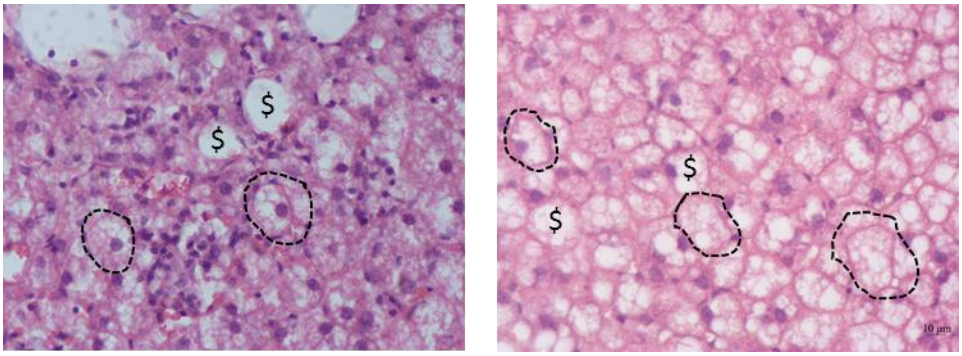

Figure 8: Hepatocyte ballooning as evaluated with the NAS score. Both images show hepatocyte ballooning outlined by dotted lines.

Addendum Q: Plagiarism report

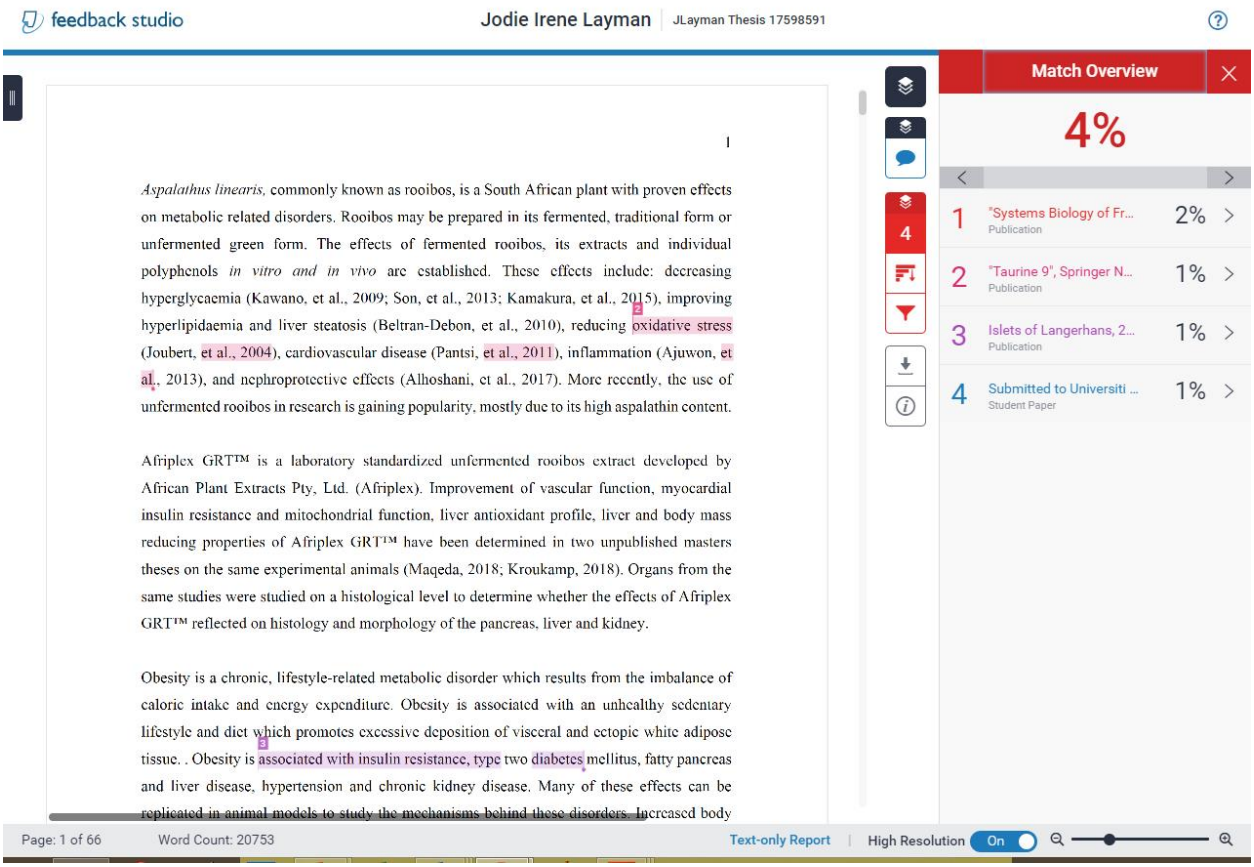

Figure 9: Plagiarism report.